D2.2
VLEO EO Satellite Aerodynamic Control Techniques and Mechanisms

Project acronym:	DISCOVERER
Grant Agreement:	737183
Project Duration:	1 January 2017 – 31 March 2021 (51 months)
Version:	1.0
Date:	30 September 2019
WP Leader:	Jonathan Becedas Rodríguez (DEIMOS)
Authors:	Nicholas H. Crisp (UNIMAN)
	Sabrina Livadiotti (UNIMAN)
	Peter C.E. Roberts (UNIMAN)
	Jonathan Becedas Rodríguez (DEIMOS)
	David González (DEIMOS)
	Valentín José Cañas Muñoz (DEIMOS)
	Constantin Traub (USTUTT)

Table of Contents

Acronyms and Abbreviations

ABEP	Atmosphere-Breathing Electric Propulsion
CMG	Control Momentum Gyroscope
DSMC	Direct-Simulation Monte Carlo
ECEF	Earth-Centred Earth-Fixed
ECI	Earth Centred Inertial
EO	Earth Observation
EUV	Extreme Ultraviolet
FMF	Free-Molecular Flow
GSE	Geocentric Solar Ecliptic
GSI	Gas-Surface Interaction
LEO	Low Earth Orbit
LQR	Linear-Quadratic Regulator
LTAN	Local Time at Ascending Node
LVLH	Local-Vertical Local-Horizontal
MPC	Model-Predictive Control
PID	Proportional-Integral-Derivative
ROAR	Rarefied Orbital Aerodynamics Research
SOAR	Satellite for Orbital Aerodynamics Research
SRP	Solar Radiation Pressure
SSO	Sun Synchronous Orbit
VLEO	Very-Low Earth Orbit

1. Executive Summary

Increasing interest in the exploitation of very low Earth orbits (VLEO) has led to novel operational concepts, including the use of aerodynamic orbit and attitude control methods. Aerodynamic forces and torques are the main source of perturbation that a spacecraft will experience at these lower altitudes in VLEO. Rather than solely using traditional attitude control actuators (reaction wheels, CMGs, and magnetorquers) or thrusters for orbit control, aerodynamic control can therefore be used as an integral aspect of operational attitude and orbit control.

A range of attitude and orbit control methods utilising orbital aerodynamic effects have been proposed in the past. In some cases these methods have been demonstrated in-orbit and ultimately used for some operational purpose. Notable examples include the GOCE mission which utilised an aerostable geometry to assist the drag-compensating propulsion system which was required to accurately map the Earth's gravitational field, and the ORBCOMM constellation which used differential drag techniques to assist the deployment of the different satellites into their intended orbital slots.

However, more complex aerodynamic control has yet to be developed and demonstrated. For Earth observation (EO) applications, the ability to provide precise and stable pointing in the presence of disturbing forces and torques is necessary. Rapid slewing capability is also often desired, requiring platform agility and the ability to offset or reject unwanted aerodynamic torques. Combinations of aerodynamic control and traditional attitude control actuators may provide the necessary performance, whilst the aerodynamics can also help to maintain these actuators, for example through momentum management. Concepts for orbit maintenance and re-tasking using aerodynamic forces have also been proposed, but are at present limited by the available material technologies which do not currently allow the generation of meaningful lift-forces in the VLEO environment. Investigation of materials which may have improved gas-surface interaction (GSI) properties in the VLEO environment is being addresses in other aspects of the DISCOVERER project.

This report documents the development of novel controllers utilising aerodynamic forces and torques and establishes their feasibility for operational use in VLEO. The VLEO environment is first described, from which a modelling toolbox was created enabling simulations of the spacecraft attitude and orbit motion to be performed in the presence of the expected perturbing forces and torques (eg. gravity, aerodynamics, solar-radiation pressure, magnetic field interactions). A review of the state-of-the-art in orbital aerodynamic control is subsequently presented, providing a basis from which the novel attitude control manoeuvres, reference aerodynamic geometries, and control surface designs were developed.

Three reference aerodynamic platform concepts were developed to which the aerodynamic control methods could be applied. Two are nominally aerostable designs, the first a shuttlecock which features an aerodynamic skirt which extends behind the satellite body, and the second an arrow or feathered configuration which features aerodynamic fins. The third geometry, a "disc satellite", was designed to be neutrally stable in the nominal configuration and takes the form of a cylindrical body with two panels extending from the flat end surfaces. For each geometry, steerable aerodynamic control surfaces were specified, enabling the generation of varying aerodynamic forces and torques and therefore control in one or more of the spacecraft body axes.

In orbit control, published studies (within the DISCOVERER project) that investigate the use of aerodynamic drag and lift for formation flight and rendezvous purposes are summarised. The second of these studies specifically investigates the performance increase that could be achieved with the development or identification of novel materials that have improved GSI characteristics and can promote specular reflection properties, thus enabling the generation of useful lift forces.

In attitude control, combinations of synergetic aerodynamic-based control and traditional attitude actuators (reaction wheels) were selected to investigate the development of pointing and trim manoeuvres. Aerodynamic control was also chosen to perform the momentum management of the

reaction wheel with the intention of avoiding saturation of the actuators in the presence of disturbing environmental torques. In order to perform the simulations of these control manoeuvres a modified PID with in intelligent integration action and gains selected using a linear-quadratic regulator (LQR) was implemented. A range of other control methods were considered, but the modified PID ultimately chosen for simplicity of implementation and robust control behaviour in order to first prove the feasibility of the selected aerodynamic control methods for the representative platform concepts.

The results of the presented case studies demonstrate the feasibility of aerodynamic pointing control and momentum management using the developed controller logic and the concept platform geometries. It was noted through the analysis of the different concept geometries that the selection of aerodynamic control surfaces is critical in providing the available control authority to perform the necessary manoeuvres. The shuttlecock geometry was not able to provide control authority in roll, while the neutrally-stable disc satellite was unable to provide control authority in pitch.

Finally, a number of improvements to the developed controllers were proposed in response to the achieved results. These include further development of the panel selection methodology to include a Jacobian formulation which may provide more efficient computation of the aerodynamic torques, and anti-saturation logic for the aerodynamic actuators to demote selection of high-drag configurations which would contribute more to orbital decay.

Within the context of DISCOVERER, the opportunity to perform in-orbit demonstration of aerodynamic control manoeuvres exists using the aerodynamics test satellite SOAR (Satellite for Orbital Aerodynamics Research. Following a consideration of the specific requirements and limitations for implementing control methods on this test satellite, a proposed set of manoeuvres for demonstration have been presented. These manoeuvres include aerodynamic-assisted pointing, aerodynamic trim, and momentum management tasks and are intended to provide proof-of-concept of operationally-relevant aerodynamic control in the VLEO environment. These manoeuvres will be taken forward for specific development and implementation on the satellite hardware within the scope of DISCOVERER Task 2.2 (reported in D2.3).

2. Deliverable Report

2.1. Introduction

Interest in the exploitation of lower orbital altitudes has recently been noted, principally for the benefits which can be afforded to Earth observation (EO) applications, for example improved resolution imagery and data or alternatively lower cost observation platforms. However VLEO also offers the possibility to utilise the increased atmospheric density at low altitudes for novel purposes, for example aerodynamics-based control or atmosphere-breathing electric propulsion (ABEP), helping to enable sustained operations in this regime.

The DISCOVERER project [1] aims to radically redesign Earth Observation satellites for sustained operation at significantly lower altitudes. The project encompasses foundational work in the understanding of gas-surface interactions in the VLEO environment, development of atmosphere-breathing electric propulsion, and implementation of novel aerodynamic control manoeuvres. These developments will also be combined to develop new concepts for EO operations in VLEO and business models to support the exploitation of these technologies.

This report documents the development of novel aerodynamic control manoeuvres, principally designed for EO satellite platforms operating in the very low Earth orbit (VLEO) altitude range. This document follows the work reported in *D2.1 VLEO Aerodynamics Requirements Document* [RD-1] which provided a comprehensive review of the state in aerodynamic attitude and orbit control and associated technologies. Following a review of the benefits of VLEO and EO applications a set of four platform concepts were outlined, and finally an initial list of aerodynamic control requirements defined for EO satellite operations in VLEO.

In Section 2.2 , the foundations for orbit and attitude modelling in VLEO is provided with a focus on the methods required to characterise aerodynamic forces and torques for representative spacecraft geometries in the relative environment.

An updated review of aerodynamic orbit and attitude control manoeuvres is provided in Section 2.3. A introduction to different controllers suitable for application to aerodynamic control manoeuvres is provided in Section 2.4, leading to the selection of the controller's which are implemented in the remainder of this work.

In Section 2.5 the development of the selected controllers is first described and some initial performance testing is presented. The aerodynamic control manoeuvres, including pointing, trim, and momentum management are then demonstrated using a set of three conceptual spacecraft geometries.

Finally, the in-orbit implementation of aerodynamic control manoeuvres on SOAR (Satellite for Orbital Aerodynamics Research) is discussed in Section 2.7 and some initial simulations presented.

2.2. Modelling of Orbital Aerodynamics

2.2.1. Aerodynamic Torques and Forces

Interaction of the surfaces of a spacecraft with the residual gas flow in Very Low Earth Orbit (VLEO) results in the production of aerodynamic forces and torques. For a given surface or body exposed to the oncoming particle flow, the magnitude and direction of the resultant force will be dependent on the relative velocity of the surface with respect to the flow v_{rel} and the atmospheric density ρ. A reference area S_{ref} and set of dimensionless force coefficients $\vec{C}_F$ (drag, side, and lift) are also required to incorporate the orientation and interaction of the surface or body with respect to the flow. The force can therefore be expressed:

$$\vec{F}_{aero} = \frac{1}{2}\rho v_{rel}^2 \frac{\vec{v}_{rel}}{|\vec{v}_{rel}|} A_{ref} \vec{C}_F$$

Equivalently, the torque produced can be also be expressed by considering the moment coefficients of the body $\vec{C}_M$ (roll, pitch, and yaw) and an additional reference length unit L_{ref}:

$$\vec{T}_{aero} = \vec{r} \times \vec{F}_{aero} = \frac{1}{2}\rho v_{rel}^2 \frac{\vec{v}_{rel}}{|\vec{v}_{rel}|} A_{ref} L_{ref} \vec{C}_M$$

Alternatively, the torque on the body can be considered as the summation of the moments produced by the external surfaces each acting at a distance from the centre-of-mass of the body.

i) <u>Atmospheric Density and Flow</u>

The density of the atmosphere reduces at an approximately exponential rate with increasing altitude. The atmospheric density in VLEO (below 450km, ie. In the lower thermosphere) is therefore rarefied and also highly variable, principally due to the variation in emitted extreme ultraviolet (EUV) radiation from the sun which is absorbed in the upper atmosphere [2]. Further characteristics of the thermosphere include the variation of molecular temperature and composition with altitude due to the relative mass of the different constituents.

Due to the low density of the atmosphere in the VLEO regime, the flow can generally be classified as free-molecular. Free-molecular flow (FMF) is characterised by the mean free path of gas molecules being much larger than the size of a satellite, and therefore the relative insignificance of particle-particle interactions, including interactions between incident and reflected particles in proximity to a surface. The dimensionless Knudsen number (the ratio between the mean free path of a particle and a characteristic dimension of the spacecraft) is typically used to determine whether the flow is continuum ($Kn \ll 1$) or free-molecular ($Kn \geq 10$). Thermospheric flows can also be classified as hyperthermal or hypothermal, depending on whether the bulk velocity of the flow, provided by the movement of a satellite through the atmosphere, is much greater than or of a similar magnitude to the random thermal motion of its constituent molecules. Molecular speed ratio is used to define whether a flow can be described as hyperthermal (typically $s > 5$), and can therefore be treated as a collimated beam of molecules.

For a surface in the VLEO environment, the assumption of FMF is generally valid (above 100km), and the force produced is dominated by the nature of the gas-surface interactions (GSI) which occur. Both incident and reflected particle-particle interactions are typically neglected.

ii) <u>Gas Surface Interactions</u>

The force produced on a surface can be equated to the rate of change of momentum between the incident and reflected gas particles. However, this process this is complicated by effects such as the differing interaction of atmospheric gas species, surface accommodation of the gas particles, and the mechanisms for energy and temperature exchange at the surface. Due to these complexities, different mathematical models for GSI in FMF are presented in the literature, providing different treatments of the underlying physical interaction between the incident gas particles and the surface.

In these models an expression for the exchange of energy or temperature (energy/thermal accommodation α), or the exchange of momentum (momentum accommodation, σ) are used to describe the averaged GSI mechanism which occurs.

Principally, two modes of particle reemission are considered by GSI models, specular reflection (no accommodation, $\alpha = \sigma = 0$) and diffuse reemission (complete accommodation, $\alpha = \sigma = 1$). Quasi-specular reemission is used in some models where the specularly reflected component of the incident flow has a distribution about a mean scattering angle. By considering values of accommodation coefficient in between these extremes, the ratio of specular (or quasi-specular) to diffuse reemission can be considered and the averaged effect which occurs on a surface can be captured.

The value of the accommodation coefficient is principally determined by the material, surface contamination (resulting from atmospheric particle adsorption), temperature, and roughness. Contamination generally increases the energy lost at the surface by incident particles and therefore increases accommodation.

Although known to be dependent on altitude (based on local atmospheric composition and density) and surface temperature, material surfaces in LEO (for currently characterised materials) are generally accepted to be highly contaminated and therefore the predominant GSI characteristic at these altitudes is diffuse with a growing specular or quasi-specular component with increasing altitude.

iii) Calculating Aerodynamic Coefficients

Analytical closed-form expressions for the pressure and shear stress or aerodynamic force coefficients for simple shapes (eg. flat-plate, sphere, cylinder) can be determined using these GSI models.

If a body can be modelled as a series of individual flat-plates or panels then the pressure and shear force coefficients can be converted to force coefficients based on the orientation of each panel with respect to the oncoming flow. The moment coefficients of the body can be similarly calculated by considering the vector from the centre of mass to the centre of each panel.

Such panel-methods can be correctly utilised for convex geometries which do not feature multiple-reflections of incident particles as only the first interaction is considered. For more complex geometries alternative numerical techniques such as Ray-Tracing Panel, Test-Particle Monte Carlo, and Direct-Simulation Monte Carlo (DSMC) may need to be used.

Under the assumption of hyperthermal FMF, and convex body geometries the panel-method can be used to determine the aerodynamic coefficient set for a body in the VLEO environment. The ADBSat (Aerodynamic Database for Satellites) tool [3] provides the capability to calculate aerodynamic coefficient sets for convex CAD or mesh-based geometries. Several different GSI models have been implemented in ADBSat. Additional shadow analysis process can also be included to allow consideration of more complex shapes. Databases of aerodynamic coefficients for varying flow incidence (body attitude), altitude, or environmental conditions can be calculated by repeated execution of the tool which can also take advantage of parallel computation.

The validation of such panel methods can be performed using DSMC modelling (eg. Mehta et al. [4]) and also by comparison to observed in-orbit objects.

2.2.2. Orbit and Attitude Modelling in VLEO

The modelling of orbital and attitude dynamics in VLEO requires careful consideration of the forces and torques which act on the spacecraft in the relevant environment. Propagation methods are widely used to perform orbit determination for satellites based on observations or predict the future trajectory or location of orbiting bodies. However, the contributing set of perturbations and method of propagation vary considerably based on the environment under investigation and the application of interest.

The dynamic environment of Earth orbits principally involves the geopotential of the Earth, the neutral and charged atmosphere, the Earth's magnetic field, and solar radiation pressure. The effects of third body gravity (eg lunar, solar), solid-Earth and ocean tides, Earth albedo and relativistic effects may also be required for more precise analysis or for specific applications (eg. GPS accuracy).

For the simulation and prediction of future spacecraft position and attitude dynamics the relative magnitude of these perturbations and the uncertainty in the contributing parameters is of significance. Whilst the future state of some parameters may be well known and predictable (for example the Earth's orbit about the sun), others are at present poorly understood, modelled, or highly unpredictable. In particular, the Earth's atmosphere (eg. density, composition, winds) is known to be highly variable and related to other factors such as the solar weather environment which is similarly characterised with high levels of unpredictability and uncertainty.

For the purpose of orbit and attitude propagation in VLEO, the uncertainties associated with modelling and prediction of the atmospheric and solar environment are more significant than many other sources of perturbations. These smaller factors can therefore be safely neglected in most analyses with the knowledge that their effects, even if secular rather than periodic, are of smaller magnitude than the uncertainty associated with the more significant perturbations.

i) Reference Frames definition

The purpose of the current section is to provide a definition of the reference frames defined in this document and implemented in the simulator to study the feasibility of the aerodynamic control manoeuvres. These comprise:

- Earth-Centered Inertial Reference Frame (ECI): the ECI reference frame has its origin located at the Earth's center of mass and it is not fixed with the Earth. The X_I axis points in the ecliptic plane of the Earth's orbit about the Sun and points towards the vernal equinox direction. The Z_I axis is aligned with the Earth axis of rotation, perpendicular to the equator. The Y_I axis lies in the ecliptic plane as well and its direction is determined according to the right hand rule;
- Earth Centered Earth Fixed Reference Frame (ECEF): the ECEF reference frame has its origin in the Earth's center of mass and, as its name suggests, it rotates with the Earth's rotation rate. The X_E axis is pointed towards the international reference/prime meridian. The Z_E axis points towards the north pole. Finally, the Y_E axis is determined according to the right hand rule;
- Orbital/Local Vertical Local Horizontal (LVLH) Reference Frame: the LVLH reference frame has its origin located at the satellite center of mass. The X_O direction coincides with the satellite velocity vector direction and lies in the satellite orbit plane. Similarly, the Z_O axis lies in the satellite orbit plane and it points towards the center of the Earth in the nadir pointing direction. Finally, the Y_O axis is determined according to the right hand rule and it is perpendicular to the satellite orbital plane;
- Flow Reference Frame: since in this work only the horizontal wind component is modelled, the X_F axis is directed along the flow vector direction and the Z_F axis points towards the center of the Earth in the nadir direction. If future development will allow vertical winds to be included in the simulation, the Z_F direction should be modified such that the X_F-Z_F plane contains the flow vector. In both cases, the Y_F axis is determined according to the right-hand rule. In practice, determination of the flow reference frame is affected by the many uncertainties associated with the estimation of the flow direction. Due to the difficulties

encountered in modelling the thermospheric wind direction, only the contribution of atmospheric co-rotation can usually be taken into account with a certain level of confidence.

- Geocentric Solar Ecliptic Reference Frame (GSE): the origin of this reference frame is located at the center of mass of the Earth and its X_S axis is directed along the Earth-Sun vector. The Z_S axis direction is given by the cross product between the Earth–Sun vector component and the Earth-Sun vector velocity component. Y_S is accordingly defined following the right hand rule;
- Body Reference Frame: the body reference frame has its origin located at the satellite's center of mass and rotates rigidly with the body. If aligned initially with the LVLH frame, the X_B axis is aligned with the satellite velocity direction, the Z_B axis is directed towards the Earth in the nadir pointing direction, and the Y_B axis is determined by the right hand rule. The X_B, Y_B, Z_B axes will be referred later on in this document as the roll, pitch and yaw axes.

ii) <u>Central Body Gravity</u>

Whilst responsible for enabling orbital motion, the variations of central body gravity which result from the aspherical gravity potential of a central body (eg. Earth) are also the largest source of perturbation to ideal two-body motion. Torque resulting from the gravity potential of the Earth may also be generated on the spacecraft body if the spacecraft has a non-uniform distribution of mass (moment of inertia matrix) [5].

The gravitational field of the Earth can be expressed in a number of ways and to varying levels of fidelity and precision. The Earth, though commonly described as a sphere, actually resembles an oblate spheroid, principally due to its rotation. The distribution of mass within the Earth further affects the true geopotential, resulting in a more complex gravitational field.

Different representations of the gravity potential are often based on spherical harmonics. For Earth, the J2, J3, and J4 models are simple analytical representations of the zonal harmonics up to degree 2, 3 and 4, which capture the principal secular effects on an Earth orbit.

For increasing propagation accuracy incorporating periodic and resonance effects, the sectoral and tesseral harmonics of increasing degree and order are considered. The necessary coefficients used in to form the potential function are obtained from an empirically determined gravitational model, for example EGM-96/08 [6,7].

iii) <u>Aerodynamic Acceleration and Torque</u>

In VLEO the perturbations due to interaction with the residual atmosphere are known to be significant. The principal contributing factors to this perturbation are the atmospheric density, the velocity vector of the spacecraft relative to the oncoming flow, and terms relating to the physical characteristics of the spacecraft.

In the calculation of aerodynamic forces and toques, the atmospheric density, relative velocity vector, and aerodynamic coefficients are all challenging parameters to determine with accuracy and certainty. The reference area also requires careful consideration in conjunction with the source of the aerodynamic coefficients to ensure compatibility. The relative velocity vector is also of importance and similarly difficult to characterise accurately. The orbital velocity of the satellite (on the order of 7 to 8 kms^{-1}) is the principal component, but atmospheric co-rotation and thermospheric winds must also be considered.

In the absence of measured or known values, the atmospheric density is typically determined using an atmospheric model. Whilst simple analytical models (eg exponential) or standard lookup tables can be used, the atmospheric density is known to be highly dynamic and varies considerably with altitude, latitude, longitude, time of day, season, and solar activity amongst other factors [14]. Representative atmospheric models are therefore complex to develop and validate even with measured data, and are associated with significant errors, biases, and uncertainties which must be considered. Current state-of-the-art atmosphere models include the NRLMSISE-00 [15], JB2008 [16], Earth-GRAM 2016 and DTM-2013 [17]. It should be noted that these models are dependent on inputs of various solar flux and geomagnetic indices which are also associated with uncertainty, particularly due to the variability and unpredictability of the solar cycle. Comparisons of atmospheric models are available in literature [8].

The Drag Temperature Model (DTM2013) [9] is a semi-empirical model which provides the temperature, density, and composition of the Earth's thermosphere. It is tuned with data provided by CHAMP, GRACE, and GOCE spacecraft. This model covers the 200–900 km altitude range and includes information from solar activity. DTM2013 was developed by including data from the DTM2009 model, but incorporates more data from GRACE and GOCE. The NRLMSISE-00 [10] is widely used in international space research because of its accuracy in comparison with other models, source code availability, integrations with different programming languages and packages, and frequency of updates.

The neutral atmosphere largely rotates with the surface of the Earth and therefore has a relative velocity that should be considered when considering interactions with an orbiting body. In addition to this general motion, thermospheric winds are also present. These winds are more variable and unpredictable and therefore associated with significant uncertainty. However, statistical representation of the wind at orbital altitudes is provided by models such as the Horizontal Wind Model (HWM07/14) [11,12].

Wind models are usually focused on the calculation of the horizontal components (zonal and meridional). The vertical component of wind velocity, usually, is much lower than the horizontal ones and it is considered negligible. Vertical components are not easily measured. Larsen et al. [13] remark in their study that there are only a few profiles of the vertical winds. The region of interest for VLEO matches the F region of the thermosphere. This region has the highest concentration of free electrons and ions in the atmosphere. A higher temperature increases the concentration of ions due to the reactions produced in the atmosphere. The solar activity, temperature and the earth field have a great impact in the winds in the thermosphere. The experimental results described by Larsen et al. [13] show different values of the vertical winds in the F region. It shows speeds below 40 m/s or 10 m/s depending on the sources they cite in their study. These measurements are one order of magnitude lower than the horizontal winds that are calculated with the Horizontal Wind Model (HWM14).

Furthermore, the models that provide information about the vertical wind were analysed. GITM [14] and MENTAT [15] are examples of models that fulfil this requirement but, in both cases, the access to the source code to integrate them in the simulations is not available or have restrictions to access it. Developing and implementing the code of these models in DISCOVERER is out of the scope of the project. Thus, if we consider that the principal disturbances that affect the spacecraft are already included in the results presented in this document, and the horizontal wind is an order of magnitude higher than the vertical component, we can conclude that we can omit the effects of the vertical wind component.

The variation in activity of the Sun and its interaction with the Earth's magnetic field can also have a significant influence on the atmosphere and ionosphere. Models for these factors are described in the section below.

iv) <u>Solar Radiation Pressure (SRP)</u>

Perturbations due to solar radiation pressure result from the interaction between the external surfaces of the spacecraft and incident solar radiation. The acceleration and torques due to SRP can be calculated by considering the solar vector to the spacecraft and the reflectivity of the external spacecraft surfaces exposed to the Sun. Coefficients for the SRP interaction of a spacecraft body can be generated by summation over a flat-plate model and databases produced for varying spacecraft attitude.

The effects of SRP are often modelled using average solar irradiance at 1AU which can be corrected for the true Spacecraft-Sun distance at a given time. However, models that account for the temporal variation in solar output can be used to improve the fidelity of simulations.

Solar output has been observed to vary on a cycle of approximately 11-years and is further characterised by high-variability at solar maximum and lower-variability at solar minimum. However, successive solar cycles can be substantially different to each other, making predictions of the solar flux at future times difficult. Despite this, methods for prediction of solar flux based on historical measurements have been developed [16]. Alternatively, for short-term simulations, static values for the solar output for an approximate can be used

v) Third Body Gravity

The contribution of third-body gravity, principally lunar and solar, can also influence the orbit trajectory. Induced periodic effects in the semi-major axis can result in perigee height variations which can affect the lifetime of the spacecraft, whilst secular variations in the node and perigee can be observed. The perturbations of multiple third-bodies can incorporated by considering their individual gravitational contributions on the spacecraft and the Earth [16].

vi) Magnetic and Electric Field Interactions

Magnetic field interactions are an important consideration regarding the attitude of a satellite. Actuators such as magnetorquers utilise interaction with the Earth’s magnetic field to perform attitude control for the spacecraft. The residual magnetic dipole of the spacecraft (from magnetised materials or internal electrical current loops) can also result in significant disturbance torques. The torque due to an applied magnetic moment can be characterised by considering the orientation of the dipole with respect to the Earth’s magnetic field [5].

The Earth’s magnetic field principally results from electrical conduction in the rotating and convecting core of the planet. Small contributions also arise in the mantle, crust, and ionosphere. The geomagnetic field varies on both short timescales due to ionospheric and magnetospheric interactions and secularly over longer timescales.

Mathematically, the Earth's magnetic field can be described using spherical harmonics. Oehler et al. [17] compare several magnetic field models. The International Geomagnetic Reference Field (IGRF-11/12) [18,19], updated approximately every five years, is the reference model popularly used in space science applications.

Further disturbances may arise from the interaction between charged components of the spacecraft with the Earth’s magnetic field, the ionosphere (charged particles), or solar wind. Significant magnetic fields generated by the spacecraft can also interact with the oncoming ionospheric plasma. However, these effects are generally small and negligible for most spacecraft designs.

2.3. Aerodynamic Control Methods for VLEO Spacecraft

A variety of different attitude and orbit control manoeuvres can be achieved using aerodynamic forces and torques that can be generated in VLEO. A review of aerodynamic control methods that have been studied and applied in the past was provided previously in [RD-1].

The aerodynamic attitude and orbit control methods of interest and their broad concept of operations are described briefly in the following sections.

2.3.1. Attitude Control

i) Aerostability

Aerostability (static aerodynamic stability) is the tendency of a body to orientate itself towards the direction of the oncoming flow, and can be a desirable feature for some spacecraft. Aerostability can be achieved through design of the external body geometry and internal mass distribution, ensuring that restoring aerodynamic torques are generated when the vehicle is not pointing in the flow direction. Commonly, addition of aerodynamic fins (eg shuttlecock, or dart designs) or appendages (feathers or aero-skirts) are used to increase the aerostability of symmetrical parallelepiped spacecraft.

A further important design consideration for aerostability is the relative magnitude of the disturbing gravity gradient torques (and possible solar radiation torques) in comparison to the restoring aerodynamic torques that are generated at varying orbital altitude.

The principal conditions for static aerostability in pitch and yaw can be described by the following equations [20], where q is the dynamic pressure, ω_0 is the angular orbit velocity, S_{ref} and L_{ref} are a reference area and length respectively, I_y and I_z are principal moments of inertia, and C_{m_α} and C_{n_β} are stability derivatives.

$$-\frac{q}{3\omega_0^2}\frac{S_{ref}L_{ref}}{I_y}C_{m_\alpha} > 1$$

$$\frac{q}{\omega_0^2}\frac{S_{ref}L_{ref}}{I_z}C_{n_\beta} > 1$$

$$I_y > I_z$$

Aerostability is therefore positively affected by reducing orbital altitude (via. increasing density and therefore dynamic pressure), and stability derivatives of greater magnitude.

Aerostability has been studied and modelled in a number of papers [21–27], and demonstrated in orbit by the DS-MO [28], PAMS [29], GOCE [30], and QbX [Armstrong, 2009] spacecraft for varying geometries.

However, whilst static stability can be achieved, aerodynamic damping forces in VLEO are not sufficient to provide passive dynamic stability. An external source of attitude damping is therefore necessary to avoid an oscillating condition about the stable equilibrium point. Passive methods (eg. magnetic hysteresis rods or viscous dampers) or active methods (e.g. magnetorquers or reaction/momentum wheels) can be used. If present, active actuators can also be used to compensate for external disturbance torques (eg. solar radiation pressure, magnetic dipole interactions).

ii) Aerodynamic Pointing

Aerodynamic torques, generated using manipulation of designed control surfaces, can be used to point a spacecraft towards a target or direction of interest. Using different combinations of control surfaces three-axis pointing can theoretically be achieved.

Pointing using aerodynamic torques currently only has a small presence in the literature. Auret and Steyn [25] consider pointing only in the roll axis with aerostabilisation use to control the pitch and yaw axes. Studies by Gargasz [31] and Virgili Llop et al. [32] approach the problem of three-axis control. These investigations indicate that the maximum pointing angle (with respect to the flow) which can be achieved is small (<5° for the material properties and geometries considered).

However, improved material properties, providing more specular reflection GSI properties, can increase the effectiveness of control surfaces and therefore provide greater pointing angle authority. The size of the control surfaces in comparison to the spacecraft body, and location with respect to the centre of mass of the spacecraft can also be used to increase the control effectiveness.

The magnitude and variability of the atmospheric density are also key factors that affect the pointing capability and performance. However, only coarse pointing accuracy is expected to be achievable without contribution of additional attitude actuators for fine control. Alternatively, if knowledge of the oncoming flow vector and atmospheric density is available, for example through active sensing, more precise control may be possible.

iii) Trim

The use of aerodynamic control surfaces can also be considered for the purpose of trim, reducing the requirements or usage of active actuators during pointing manoeuvres.

Compensation of atmospheric co-rotation is the most obvious application for the use of trim, allowing a spacecraft to point in a non-flow oriented direction, whilst also avoiding the build-up in momentum of reaction wheels due to the constant bias.

Trim can also be used to compensate for asymmetric geometries presented to the oncoming flow. For example as an asymmetric spacecraft is pointed out of the ram direction towards a selected target, a combination of control surfaces rather than internal actuators can be used to compensate for any disturbing aerodynamics torques which are generated.

Trim in this manner was demonstrated in orbit by the MagSat spacecraft, which utilised an extendible aerodynamic boom with controllable length to assist the yaw control of the spacecraft [33,34].

iv) Momentum management

In addition to the momentum management which can be afforded by utilising aerodynamic trim where possible, active aerodynamic control can be used to reduce the rates of reaction wheels and control momentum gyroscopes (CMGs), helping to avoid saturation and loss of control authority. This is often termed momentum dumping or desaturation.

Due to the dependency of internal momentum accumulation on the oncoming flow direction in VLEO, reaction wheel management or momentum dumping is most effectively applied on an aerostable geometry when pointing nominally in the ram direction. However, given appropriate control surfaces, the principals of aerodynamic momentum management can be applied in combined with pointing or trim manoeuvres.

In order to provide momentum management using aerodynamics, the control surfaces must be used to generate external torques which oppose the accumulated momentum in the reaction wheels, thus requiring them to reduce their speed in order to maintain the orientation of the spacecraft.

2.3.2. Orbit Control

i) Relative motion and collision avoidance

Concepts for aerodynamic orbit maintenance uses drag and lift forces to provide relative motion between two spacecraft or a spacecraft with a reference orbit or condition. Early studies considered only the drag force to provide in-plane manoeuvring [35–41], however, more recently the use of lift forces which can provide out-of-plane relative motion have been considered [42,43]. Use of differential drag to provide collision avoidance manoeuvres have also been proposed [44].

Differential aerodynamic forces can be generated through the use of either dedicated moving control surfaces (or dual-use, eg. solar arrays), or use of the attitude of the spacecraft body itself to generate a variation in the drag force experienced. However, in either case, a capable attitude control system is required in order to provide the necessary orientation of the spacecraft with respect to the oncoming flow.

The ORBCOMM constellation used a combination of the solar array position and spacecraft yaw angle to provide constellation maintenance over the lifetime of the system [45]. Further in-orbit demonstration of differential drag formation maintenance has been performed by the Aerocube-4 [46] and Planet Dove [47] spacecraft, both of which used attitude control to increase the area of the spacecraft exposed in the ram flow direction and therefore provide variable drag.

Constellation deployment using nodal (RAAN) precession assisted by differential drag has also been proposed [48]. However, similarly to the other differential drag methods discussed above, the extended manoeuvre duration and contribution to orbital decay are significant limitations.

However, the implementation of these manoeuvres is at the expense of increasing the drag force experienced by the spacecraft, therefore contributing to orbital decay. Furthermore, the rate of relative motion between spacecraft may be small, leading to extended manoeuvre or drifting times to generate the desired separations or rendezvous.

Atmospheric re-entry interface targeting using aerodynamic drag exploits the problem of incurring orbital decay during manoeuvring. Under this concept, modulation of the spacecraft drag (using either the body attitude or external control surfaces) during its final orbits is used to locate the atmospheric re-entry interface both in latitude and longitude [49]. Given a sufficiently high initial orbital altitude for the manoeuvre, any latitude allowed by the orbital inclination and any global longitude can be achieved.

ii) Secular modification of orbital parameters

Out-of-plane forces generated using aerodynamic lift can also be used to produce secular variations in inclincation, RAAN, and AoL or AoP. Inclination correction for a sun-synchronous orbit (SSO) naturally descending in altitude has been proposed [50]. However, for current spacecraft materials, drag-compensation is required in order to reconcile the achievable lift-to-drag ratio with the rate of orbital decay.

In a similar manner, aerodynamic lift could be used to control the nodal regression rate of SSOs, enabling a desired variation in LTAN or reducing the need for corrective propulsive manoeuvres to maintain regular revisit of a target under the same illumination conditions.

In order to provide the necessary out-of-plane forces, control surfaces or asymmetric external spacecraft geometries are required. However, the orientation of these surfaces with respect to the flow must be controlled over the orbital period to ensure application of the force in the correct direction to provide the desired secular effect.

2.3.3. Effect on Orbit Lifetime

In low orbits, atmospheric interaction significantly affects the satellite lifetime. The density increases very quickly as the altitude of the orbit decreases, which causes the spacecraft orbit to decay through ever increasing drag. This means that in VLEO the satellite lifetime is considerably shorter than in higher orbits (of course, if the decay is not compensated with a propulsion system).

The lifetime in orbit directly depends on the mass to area ratio of the satellite (this is the relation between the frontal area of the satellite and its mass.). This was demonstrated in our recent publication in [51]. Figure 1 depicts the orbit lifetime for different CubeSat geometries at different altitudes. All satellites were considered to be flying with constant attitude, in which the frontal face was perpendicular to the tangential direction of the orbit.

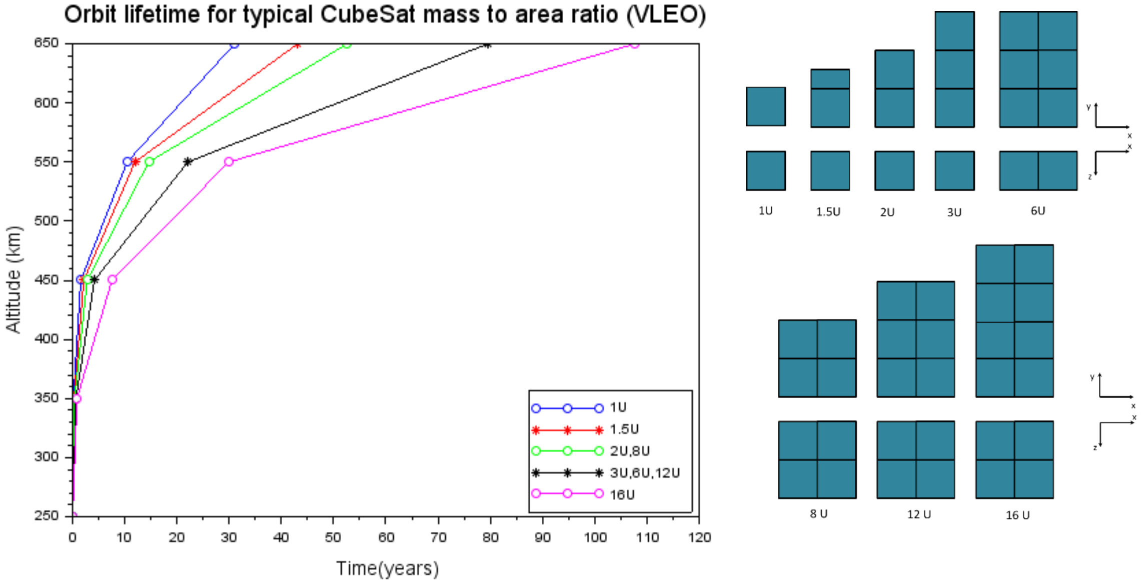

Figure 1 Orbit lifetime for several types of CubeSats and launch altitude

The 1U CubeSat had a mass to area ratio of 0.01, 2U and 8U had the same mass to area ratio, which was 0.005; 3U, 6U and 12U had the same mass to area ratio, which was 3.33·10-3, and 16U had a mass to area ratio of 2.5·10-3. The picture shows that the 1U satellite was the most unfavourable case because it had the higher mass to area ratio, while the 16U was the most favourable case among all the configurations analyzed, again, for having the lowest mass to area ratio of all the configurations studied.

From this analysis one can deduce that in order to be able to perform missions with a long lifetime a drag compensation system is needed for VLEO. It can also be deduced that it is convenient to have a small mass to area ratio. In the subsequent analysis the 3U configuration will principally be used to demonstrate aerodynamic control feasibility as it has a small mass to area ratio. The results are representative of the SOAR mission and can therefore facilitate the selection of aerodynamic manoeuvres and control methods for implementation and in-orbit testing.

2.3.4. Initial Pointing Analysis

In order to investigate aerodynamic stabilization and pointing manoeuvres an initial analysis was performed to determine the control capability when only aerodynamic control interactions are taking place during operation. The following results were presented by D. González [52].

Simulated external torques were the included: gravity gradient, magnetic field, and aerodynamic torque. A PID (Proportional Integral Derivative) controller was selected to manage the aerodynamic panels for both a shuttlecock and feather configuration. The orbit parameters are defined in Table 1. The dimensions of the aerodynamic panels for both the shuttlecock and feather configuration were 90 cm x 10 cm.

Table 1 Orbit parameters for the initial pointing performance analysis

Type of orbit	Altitude (km)	Inclination (degrees)	Argument of Perigee (degrees)	Eccentricity
VLEO	350	50	90	0.001

The attitude stability of the feather configuration was studied in pitch, raw and yaw axes. An independent simulation was performed for each axis. Figure 1Figure 2 shows the results for each simulation. The settling time was considered the moment when the difference between the signal and the reference is lower than one degree, as defined in D2.1 for optical coverage missions such as the Flock constellation. The maximum manoeuvrability is reached in roll axis, with a settling time of 172 seconds (2.87) minutes. The pitch and yaw axes behaved similarly to each other and showed a settling time of 607 seconds (10.11 minutes) and 812 seconds (13.53 minutes), respectively. In this configuration, lift primarily is used in the manoeuvres.

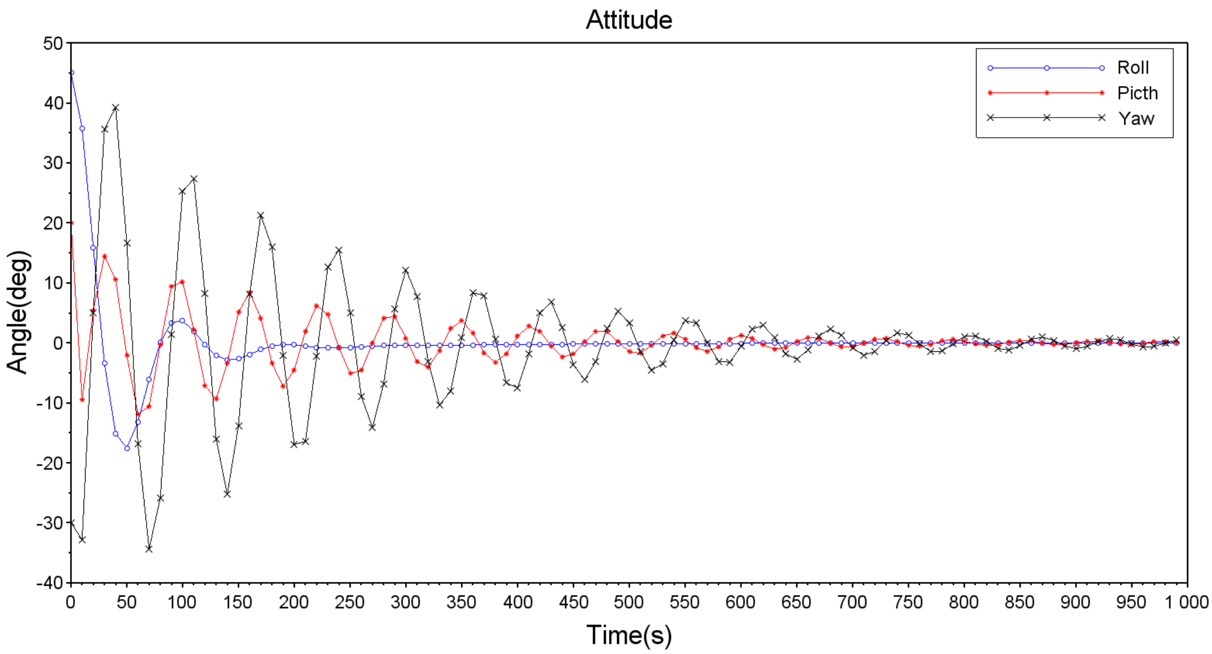

Figure 2 Attitude stabilisation for the feather configuration

Table 2 shows the results obtained for a pointing manoeuvre. The target angle was 15 degrees. The settling time and the overshoot are presented for different accommodation coefficients, which depend on the material used for the fins, the temperature and the roughness of the surface. The higher the accommodation coefficient the higher the settling time and the overshoot.

Table 2 Pointing manoeuvre time as a function of the accommodation coefficient.

Accommodation coefficient	Settling time (s)	Overshoot (%)
0	4281	32.73
0.2	5426	32.86
0.4	9022	33.01
0.6	22513	33.13
0.8	68319	36.06
0.95	-	-

The same analysis was carried out for the shuttlecock configuration. Figure 3 shows the results of the attitude stabilization for that geometry. In this case, drag is mainly used in the manoeuvres. The stabilization is faster than with the feather configuration. However, this configuration has lack of roll controllability. It would need the use of a reaction wheel or magnetorquers to have controllability in the roll axis. For instance, pitch and yaw axes had a settling time of 183 seconds (3.05 minutes) and 197 seconds (3.28 minutes), respectively: one order of magnitude less than with feather configuration: 10.11 minutes and 13.53 minutes respectively.

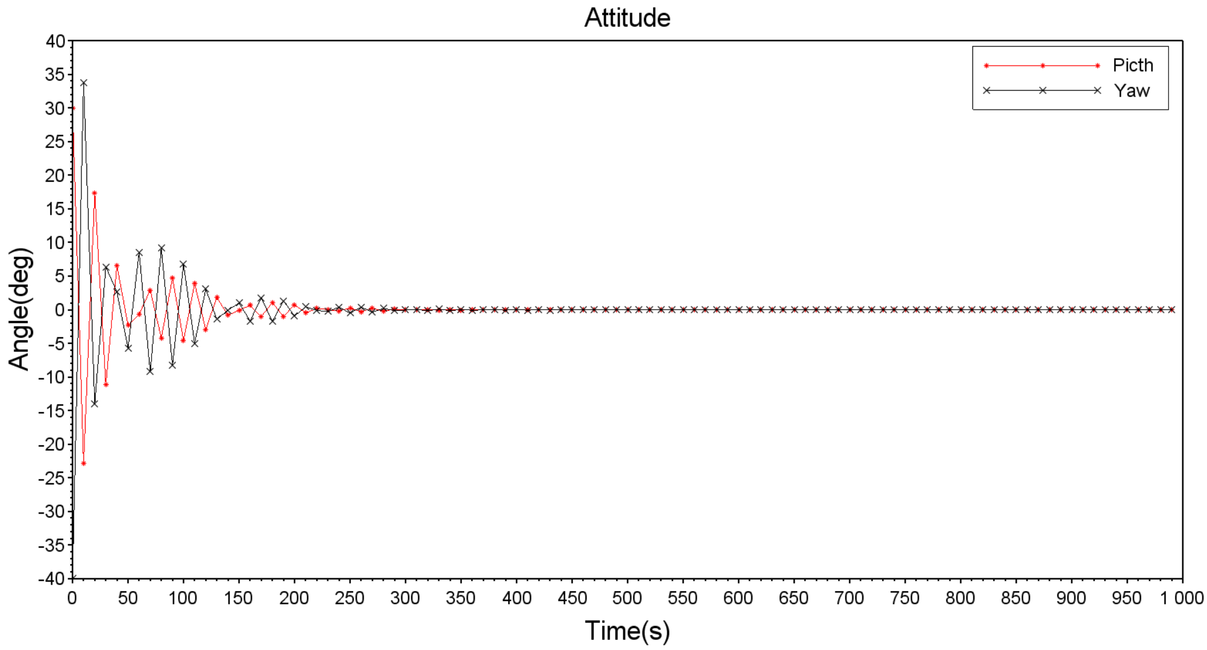

Figure 3 Attitude stabilization for the shuttlecock configuration.

Table 3 shows the comparison of the pointing manoeuvre for both configurations feather and shuttlecock with different pointing angles. The settling time was lower for the shuttlecock configuration but the overshoot was higher. In the case of the feather configuration the range of the pointing angles was lower than in the shuttlecock configuration. From a pointing angle of 18 degrees this configuration cannot reach a steady state using a PID controller for the fins.

Table 3 Comparison of pointing manoeuvre characteristics for the feather and shuttlecock configurations.

	Feather		Shuttlecock	
Pointing Angle	**Settling Time**	**Overshoot (%)**	**Settling Time**	**Overshoot (%)**
5	3523	37.8	253	79.3
10	3271	35.7	261	77.8
15	4116	29.5	272	73.7
20	-	-	279	69.1
25	-	-	312	62.1
30	-	-	433	51.5
35	-	-	673	42.1
40	-	-	-	-

These results show that it is possible to perform some manoeuvres in VLEO using only aerodynamic actuators. Both the shuttlecock and feather demonstrated good behaviour in passivation manoeuvres, but show limitations in terms of the settling time and the maximum range that can be reached in pointing manoeuvres. The shuttlecock also does not have a good control on the roll axis, which means that in most cases the spacecraft should need at least one reaction wheel to complement the aerodynamic fins for roll axis controllability.

In order to have higher performance and more complete control in pointing manoeuvres it is therefore necessary to have reaction wheels with control on all three axes. This is particularly noted for currently characterised and identified materials which have an accommodation coefficient close to 1 and therefore are unable to promote the production of life forces. In this case of combined aerodynamic and traditional control actuators, the capabilities of the aerodynamic fins would also enable a momentum management system to be set up to avoid saturation or singularity of the momentum exchange devices.

2.3.5. Satellite Formation Control using Aerodynamic Forces

The application of aerodynamic forces is not restricted to the control an individual satellite's attitude or orbit but can also be used to control the relative motion of several spacecraft flying in formation (see Section 2.3.2). The developments in this research field made within the scope of the DISCOVERER project have largely been published and will therefore be summarised in the following section.

Following the chronology of the respective publications, the summary is structured in three main blocks: i) Literature review and gap analysis ii) Robust control of the out-of-plane relative motion via aerodynamic lift and iii) Improvements to the feasibility range and manoeuvre success for a rendezvous using aerodynamic lift.

i) <u>Literature review and gap analysis</u>

In order to get a detailed overview of the current state of the art, an extensive literature review on lift and drag-based satellite formation control has been conducted.

The review revealed that in the field of differential drag, the state-of-the-art in terms of control theory is quite advanced. In particular, the rendezvous scenario has been dealt with in depth. However, the development of the respective hardware required to realize the proposed control strategies is still lacking. In particular, the frequently used bang–bang type control, which includes the assumption that the attitude is controlled by other means and that the drag magnitude can be changed discretely and instantly, is more of theoretical nature and not realisable as such. Therefore, the focus of future research efforts should be shifted from control theory development towards a transformation of the theoretical approaches into flyable hardware. Differential lift, on the other hand, was not considered an option until circa 2011 and the progress made since then has been very limited. Linearized models and constant density assumptions have been used to gain first insights and derive analytically created open-loop control sequences, from which several even caused collisions. Only very rarely have robust control methods and the dynamic nature of the atmosphere, uncertainties, or noise been considered at all.

Based on the gained insights, key gaps that need to be addressed to make the methodology applicable in a real-world scenario were revealed. These include the analysis of potential benefits resulting from using surface materials promoting specular reflection, the removal of the constant drag and lift coefficient assumption as well the development of robust guidance and control strategies able to cope with the dynamic nature of the available control force and the uncertainty it inevitably contains.

The results were published and presented as a conference paper [53] and later on in a further developed version as a peer-reviewed journal publication [54].

ii) <u>Robust control of the out-of-plane relative motion using lift</u>

In the following, effort was provided to address the gaps revealed in the literature review. In a first step, a robust control method to zero out the out-of-plane relative motion of two satellites during a rendezvous manoeuvre was developed. The proposed full manoeuvre sequence was shown to be successful in high-fidelity propagations, taking all major perturbations into account, and represents the first ever presented manoeuvre sequence which robustly zeros all translational degrees of freedom using aerodynamic forces.

In a second step, the developed simulation infrastructure was used to analyse possible benefits of advanced satellite surface materials with reduced levels of energy accommodations. The results showed that due to the higher available differential lift accelerations, the manoeuvre times as well as the orbital decay during the manoeuvre could be significantly reduced.

The results were published in peer-reviewed journal publication [43].

iii) Improvements to the feasibility range and manoeuvre success for a rendezvous using aerodynamic lift

In parallel, the effectiveness of two possible options to increase the feasibility range of using differential lift (proposed in [53,54]) were analysed in a Monte-Carlo approach by applying them to the analytic control algorithms introduced in literature. Moreover, additional modifications to the algorithms were made to reduce the manoeuvre time of one of the respective control phases. The results show that the analysed options noticeably improve the feasibility range as well as the success rates of the algorithms. Again, due to the significant increase of differential lift acceleration for reduced levels of energy accommodation, the feasibility range of the lift-based control algorithms is enlarged considerably. In addition, the implemented modifications are shown to consistently reduce the manoeuvre time of the respective control phase.

The presented analysis improves the current state of the art of the analytically designed rendezvous trajectories and provides valuable new insights into the methodology of using differential aerodynamic forces as a means of relative motion control.

The results were published and presented as a conference paper [55].

2.4. Applicable Control Methods

i) Proportional-Integral-Derivative (PID) Control

In the last few decades, control theory has made significant progress in the development of new and sophisticated control techniques able to cope with uncertainties in the system modelled. However, improvement in performance is generally accompanied by increased complexity in the controller principles and implementation. As a result of this, industrial operations typically prefer traditional types of controller, among which PID is by far the most popular. The simple principles on which the PID is built, the ease of implementation, the good performance achievable through a proper tuning, and its widespread commercial availability are the principle reasons for its success.

The PID control loop uses the computed error at the current time $e(t)$ between a desired state and the current measured state and attempts to correct it through the application of a control input computed as a function of a proportional, integral and derivative actions.

$$u(t) = K_p e(t) + K_i \int_0^t e(\tau) d\tau + K_d \frac{de(t)}{dt}$$

In the most general case, the proportional term has an impact on the speed and the oscillatory nature of the response by means of the overshoot value and the rise time. The integral term represents the accumulation of the error over time and its presence is useful if a null steady state error is to be achieved with the system being subjected to constant external disturbances. The derivative term works on the rate of change of the error, thus providing some information on the future evolution of the error. Its variation mainly affects the overshoot value and the settling time introducing damping into the system.

Tuning of the respective proportional, derivative and integral gains (K_p, K_d, and K_i) is crucial, since a bad selection may cause the system to be unstable or too oscillatory in response. Other performance objectives associated with tuning also clash with each other (eg. speed of response and small steady-state error).

Despite its simplicity, traditional PID controllers are not robust enough against uncertainties in the model plant (mainly the inertia matrix and external disturbances). Further enhancement of the controller performance can be achieved through the integration of robust, adaptive and fuzzy techniques.

ii) Robust Control

Robust Control deals with designing a control system able to cope with the uncertainties that characterise both the actual system dynamics and the environment in which the controller is meant to operate. The design of the controller relies on a process model that, even when accurate, represents just an approximated description of the actual dynamics. A controller is thus said to be robust when it is able to provide a consistent performance level against model uncertainties (un-modelled/unknown dynamics, environmental disturbances, sensor noise, or unpredicted changes in the plant). This means that the controller needs to be designed to have low sensitivity to uncertainties, so that the impact of these is minimised. Some advanced techniques are proposed in the frame of robust control theory. However classic controllers can show robust behaviour if this requirement is considered during the design process.

iii) Adaptive Control

Adaptive Controllers are designed to adjust in real time to deal with any uncertainties in the modelled system dynamics. According to this, the performance remains substantially unvaried over the time required to perform the control action. This characteristic makes adaptive controllers especially suitable when:

1. The controller needs to cope with unknown or un-modelled system dynamics and uncertainties;
2. The controller is required to provide different performance profiles as time changes;
3. The controller needs to cope with deterioration in the system plant with time.

The general learning structure of adaptive controllers consists of (i) a component providing an estimation of the dynamics of the process and (ii) a modification algorithm that varies the controller features according to (iii) a decision-making function.

Adaptive controllers are generally categorised as direct or indirect methods, depending on whether the process estimation is directly or indirectly used to adjust the controller parameters. Measurement of the plant dynamics is a difficult task to perform and the advanced nature of these controllers demands a certain level of experience in control engineering to be implemented successfully. The employment of adaptive controllers in industrial processes is therefore limited and generally restricted to applications for which the increased complexity in the controller structure is justified by the stringent requirements imposed on the system.

iv) Optimal Control

Optimal control theory is based on the mathematical framework of variational calculus. Given a set of initial conditions, a controllable system evolution (trajectory) depends on the control input provided. The aim of optimal control to identify amongst all the possible trajectories capable of driving the system from an initial to a final state, those that minimise a certain cost function, under some constraints regarding both time (fixed finite time or free) and the physics of the system. Optimal control theory-based controllers have achieved widespread success in space applications because of the benefits which can be provided. For example, optimal satellite attitude\orbit control can be achieved minimising the amount of fuel required to perform the manoeuvre and thus maximise the payload.

v) Linear Quadratic Regulator (LQR)

A LQR is a linear feedback controller derived in the more generic frame of optimal control theory. The controller is designed to provide the optimal set of gains (K) that minimise a performance index described by a quadratic cost function. The optimal solution is found applying the maximum principle and solving a two-points boundary value problem or the Riccati ODE Equation. The LQR achieved success and diffuse implementation due to its intrinsic stability and robustness characteristics in the presence of disturbances (large gain and phase margin). However, for the LQR to be applied, the system needs to be described by a set of linear or linearised differential equations. When the controller is implemented on the real nonlinear satellite dynamics, robustness performance is expected to be inferior.

vi) Model Predictive Control (MPC)

MPC are a set of advanced optimal controllers which rely on the accuracy of a process model to predict the future evolution of the controlled variables (output). The controller is able to cope with Multiple Input, Multiple Output (MIMO) systems subjected to inequality constraints in both input and output. The difference between the measured and the predicted controlled variables is provided in input to a prediction block in a feedback loop. The input variables are altered according to an optimisation algorithm that, at each sample time, provides the control action to be applied to move the predicted outputs towards a reference value. The optimal online algorithm can be implemented in a linear or in a quadratic formulation, according to the form of the optimisation cost function. In its quadratic formulation MPC is similar to the more traditional Linear Quadratic Regulator (LQR), even though for the former a new solution is computed at each time step. MPC performance is sensitive to the accuracy of the process model: model inaccuracies can lead to controller deterioration making their performance inferior to that of traditional controllers.

2.4.1. Controller Selection

Selecting the most appropriate control strategy for the implementation of the aerodynamic attitude control in VLEO is a challenging task. The number of uncertainties affecting the problem, the little knowledge of the phenomena that drives density fluctuations in the thermosphere, and the inability to model with accuracy some of the disturbances affecting the satellite dynamics demands robustness or adaptive characteristics of the controller.

Table 4 Comparison of different control techniques.

CONTROL TECHNIQUE	ADVANTAGES	DISADVANTAGES
Proportional-Integrative-Derivative (PID)	- Preferred control strategy in industrial processes; - Simple implementation; - Wide commercial availability; - Good results achievable with limited experience.	- Potential lack of robustness against external disturbances and uncertainties in the inertia matrix.
Robust Control	- Constant performance level in presence of uncertainties; - Low sensitivity; - Traditional controllers can be designed to be robust.	More advanced techniques may require: - Complex implementation; - May not be suitable for the specifications of the platform.
Adaptive Control	- Real time adjustment; - Varying performance profiles achievable; - Strong reliability in presence of uncertainties or hardware deterioration.	- Difficult to implement; - Experienced required; - Increased complexity; - Bad performances if poorly implemented.
Optimal Control (LQR)	- Stability and robustness in presence of uncertainties. - Relatively easy to implement.	- Inferior performances to be expected when implemented on non-linear plants.
Optimal Control (MPC)	- Indicated for MIMO systems with inequality constraints; - Stability and robustness in presence of uncertainties.	- More complex implementation; - Performances sensitive to the level of accuracy in the process model.

Advanced adaptive or model predictive controllers are well suited for this task. However, considerable experience is required to achieve the successful implementation of these controllers for the system. Furthermore, their increased level of complexity may not be supported by the limitation of the platform.

Traditional PID controllers are easier to implement due to the straightforwardness of their formulation, such that even non-expert users can achieve good results. Their inherent simplicity also makes them more suitable when the platform requirements and specification pose some limits on the controller implementation. A classical PID can be modified to have a robust behaviour against uncertainties, thus making them applicable for aerodynamic attitude control tasks in VLEO.

Optimal LQR controllers have been shown to grant robust, even if slightly deteriorated, performance when the control law is implemented on real non-linear satellite dynamics [56,57]. Compared to PIDs, the gain matrices of the LQR can be selected by following certain criteria for the control actuation and state space vector. A desired performance for a given application can therefore be achieved more easily.

According to this analysis of the described controllers, summarised in Table 4, a combined approach using PID and LQR controllers were selected for this study to provide proof of concept and feasibility of the different aerodynamic control manoeuvres. The implementation of these controllers is provided in detail in Section 2.5.3.

2.5. Aerodynamic Control Applied to Platform Concepts

Representative mission concepts with different attitude and orbit control requirements were previously identified in the *DISCOVERER Deliverable 2.1 VLEO Aerodynamics Requirements Document* [RD-1]:

– Optical Coverage

High resolution optical imaging capability with a wide swath and large coverage area. Pointing accuracy and agility requirements are relatively low. These platforms are typically used in a nadir pointing mode with some small angle off-axis viewing capability.

– Optical Very-High Resolution (VHR)

Very-high resolution optical imaging combined with higher requirements on pointing accuracy, slewing and agility performance, and imaging stability.

– Synthetic Aperture Radar (SAR)

Imaging using SAR requires a side-looking radar antenna which is able to achieve a higher resolution image than a standard radar instrument. Pointing accuracy requirements can be high, but agility is generally more relaxed.

2.5.1. Platform Concepts

Application of the different aerodynamic attitude control manoeuvres described previously is dependent on the platform design and control performance that can be realised.

Within the wider DISCOVERER project, activities in WP5 (System Design and Long-Term Business Opportunities) and the *DISCOVERER 3rd General Assembly Brainstorming Session #1* have focused on the formation and development of concepts for VLEO platforms. A set of notional platform concepts, marrying the above mission concepts with a notional platform design have been formalised in order to explore and demonstrate the feasibility of aerodynamic attitude and orbit control manoeuvres.

These concepts are not intended to be a comprehensive set of possible platform designs and do not at present consider aspects such as the integration of atmosphere-breathing electric propulsion (ABEP) or steerable optics which may have significant impact on pointing, agility, and stability requirements.

A more thorough exploration of these design concepts including consideration of novel propulsion systems and different payload types will be provided in the DISCOVERER D5.4 report.

i) <u>Fixed Aerostable</u>

A simple aerostable platform is well-suited to optical coverage and SAR missions for which only modest roll-axis manoeuvres are expected to be necessary for repointing and off-nadir imaging.

For an elongated satellite (in the longitudinal axis), a carefully designed or selected centre-of-mass can produce aerodynamically stabilising torques. Aerodynamic surfaces behind the centre of mass can be used to further promote the platform stability. Steerable aerodynamic control surfaces (fins or feathers) can be used to provide reaction wheel desaturation torques and some roll manoeuvring capability. Examples of fixed aerostable configurations include the Cosmos “space arrows” [28], the “stove pipe“ PAMS configuration [29], the QbX space darts satellites [24] and GOCE [30], with its tail fins designed to provide passive stabilisation.

ii) <u>Aerostable with Control</u>

For higher-resolution imaging and SAR applications, increased satellite pointing capability is required. Whilst aerostability may generally be a desired quality, an aerodynamically-stiff platform may also compromise the agility of the platform. A controllable centre-of-mass of the spacecraft may enable more versatile operations by providing control over the platform stability characteristics.

Aerodynamic control surfaces can assist out-of-flow pointing and provide aerodynamic trim to avoid rapid saturation of attitude control actuators. Using a suitable combination of control surfaces, aerodynamic torques can be provided in 3-axes. The aerodynamic control surfaces can also assist in reaction wheel desaturation. Active aerodynamic attitude control is yet to be demonstrated on orbit. Possible geometries that could be implemented for this purpose are the feathered configurations of SOAR (Figure 7, top right) [58] and ΔDSat [59]. CubaSats geometries for aerodynamic attitude control were also proposed by Auret [25] for aerodynamic roll control and Gargasz [31].

iii) Neutrally Stable

A neutrally-stable spacecraft can offer high agility and slewing performance which may be desirable for some very-high resolution optical applications. Aerodynamic control surfaces can be incorporated to assist manoeuvring and provide attitude actuator desaturation capabilities. However, the platform must also be robust against sources of disturbance to ensure that the control performance is not detrimentally affected.

One such concept is a disc-shaped satellite which can provide neutral stability and remains area-invariant with respect to the flow during pitching and rolling manoeuvres. This avoids the generation of unwanted disturbing torques due to variation in the oncoming flow. Aerodynamic control surfaces, in the form of panels extending from the sides, can be utilised to provide control torques or trim as required. An example of such a configuration is the disc satellite discussed later on in this work and shown at the bottom of Figure 7.

2.5.2. Control Surface Mechanisms

Whilst the platform concepts presented previously in Section 2.5.1 are notional, some attention should be paid to the mechanisms by which the proposed control surfaces can be actuated to achieve the desired aerodynamic control.

For the current concepts, two principal methods of surface-body attachment and actuation have been proposed: hinged and rotating. For hinged control surfaces, linear actuators with linkages and motors are the most common mechanisms. Correspondingly, for rotating control surfaces, motors and geared-systems typically provide the required motion. In both cases, examples of mechanisms matching these descriptions have been demonstrated in-orbit, typically for motion of solar arrays.

In practice, these mechanisms will need to be designed to provide reliable performance throughout the mission. The actuation capability provided by these mechanisms may also result in constraints or limitations on the fidelity and precision of control which can be achieved, for example the accuracy and rate at which the aerodynamic control surfaces can be moved between desired positions.

With future research and technology development more exotic control surfaces can also be conceptualised. For example, if the GSI characteristics of a surface can be actively modulated, control authority could be provided without additional deployable or moving surfaces. Possible mechanisms for this include louvers (either mechanical or MEMS) with varying GSI character, or novel materials that can change their surface properties for example through the application of an electric current.

2.5.3. Controller Development

i) Modified PID

A quaternion feedback PID controller with constant gains was selected for the implementation of combined aerodynamic and reaction wheel attitude control techniques. The PID form of the controller was preferred to the simple PD form to support the system stabilisation in presence of external disturbances. However, if the integral term helps to reduce the steady-state error, the build-up of the integral action over time may lead to the saturation of the reaction wheels on board. The actuator saturation problem is usually handled by implementing an anti-windup logic to modify the control signal to avoid saturation. An alternative approach using an intelligent integrator can be used to directly modify the magnitude of the integral action when the system error feedback is not within a certain range. The second approach was selected for the current implementation, and the traditional PID controller was modified to include the intelligent integrator logic proposed in [60] as a variation of the Wie et al. [61] quaternion feedback regulator:

$$\boldsymbol{u} = \gamma\boldsymbol{\omega} \times \boldsymbol{H} - K_p\boldsymbol{q}_e - K_D\boldsymbol{\omega} - K_i\boldsymbol{\xi}$$

Where ω is the body angular velocity vector, H is the total angular momentum, q_e is the quaternion error, and ξ is the integral error signal manipulated by the intelligent controller. The tuning of the three control law gain matrices (K_p, K_d, K_i) was achieved using a LQR. The penalty matrices for the state variables (Q) and the control signal (R) were selected based on a trade-off between the speed of response and the control effort imposed on the actuators.

If tuned for a particular instance, general PID performance may deteriorate in the presence of uncertainties in the plant model description. The robustness of the modified continuous-time controller was tested against uncertainties in the satellite inertia matrix (Table 5) and its performance was compared against those of a traditional PID controller. PID controllers implemented with appropriately tuned gains provide excellent performance when applied to the plant of the system they were designed for. However, if any uncertainties or un-modelled dynamics affect the plant, the performance may deteriorate considerably.

Nominal Case	$\boldsymbol{I} = \begin{bmatrix} \mathbf{0.0575} & \mathbf{0} & \mathbf{0} \\ \mathbf{0} & \mathbf{0.0725} & \mathbf{0} \\ \mathbf{0} & \mathbf{0} & \mathbf{0.0725} \end{bmatrix} \boldsymbol{kg \cdot m^2}$
Case A	$I = \begin{bmatrix} 0.1075 & 0 & 0.0003 \\ 0 & 0.1066 & 0 \\ 0.0003 & 0 & 0.1166 \end{bmatrix} kg \cdot m^2$
Case B	$I = \begin{bmatrix} 0.1275 & 0.0001 & 0.003 \\ 0.0001 & 0.1266 & 0 \\ 0.0030 & 0 & 0.1866 \end{bmatrix} kg \cdot m^2$
Case C	$I = \begin{bmatrix} 0.0075 & 0.0001 & 0.003 \\ 0.0001 & 0.0666 & 0 \\ 0.003 & 0 & 0.0066 \end{bmatrix} kg \cdot m^2$
Initial Orbit Parameters	$h = 250\ km;\ i = 70°;\ e = 0;\ \Omega = 0°;\ \nu = 0°$

Table 5: Initial orbit parameters and spacecraft inertia matrix values used to test the modified PID [60] *control law robustness against uncertainties.*

For all the cases described in Table 5, the feathered geometry of SOAR was taken as reference and atmospheric co-rotation, thermospheric winds, gravity gradient, solar radiation pressure and aerodynamic torques were included in the simulation. SOAR is an aerostable configuration satellite, which has four fins that extend from the rear of the 3U CubeSat main body. Further information on the SOAR satellite and mission is provided later in Section 0.

To test the robustness of the controller, the reaction wheels were used as the only actuators and the aerodynamic surfaces were kept in their nominal configuration (0° deflection angle). The test is thus performed for an aerostable configuration as an illustrative case. A more challenging LVLH, rather than inertial-pointing, attitude was assumed for the satellite. Figure 4 shows the rotation described by the body reference frame with regards to the orbital LVLH reference frame from an initial offset of $20°, -20°, 20°$ in roll, pitch and yaw respectively. The controller, designed for the nominal inertia matrix value, shows a robust response to inertia matrix uncertainties. The simulations of cases A and

C show very similar time response to the nominal case. In the more challenging scenario described by case B, the performance is slightly degraded and the response shows more oscillatory behaviour in roll, pitch and yaw. However, stability is still granted.

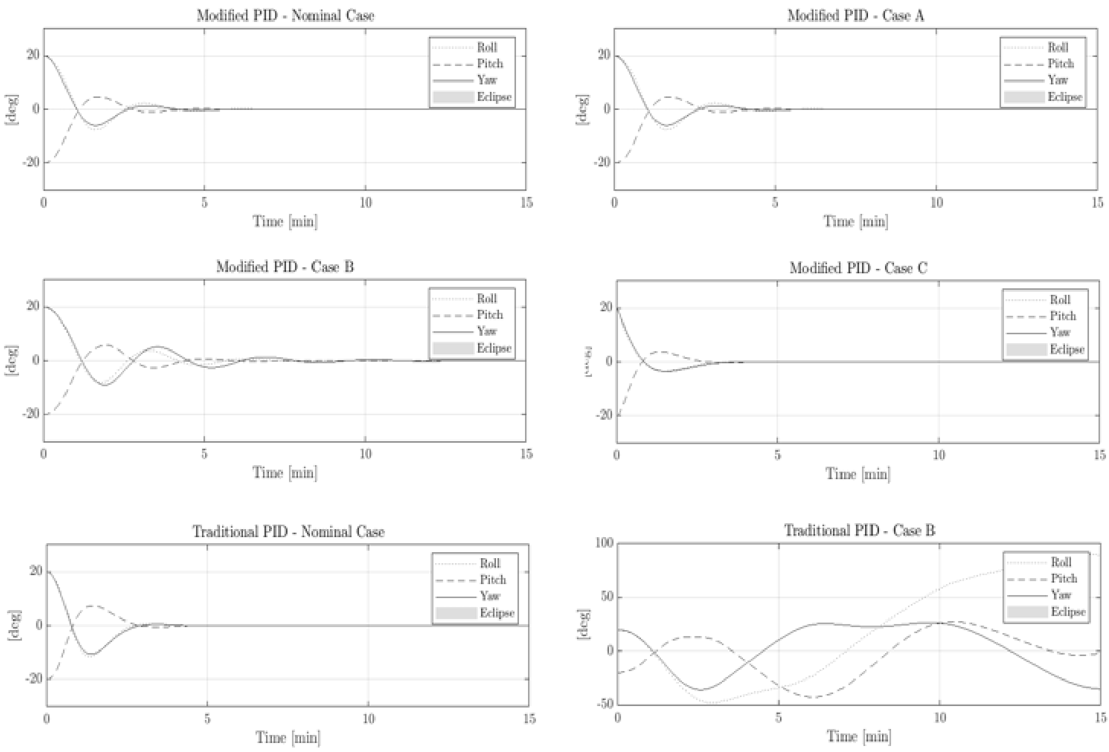

Figure 4: Modified and traditional PID continuous time control law performance. Results refer to the implementation of an attitude control manoeuvre performed by the reaction wheels. The figure shows the time histories of Euler angles about the LVLH orbital reference frame for the inertia uncertainties scenarios identified in the current section.

For comparison, the traditional PID controller implemented with the same gain matrices shows a comparable performance in the nominal case (Figure 4, bottom left) but seems to be unable to perform the attitude control task in the scenario described by Case B due to reaction wheel saturation (Figure 4, bottom right).

The controller implemented for the reaction wheel momentum management task is an optimal infinite-horizon LQR. The linear feedback control law in the continuous time derivation has the form:

$$\boldsymbol{u} = -K\boldsymbol{x}$$

Where x is the vector of state space variables and K is the constant gain matrix according to which the control law minimise the following cost function:

$$J = \int_0^\infty (\boldsymbol{x}^T Q\boldsymbol{x} + \boldsymbol{u}^T R\boldsymbol{u})dt$$

Where $Q \geq 0$ and $R \geq 0$ are symmetric positive semidefinite matrices defining the weights for the state variables ($\boldsymbol{x}$) and the control action ($\boldsymbol{u}$). Due to the limited control authority provided by the aerodynamic surfaces, desaturation using these actuators might be unsuitable when high constraints are imposed on the unloading controller by the mission requirements. In this scenario, the attitude control task (reaction wheels) and the momentum management task (aerodynamic surfaces) can be performed simultaneously. The purpose of the aerodynamic momentum management controller is to keep the reaction wheels within the saturation limits without hindering the attitude control loop (modified PID) excessively. To achieve this, the gains of the LQR were selected so that a large separation exists between the two loops in terms of time responses.

For the implementation of the aerodynamic control manoeuvres, the design of the algorithm that selects the optimal configuration of the control surfaces for a given angle of attack and sideslip is crucial. The logic behind the controllers is shown as simplified flowcharts for the Attitude Control Loop (Modified PID) and the Momentum Management Control Loop (LQR) in Figure 5 and Figure 6 respectively.

ii) Optimal Control Surface Deflection

Determination of the aerodynamic coefficients relies on the adaption of ADBSat, a tool that implements a panel method for aerodynamic coefficient estimation, for control purposes. The geometry of the satellite is firstly imported as a 3D triangular mesh. An algorithm successively reads the surface mesh and identifies the geometric elements (i.e. faces and vertices) belonging to the control surfaces and those belonging to the satellite main body. For each control surface, a range of angles of deflection is defined and the possible permutations associated with multiple independent surfaces are defined. The choice of angular step size is important as the computational effort can increase significantly for a large number of permutations of multiple control surfaces. Dimensional aerodynamic coefficients, more suited than the non-dimensional ones for control and propagation purposes, are then computed for the main body and the control surfaces separately through the determination of the normal and the shear stress coefficients. The normal and the tangential unit vectors on each element of the surface mesh depends on the surface geometry (normal unit vector) and the direction of the incoming flow (tangential unit vector). According to this, the current angle of attack and angle of sideslip are estimated at each sampling time from the attitude with regards to the flow direction. In the case of the control surfaces, the direction of the normal unit vector also relies on the angle of deflection of the surface. The routine reads each line of the matrix containing the different combination of the control surface deflections and applies the required rotation matrices to the elements of the 3D surface mesh that belong to the corresponding control surface. The overall aerodynamic torques induced on the satellite for the current angle of attack and sideslip are computed summing the contribution coming from the body to that coming from each permutation of the control surfaces. Whilst no control action can be imposed on the body, it can be usefully employed to determine the optimal panel configuration for the current attitude with regards to the flow.

The best match with the desired control torques provided by the attitude/momentum management controller is found computing the minimum Euclidean distance between the desired control torques and the dimensional momentum coefficients multiplied for the value of the dynamic pressure at the current altitude. If multiple configurations have the minimum Euclidian distance to the desired values, the option that induces less aerodynamic drag is selected such that the mission lifetime is least compromised.

This algorithm is a first attempt to study the feasibility of 3-axes aerodynamic control manoeuvre that of course demand some improvements. To find a model capable of describing an aerodynamic surface varying with a high number of independent variables is a very challenging task in the implementation of aerodynamic control manoeuvres. This is especially true if no limitation is imposed on the possible values that can be selected for the angle of deflection of the panels in the possible range of selection. In this case, describing the aerodynamic output by simple linear fits may introduce some error on the expected aerodynamic torques induced by a certain configuration in output. At the same time, limiting the panel configuration has an impact on the achievable control authority and thus the feasibility of the manoeuvres.

Further developments will focus on making this algorithm more realistically implementable on SOAR for on-orbit demonstration. Currently, the algorithm implementation is sufficient to *mathematically* demonstrate the feasibility of the different manoeuvres. However, some improvements are needed to meet the physical constraints of a real platform. Possible improvements include (i) the translation of the algorithm from a numerical to a symbolic Jacobian derivative based approach, (ii) introducing further penalization on the aerodynamic control actuation and (iii) adding saturation avoidance logic on the aerodynamic control panels. Further discussion of these improvements is provided in Section 2.6, after discussing the simulation results.

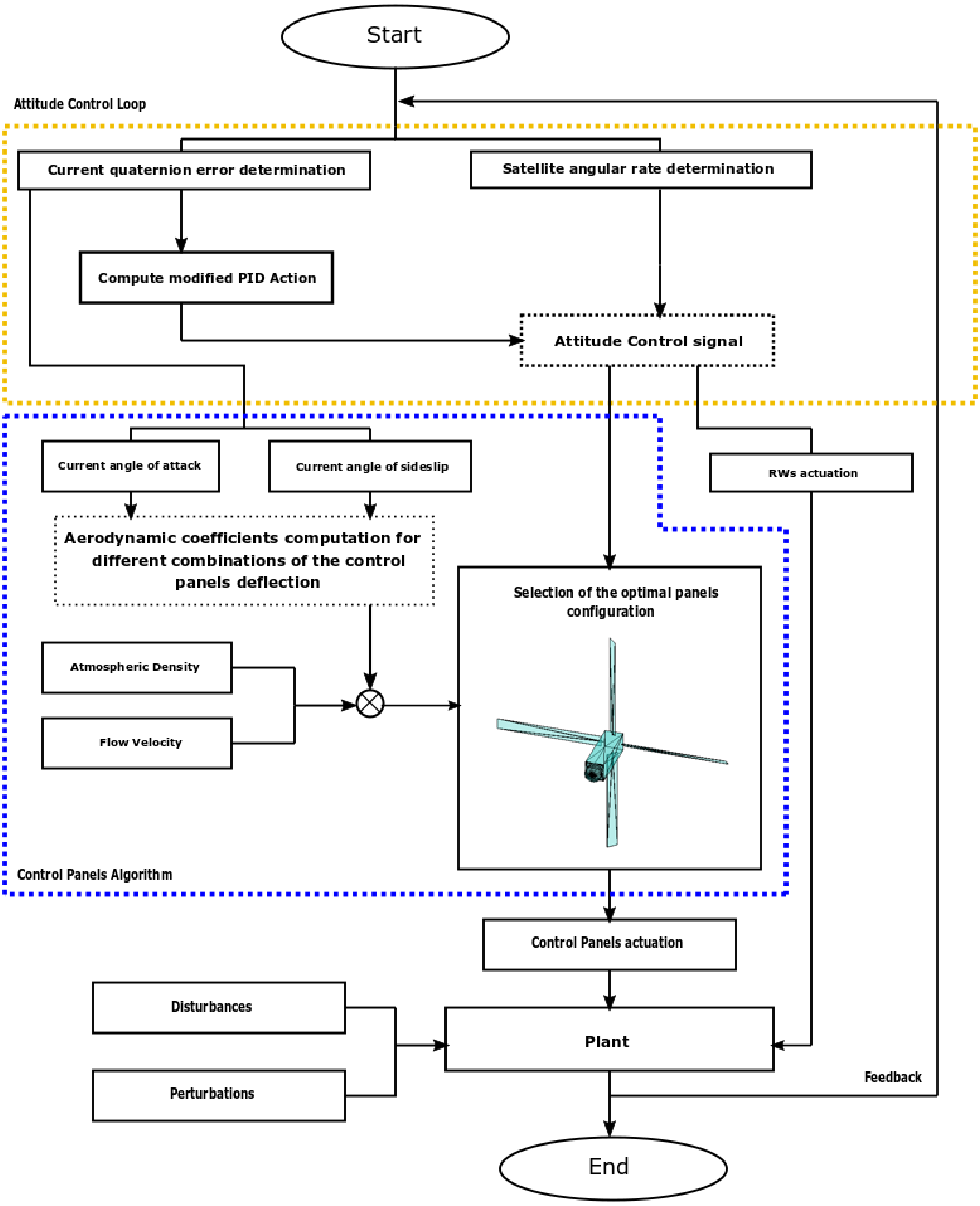

Figure 5: Block diagram describing the interaction between the attitude control loop (modified PID) and the algorithm that selects, for a given attitude, the optimal panel configuration to provide the desired control torque.

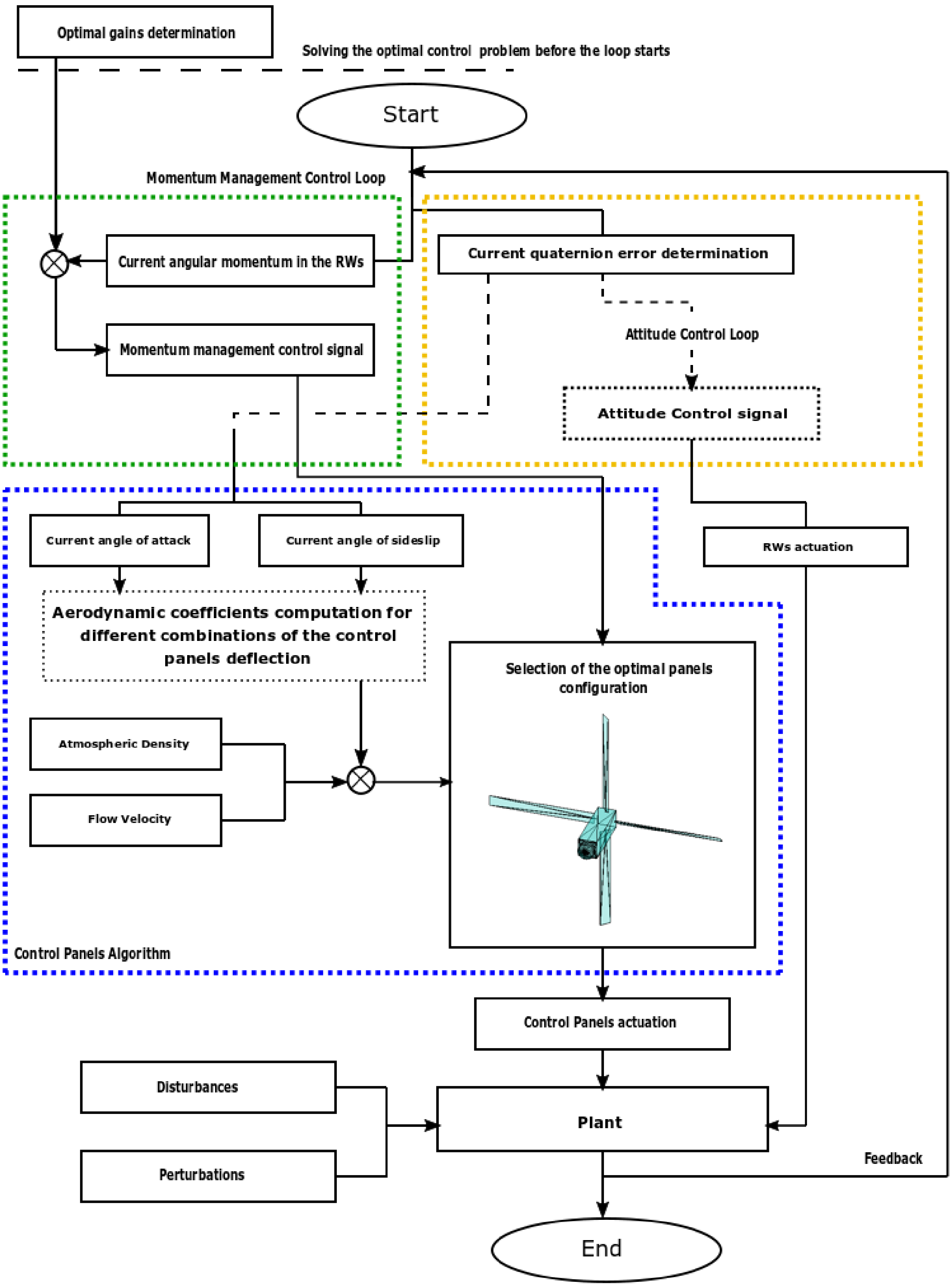

Figure 6: Block diagram describing the interaction between the momentum management control loop (LQR) and the algorithm that selects, for a given attitude, the optimal panel configuration to provide the desired control torque. For the momentum management task, the attitude control loop interacts exclusively with the reaction wheels.

2.5.4. Performance of Aerodynamic Control Manoeuvres

The feasibility of the aerodynamic control manoeuvres described in the previous sections was investigated for the three representative geometries illustrated in Figure 7 in their nominal configurations, two aerostable and one neutrally stable.

The fin or feathered configuration (Figure 7, top left) that will be used by the 3U CubeSat SOAR features four aerodynamic panels that can rotate independently thus providing control torques in roll, pitch and yaw simultaneously. Aerodynamic control in roll can be generated by inducing opposite lift forces on opposed fins (fins counter-rotated at the same angle). Similarly, aerodynamic torques in pitch and yaw can be induced by panel co-rotation or by introducing asymmetry in the body configuration with regards to the incoming flow. Optimal control authority in 3-axis can be achieved through a proper selection of the configuration of the four independent panels. In this study the panels have been each given a length of 0.58 m and width of 0.065 mm, providing an area of 0.037 m^2 each.

The shuttlecock geometry (Figure 7, top right) is also a nominally aerostable configuration characterised by four panels creating an aerodynamic stabilising skirt extending from the rear of the satellite main body. To enable control, this configuration allows the four rear panels to hinge about their attachment, thus varying the surface exposed to the incoming flow and consequently the aerodynamic torques induced about the CoM. Because of the configuration of the surfaces, control authority in the roll axis is expected to be inferior to that of feathered configurations. The geometry used herein is consistent with that of the 3U CubeSat concept of Rawashdeh and Lumpp [26] which features panels with length of 300 mm and width 100 mm, providing an area of 0.03 m^2 each.

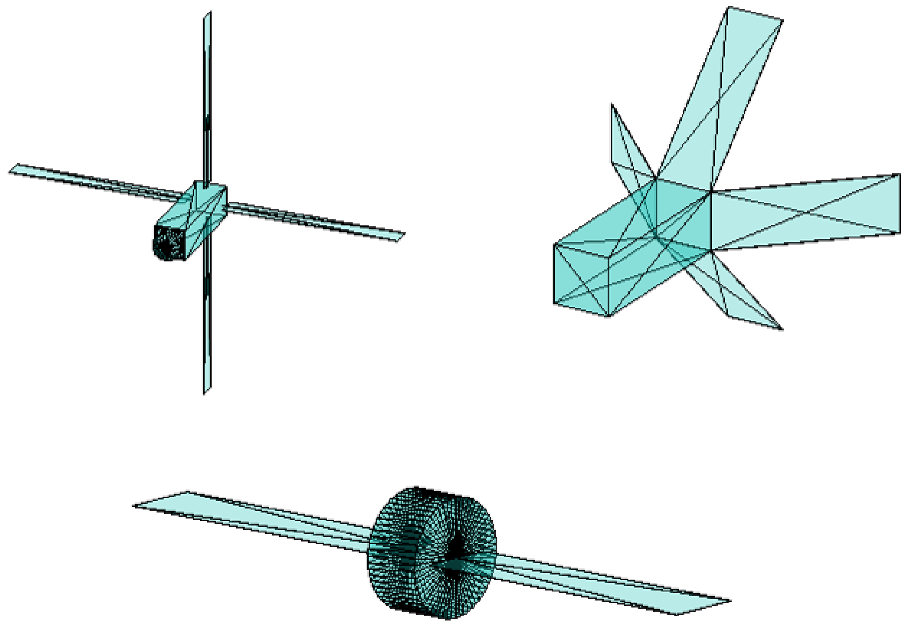

Figure 7: Satellite geometries employed to test the feasibility of the aerodynamic attitude control manoeuvre: feathered (top left); shuttlecock (top right) neutrally-stable disc satellite (bottom).

The disc satellite geometry (Figure 7, bottom) is a novel configuration given by an extension of the geometric concept proposed in [RD-1]. Two opposing control panels extend from a cylindrical main body which is oriented with the curved surface pointing into the incoming flow direction. Similar to the feathered configuration, varying the relative angle of the panels allows aerodynamic torques in the roll and yaw axes to be produced. Because the panels are not offset with respect to the CoM in the longitudinal axis, control authority in pitch is expected to be null. The configuration is neutrally stable in its nominal configuration: the rotation of the lateral panels endows the satellite with aerodynamic controllability in roll and yaw. Aerodynamic control in pitch could be achieved creating an offset between the location of the centre of pressure of the panels and the centre of mass. In the study, a cylindrical diameter of 0.30 m is used, and panels of length 0.8 m and width 0.2 m are specified, providing an area of 0.16 m^2 each.

In the following sections, the feasibility of some attitude control manoeuvres will be investigated for these three geometries. Further results referring to the intended mission implementation of SOAR (the feathered geometry) will also be discussed separately in Section 0. The selected manoeuvres, in particular, comprise aerodynamic attitude control, aerodynamic trim and aerodynamic momentum management of the angular momentum stored in the reaction wheels. The hardware specifications assumed for the reaction wheels to perform simulations are summarised in Table 6.

Configuration	4 reaction wheels in a tetrahedral configuration
Spin axis moment of inertia	$654.5\text{x}10^{-9}$ [kgm^2]
Maximum angular momentum storage	$1.2\text{x}10^{-3}$ [Nms]
Maximum Torque	$23\text{x}10^{-6}$ [Nm]
Resolution	$7.2*10^{-8}$ [Nm]

Table 6: Definition of the hardware performance for the reaction wheels configuration.

To resemble the environmental conditions that will characterise the SOAR mission, simulations are run assuming low solar activity, thus partially reducing the uncertainties related to fluctuations in the thermosphere density [62]. Disturbances to the plant include solar radiation pressure (SRP), gravity gradient and undesired aerodynamic torques.

Aerodynamic coefficients are computed using Sentman's model [63] to represent the aerodynamic performance of materials at the current state of the art. The thermal accommodation coefficient α, on which the aerodynamic coefficient estimation relies on, is assumed to vary according to the atomic oxygen concentration/altitude in the range of approximately 0.9 to 1 [64].

To optimally achieve the attitude and momentum management control tasks, the control surface configuration at any time is selected by considering all the control surfaces independently. No limit is therefore imposed on the relative orientation of opposing sets panels (in terms of synchronised co/counter-rotation).

Movement of the control surfaces is also limited to a minimum interval of 2s interval between changes. This value was selected in the attempt to provide a conservative estimation of the rate of angular rotation of the panels for SOAR: it is thus deriving from some assumptions regarding the setting time of the panels and the time required to perform a ±90° degrees rotation from the nominal minimum drag configuration.

Control surface shadowing from the incoming flow is also neglected as the error introduced is expected to be small compared to other sources of uncertainties (eg. environment, reference area, aerodynamic coefficients estimation, atmospheric density model accuracy). Uncertainties on the expected induced aerodynamic control torques are also added to test the robustness of the controller. To reproduce a digital implementation of the controllers described in Section 2.5.3, control laws are implemented in the discrete-time domain, assuming a sampling frequency of 1Hz.

In the following sections, a variety of the previously described aerodynamic control manoeuvres are investigated for each platform concept:

- A Shuttlecock Configuration
  - A1 Aerodynamic pointing and trim:
    - A1.1 Aerodynamic pitch and yaw control combined with reaction wheel roll control;
  - A2 Aerodynamic momentum management:
    - A2.1 Aerodynamic momentum management of reaction wheels for a satellite assumed to have a constant offset with regards to the LVLH reference frame.
- B Disc Satellite Configuration
  - B1 Aerodynamic pointing and trim:
    - B1.1 Aerodynamic roll combined with reaction wheel pitch and yaw control;
    - B1.2 Aerodynamic pitch & yaw combined with reaction wheel roll control;
    - B1.3 Aerodynamic roll & yaw control combined with reaction wheel pitch control.
- C Feathered (SOAR) Configuration
  - C1 Pointing and trim:
    - C1.1 Aerodynamic roll control combined with reaction wheel pitch and yaw control;
    - C1.2 Aerodynamic pitch & yaw control combined with reaction wheel roll control;
  - C2 Momentum management:
    - C2.1 Reaction wheel attitude control manoeuvre performed in parallel with the aerodynamic momentum management task.

A Shuttlecock Configuration

A1.1 Aerodynamic Pitch & Yaw Control + Reaction Wheel Roll Control

In the current section aerodynamic control about the pitch and yaw axes are investigated for the Shuttlecock geometry. Conventional actuators (reaction wheels) are employed to exclusively control the satellite attitude in roll. Initial conditions provided in input for the simulation include:

Initial orbit parameters	$alt = 280\ km,\ i = 50°,\ e = 0,\ \Omega = 0°, \nu = 0°$
Initial attitude (RPY in LVLH)	$\varphi_0 = 5°,\ \vartheta_0 = -10°,\ \psi_0 = 7°$
Initial body rates (in LVLH) [°/s]	$\omega_{BO,i} = [0,0,0]$
Desired final attitude (RPY in LVLH)	$\varphi_f = 0°,\ \vartheta_f = 0°,\ \psi_f = 0°$
Desired final body rates (in LVLH) [°/s]	$\omega_{BO,f} = [0,0,0]$

Table 7: Initial and final parameters for aerodynamic pitch and yaw control + reaction wheel roll control for the shuttlecock configuration.

Figure 8 shows the evolution of the satellite attitude about the LVLH orbital reference frame. The controller is able to correct the initial attitude offset and restore the desired LVLH pointing configuration. As can be seen in the middle portion of Figure 8, the reaction wheels do not provide any control torques about the pitch and yaw axes, indicating that the control task is effectively achieved through the only generation of the aerodynamic control torques.

The plot of the body rates in Figure 8 shows how the initial body rates evolve till the desired null angular velocity is achieved in roll, pitch and yaw. The satellite inertial angular velocity of the body frame (ω_{BI}) consists of the sum of two components: the first one is the satellite body rate with regards to the orbital reference frame (ω_{BO}) and the second is the orbit rate (ω_0) with regards to the inertial reference system:

$$\omega_{BI} = \omega_{BO} + A_{OB}[0, -\omega_0, 0]^T$$

Where A_{OB} denotes the transformation matrix from the orbital to the satellite body reference frame. The plots of Figure 8 show the total inertially referenced body rates ω_{BI}. The initial tumble in the pitch and yaw angular velocity is successfully corrected by the panels. The offset in pitch is explained by the fact that when $\omega_{BO,y} = 0$ [deg/s] the inertially referenced satellite body rate in pitch cannot be null since the satellite is pitching to follow the orbit.

The bottom of Figure 8 also shows the time history of the set of control panels oriented along the Y_B and Z_B body axes. Y+ and Y- denote the panel extending along the positive and negative body Y_B axis direction, respectively. Similarly, Z+ and Z- define the panels directed along the positive and negative body Z_B axis direction. Positive angles of deflection of the panels are defined according to the right-hand rule. In Figure 8 a null angle of deflection implies that the panel is in the minimum drag configuration, vice versa for a 90° panels rotation. As can be seen, after achieving the control task the panels do not come back to the nominal configuration (45°) but are still actuated to perform aerodynamic trim, which consists in varying the aerodynamic torques induced on the control surfaces to reject disturbances and keep the satellite in the desired attitude. During the aerodynamic trim, there are time intervals in which the panels tend to move persistently between minimum and maximum drag configurations. Whilst this adequately preserves the target attitude, it is mechanically impractical for a real platform. Moreover, continuous switching from higher to minimum drag configuration will only make a small difference in the mitigation of orbital decay in comparison with maintaining the higher drag configuration.

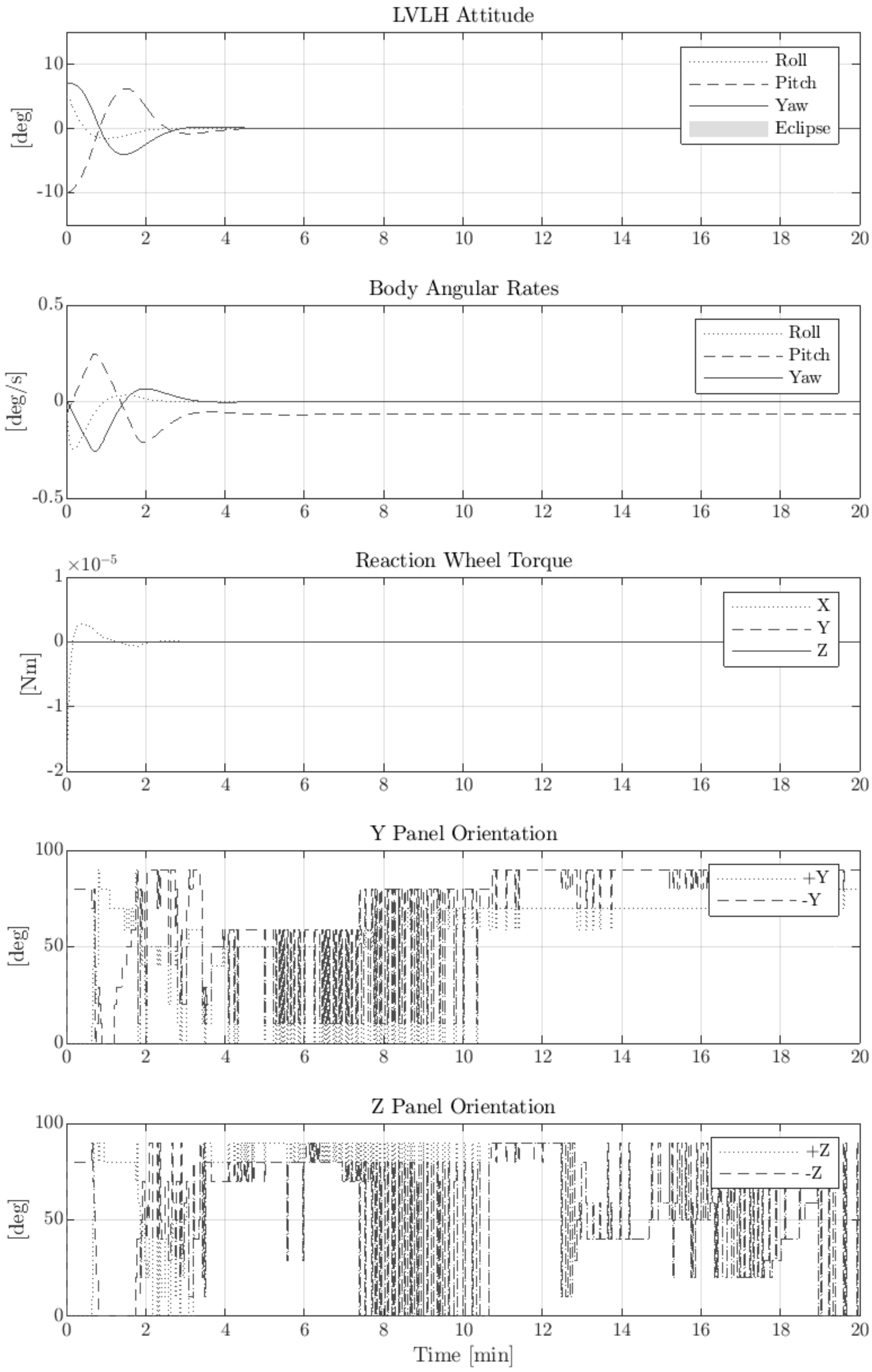

Figure 8: Aerodynamic pitch & yaw control + reaction wheels roll control for the Shuttlecock satellite geometry: 1) Euler angles time history about the LVLH reference system; 2) Inertial angular body rates evolution with time; 3) Control torques provided by the reaction wheels in body axes; 4) Orientation of the panels extending along the Y_B body axis; 5) Orientation of the panels extending along the Z_B body axis.

This undesirable behaviour results from the excessive sensitivity of the panels algorithm. During the aerodynamic trim task, small variations in the control signal provided by the modified PID correspond to considerable variation in the selection of the panel configuration and consequently the panel activity increases. Despite being different, the selected configurations provide very similar aerodynamic control torques. Further modification of the algorithm in setting the panel configuration is therefore needed. This will likely result in some degradation of the in the overall attitude control performance, but it will result in more realistic results which can be achieved by typical platforms. These improvements will be discussed in Section 2.6.

It is also important to mention in this context that for the shuttlecock design the variation in the amount of control surface exposed to the flow (projected areas) during actuation is considerable. Employing such a geometry to perform attitude control tasks may have a measurable impact on the satellite rate of decay, which should be evaluated especially when lower altitudes are selected. Some strategies should also be employed to maintain the desired stability margin, unless variation of this property with the control surface position is desired for specific purposes (i.e. improving agility).

A2.1 Aerodynamic momentum management

The aerodynamic torques induced by a control surface can be employed not only to perform attitude control tasks, but also to keep momentum exchange devices within their prescribed saturation limits. Secular torques acting on the satellite can increase in the angular velocity of reaction wheels for example, leading to the saturation of their internal actuators. Orbital aerodynamics can be exploited for this task through the utilisation of aerodynamic control surfaces to produce external torques to dump the momentum stored in the reaction wheels rather than traditional unloading devices such as magnetorquers or reaction thrusters.

This method may prove to have some advantages over magnetic coils employment. For example, the performance can become independent of knowledge of the Earth's magnetic field and dumping torques can be produced even in directions not perpendicular to the magnetic field vector. On the other hand, the estimation of aerodynamic torques can be affected by numerous uncertainties and the control authority (and thus the range of applicability) may vary considerably with the solar activity. Furthermore, the time required to desaturate the wheels might be impractical or incompatible with other mission requirements (e.g. target pointing). Because of this, it seems reasonable to investigate whether aerodynamic torques can be employed to maintain the momentum of reaction wheels within their prescribed saturation limits whilst they are being used to perform an attitude control task. In this way, it might be possible to perform the two activities in parallel with the advantage of no interruptions.

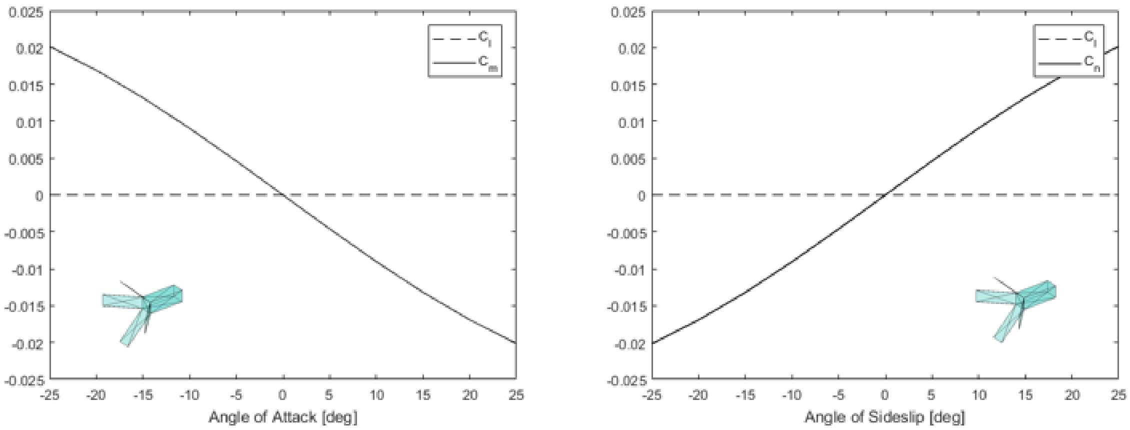

Figure 9: Shuttlecock aerostability characteristics for the nominal configuration. A proper selection of the relative distance between the centre of mass and the centre of pressure provide aerodynamic passive stabilisation. Stability is granted in pitch when the derivative of the pitch momentum coefficient with regards to the angle of attack is negative. Passive stability in yaw is given by the yaw momentum coefficient having a positive derivative with regards to the angle of sideslip.

Simulations were performed for a 250 km circular orbit and 50° inclination, assuming a constant offset in pitch and yaw with regards to the LVLH frame of 5° and 3°, respectively. Keeping the satellite in such a configuration in the lower VLEO altitude range is quite demanding for the reaction wheel authority (Figure 10, bottom). The four tetrahedrally mounted wheels become saturated within 20 minutes. When this condition arises, the satellite is no longer controllable and because of its aerostable characteristic it will start oscillating about the direction of the velocity vector with increased angular body rates (Figure 10, top & middle). The uncontrolled satellite motion after reaction wheel saturation demonstrates the aerostability in pitch and yaw predicted by the simplified aerodynamic derivatives (Figure 9). However, the roll motion appears to be unstable. The larger perturbation in the satellite motion about the yaw axis is attributable to the effects of atmospheric co-rotation on inclined orbits. It is important to note that predicting the flow direction a priori is difficult because of the number of uncertainties involved in this estimation. Any control action about the flow pointing direction is limited by the lack of knowledge of the thermospheric wind direction. Only atmospheric co-rotation can be integrated with a certain level of accuracy.

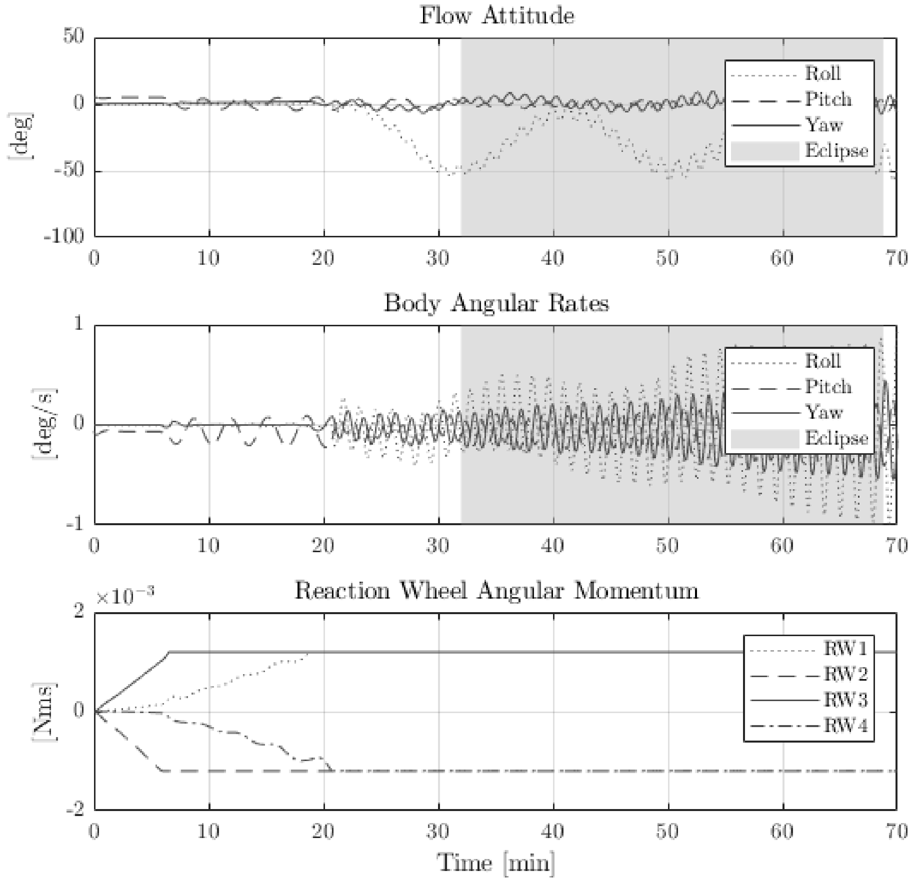

Figure 10: Time histories of the Euler angles and the satellite body rates. After the reaction wheels achieve the saturation condition (bottom), the satellite experiences an uncontrolled motion. Due to its aerostable configuration it starts oscillating about the flow direction (top) with increasing angular body rates (middle).

The aerodynamic momentum management task was subsequently simulated using the same environmental and initial orbit conditions of Figure 10. In this case, it was assumed that the reaction wheels had to keep the satellite aligned with an offset in pitch and yaw of 5° and 3° with regards to the LVLH reference frame. The initial momentum stored in the reaction wheels was assumed to be initially null. Comparing Figure 10 with Figure 11, it can be noticed that aerodynamic torques are capable of counteracting the effect of disturbances on the reaction wheel angular velocity, thus maintaining the angular momentum in each reaction wheel close to the initial null value.

The momentum management algorithm seems also to be performed without unacceptably compromising the reaction wheel attitude control task performed in parallel (Figure 11, top). Figure 11 shows that the reaction wheels are still capable of performing the attitude control manoeuvre and keep the satellite aligned with the desired direction. The controller also proves to be robust against variation in the environmental disturbances acting on the system between periods of eclipse. The manoeuvre performance seems also to be achievable with reasonable panel activity. Time intervals in which the control panels operate in the maximum or nearly maximum drag configuration are however still present, possibly having an undesired impact on the orbital rate of decay. The problem may be solved employing drag compensation devices such as Atmosphere Breathing Electric Propulsion (ABEP) systems. Alternatively, the requirements on the wheels momentum management can be relaxed and some more restrictions can be introduced on the panel deflection both in terms of angular range and rate of change.

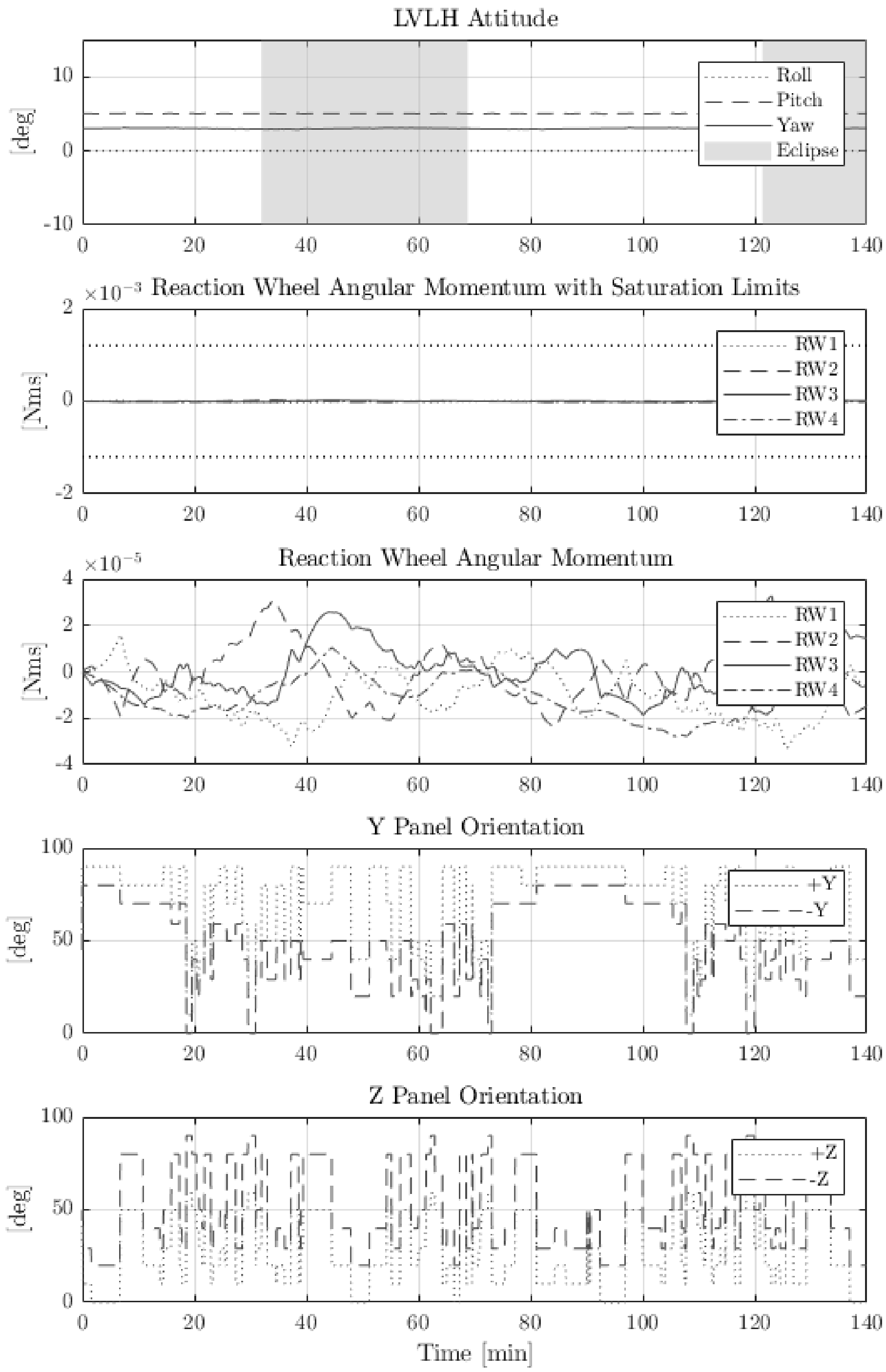

Figure 11: Aerodynamic management of the angular momentum stored in the reaction wheels: 1) Time history of Euler angles about the LVLH reference frame. The reaction wheels are commanded to maintain a desired offset in pitch and yaw of 5° and 3° respectively; 2) Evolution with time of the angular momentum stored in each reaction wheel. The dotted lines identify the upper and lower saturation limits; 3) Close-up view to the momentum stored in each reaction wheel. The results are the same of the plot in 2) but shown with a different scale; 4) Orientation of the panels extending along the Y_B body axis; 5) Orientation of the panels extending along the Z_B body axis.

B Disc Satellite (Neutrally Stable Configuration)

The Disc satellite configuration is designed to be neutrally stable: this means that in the nominal configuration, any variation in the satellite attitude does not produce any variation in the aerodynamic momentum coefficient, whose value remains equal to zero (Figure 12).

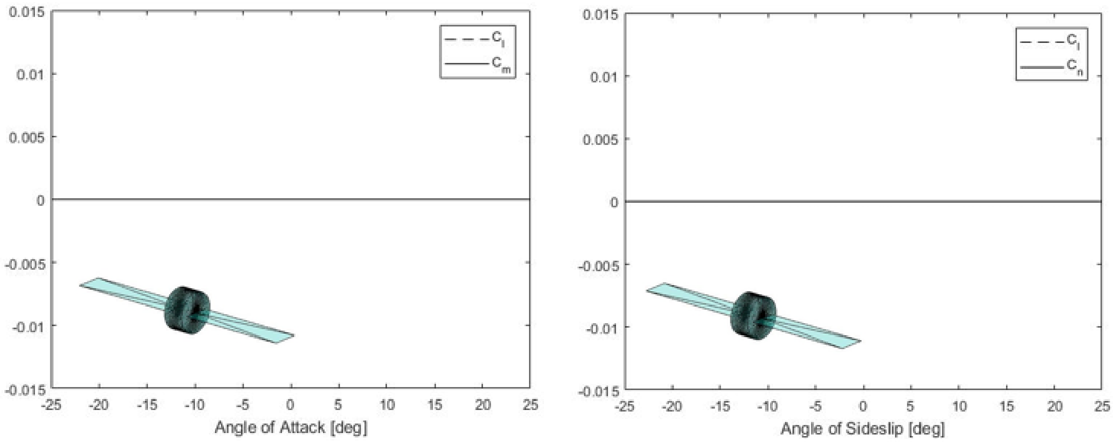

Figure 12: Neutrally stable design for the Disc Satellite in the nominal configuration obtained adapting ADBSat for control purposes. The centre of mass is designed to be coincident with the geometric centre, so that unwanted torques in pitch and yaw are suppressed.

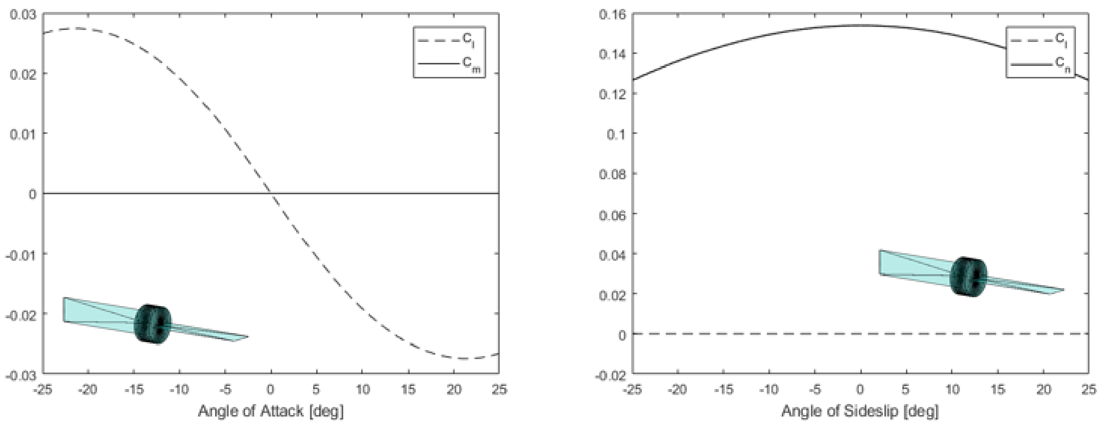

Figure 13: Aerodynamic behaviour of the Disc Satellite for a non-nominal configuration obtained adapting ADBSat for control purposes. The panel oriented along the negative Y_B is kept in its nominal configuration while the panel oriented along the positive Y_B body direction is rotated of 90°. As expected, variations in the satellite configuration do not produce any aerodynamic torques about the pitch axis.

The neutrally stable characteristic is however expected to change with the angle of deflection of the panels (Figure 13. Since the panels extend only along the Y_B direction and their geometric centre is aligned with the CoM in Z_B, the control authority in pitch is expected to be null even for considerable angles of deflection (Figure 13). Moreover, any non-symmetrical counter rotation of the control surface will induce a torque in yaw as well. If the induced yaw torque is not considered for control purposes it may eventually deteriorate the performance of the system.

B1.1 Aerodynamic Roll + Reaction Wheel Pitch & Yaw Control

The capability of the panels to perform a roll control manoeuvre was evaluated for the disc satellite geometry. The manoeuvre is performed in synergy with reaction wheels that control the pitch and yaw motion. The following initial and final conditions are given:

Initial orbit parameters	$alt = 280\ km,\ i = 50°,\ e = 0,\ \Omega = 0°, \nu = 0°$
Initial attitude (RPY in LVLH)	$\varphi_0 = -15°,\ \vartheta_0 = 5°,\ \psi_0 = -5°$
Initial body rates (in LVLH) [°/s]	$\omega_{BO,i} = [0,0,0]$
Desired final attitude (RPY in LVLH)	$\varphi_f = 0°,\ \vartheta_f = 0°,\ \psi_f = 0°$
Desired final body rates (in LVLH) [°/s]	$\omega_{BO,f} = [0,0,0]$

Table 8: Initial and final parameters for aerodynamic roll control + reaction wheel pitch and yaw control for the Disc satellite configuration.

The time histories of the Euler angles about the orbital LVLH reference frame and the satellite inertial body rates are shown in Figure 14. The aerodynamic panels are able to provide the roll control torque demanded to perform the reorientation task without receiving support from the reaction wheels (Figure 14, third picture from the top). The low orbit altitude and the large control surfaces employed enable the desired attitude to be achieved within 20 minutes. Reaction wheels saturation is avoided by constraining the panels to symmetrically counter-rotate (Figure 14, bottom). For the geometry considered, any asymmetry in the satellite configuration with regards to the incoming flow would have no effect on the torque induced in pitch but will induce a torque in yaw. This torque may interfere with the reaction wheels control task and eventually drive the conventional actuators towards saturation, especially when lower altitudes orbits are considered.

The algorithm that determines the panel configuration was designed for non-neutrally stable configurations (feathered and shuttlecock designs). Because of this, once the satellite attitude has been restored, the panels are not ordered back to their nominal configuration but are still actuated to perform aerodynamic trim, i.e. counteract external disturbances to preserve the desired attitude. If this feature can be considered desirable for aerostable configurations, the same cannot really be said for neutrally stable platforms due to their advantageous geometrical configuration. The panel orientation persistently varies during the trim task between the minimum and the maximum or nearly maximum drag configuration with obvious undesired consequences on the satellite mission lifetime.

This implies that the panel configuration algorithm, which also needs to be improved for SOAR, demands further modifications if is to be implemented on a neutrally stable platform. In this regard, the panel configuration algorithm should be modified to take into account the aerodynamic advantages provided by a neutrally stable geometry (see Figure 12) and return the panels to their nominal configuration. In this way the disturbances experienced by the satellite in orbit and the aerodynamic drag induced by the external surfaces could be reduced.

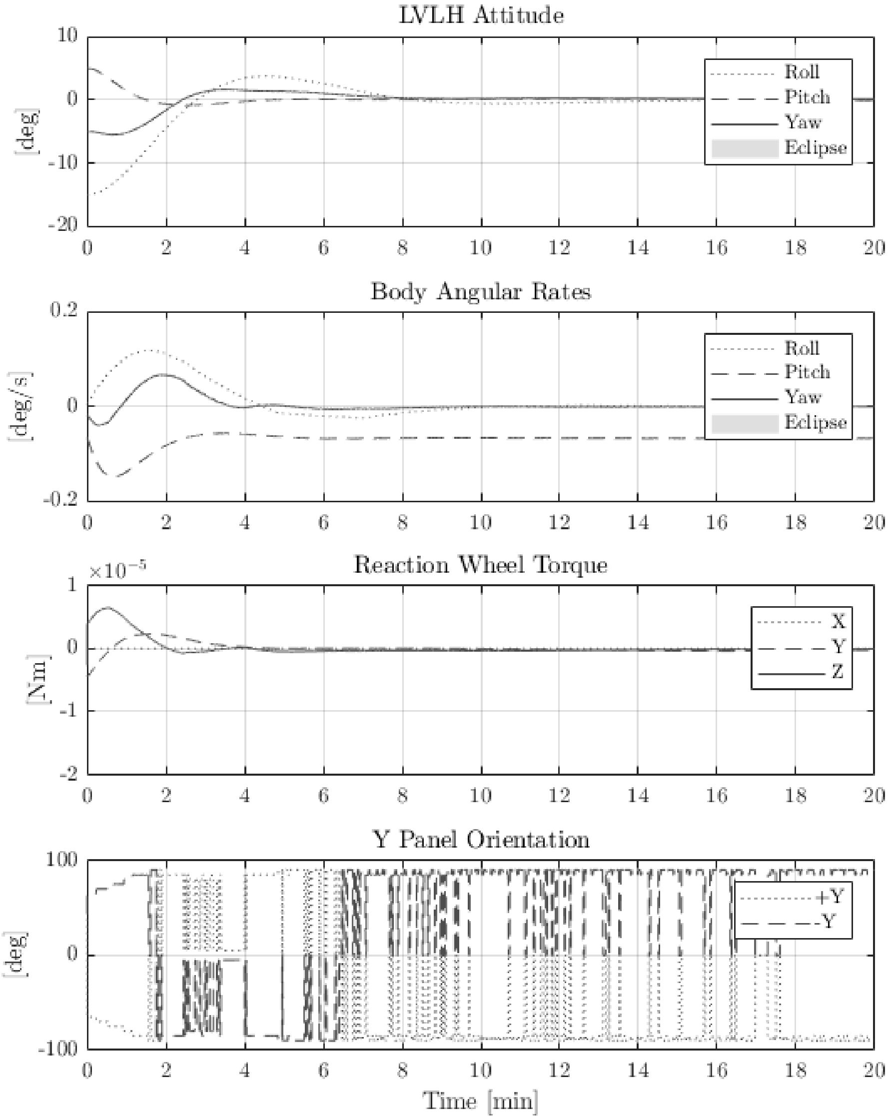

Figure 14: Aerodynamic roll control + reaction wheel pitch & yaw control for the Disc satellite configuration: 1) Euler angles time history about the LVLH reference system; 2) Inertial angular body rates evolution with time; 3) Control torques provided by the reaction wheels in body axes; 4) Orientation of the panels extending along the Y_B body axis.

B1.2 Aerodynamic Pitch & Yaw + Reaction Wheel Roll Control

Aerodynamic control in pitch and yaw was evaluated for the disc satellite geometry for the following initial conditions:

Initial orbit parameters	$alt = 300\ km,\ i = 50°,\ e = 0,\ \Omega = 0°, \nu = 0°$
Initial attitude (RPY in LVLH)	$\varphi_0 = 5°,\ \vartheta_0 = -5°,\ \psi_0 = 10°$
Initial body rates (in LVLH) [°/s]	$\omega_{BO,i} = [0,0,0]$
Desired final attitude (RPY in LVLH)	$\varphi_f = 0°,\ \vartheta_f = 0°,\ \psi_f = 0°$
Desired final body rates (in LVLH) [°/s]	$\omega_{BO,f} = [0,0,0]$

Table 9: Initial and final parameters for aerodynamic pitch & yaw control + reaction wheel roll control for the Disc satellite configuration.

Similarly to the case discussed for the shuttlecock configuration, reaction wheels are employed to correct the attitude in roll. As expected the satellite geometry is not able to provide sufficient control authority to perform the pitch control manoeuvre (Figure 15). This result depends on the fact that the geometric centre of the control panels is aligned with the satellite centre of mass, so that no offset is present in the longitudinal axis. If aerodynamic pitch control is to be implemented on a similar geometry, the panels or the centre of mass needs to be moved in the Z_B axis. Alternatively, multiple sets of panels could be considered.

For the current configuration, however, the panels seem to be still able to provide reasonable stabilisation of the satellite attitude in yaw. According to this, it seems legitimate to verify if any aerodynamic roll and yaw control can be implemented for this geometry.

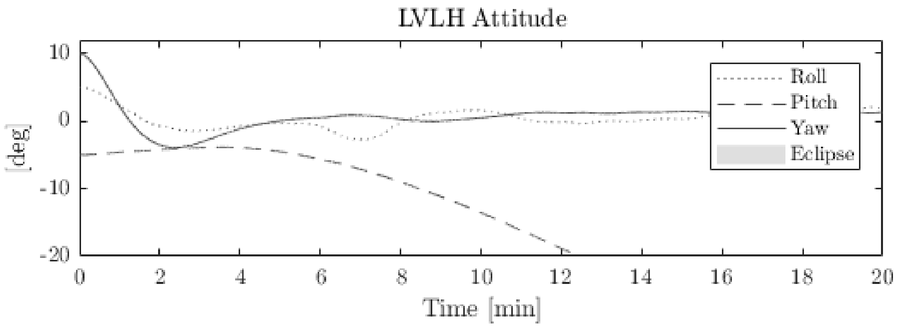

Figure 15: Aerodynamic pitch & yaw control + reaction wheel roll performance for the Disc satellite geometry. The plot shows the evolution of the Euler angles about the orbital LVLH reference frame with time. As expected by some design considerations, the aerodynamic control paddles do not provide sufficient authority to stabilise the attitude in pitch.

B1.3 Aerodynamic Roll & Yaw + Reaction Wheel Pitch Control

In the following case, a control manoeuvre to return the satellite in the desired pointing direction from a given offset with regards to LVLH orbital frame is studied. The initial orbital and attitude conditions include:

Initial orbit parameters	$alt = 250\ km,\ i = 50°,\ e = 0,\ \Omega = 0°, \nu = 0°$
Initial attitude (RPY in LVLH)	$\varphi_0 = 14°,\ \vartheta_0 = 5°,\ \psi_0 = -5°$
Initial body rates (in LVLH) [°/s]	$\omega_{BO,i} = [0,0,0]$
Desired final attitude (RPY in LVLH)	$\varphi_f = 0°,\ \vartheta_f = 0°,\ \psi_f = 0°$
Desired final body rates (in LVLH) [°/s]	$\omega_{BO,f} = [0,0,0]$

Table 10: Initial and final parameters for aerodynamic roll & yaw control + reaction wheel pitch control for the Disc satellite configuration.

The controller is set so that the reaction wheels solely perform the pitch control task, while the roll and yaw axes control is pursued by the aerodynamic control surfaces. According to the time histories of the Euler angles (Figure 16, top), coarse aerodynamic control is achievable even though the aerodynamic roll and yaw control task for this geometry seem to be partially conflicting. The aerodynamic controller appears to be able to keep the error in roll close to zero, even though the initial value of the offset is relatively large in the small angles manoeuvre domain. An undesired and noisier behaviour, in comparison with the results obtained for the shuttlecock configuration or the disc satellite roll control manoeuvre, is also observed in the evolution of the satellite inertial body rates with time (Figure 16, second from the top), with some undesired disturbance about the desired null angular rate value in roll and yaw.

The efforts of the control panels whilst performing this manoeuvre are intense (Figure 16, bottom). The panels oscillate persistently between nearly-opposite configurations in very short time intervals (~2s). This condition is likely to not be mechanically implementable on a real platform and highly undesirable especially in the lower VLEO altitude range.

Possible future developments may include a better design selection for the aerodynamic attitude task to be performed. This might include, among others, the selection of multiple smaller aerodynamic control panels which are sized to play a role in both disturbing and stabilising the roll and yaw attitude motion. Moreover, the algorithm that selects at each allowed interval of time the optimal panel configuration was derived for aerostable configurations (specifically SOAR) and adapted to a neutrally stable platform. Because of this, the panel selection criteria intrinsically suffers from neglecting fundamental features provided by the neutrally stable design of the disc satellite. Better performance is expected to be observed by commanding the control panels to maintain the nominal minimum drag configuration once the attitude task is coarsely achieved. In this way the advantages provided by the satellite design can be exploited and the disturbance torques acting on the body can be reduced.

Similar to the shuttlecock configuration, high sensitivity in the panel selection algorithm causes the panel configuration to be rapidly changed despite producing only small variations in the induced aerodynamic torques. The undesired behaviour observed in Figure 16 may be able to be mitigated by improving the implementation of the algorithm as discussed later in Section 2.6.

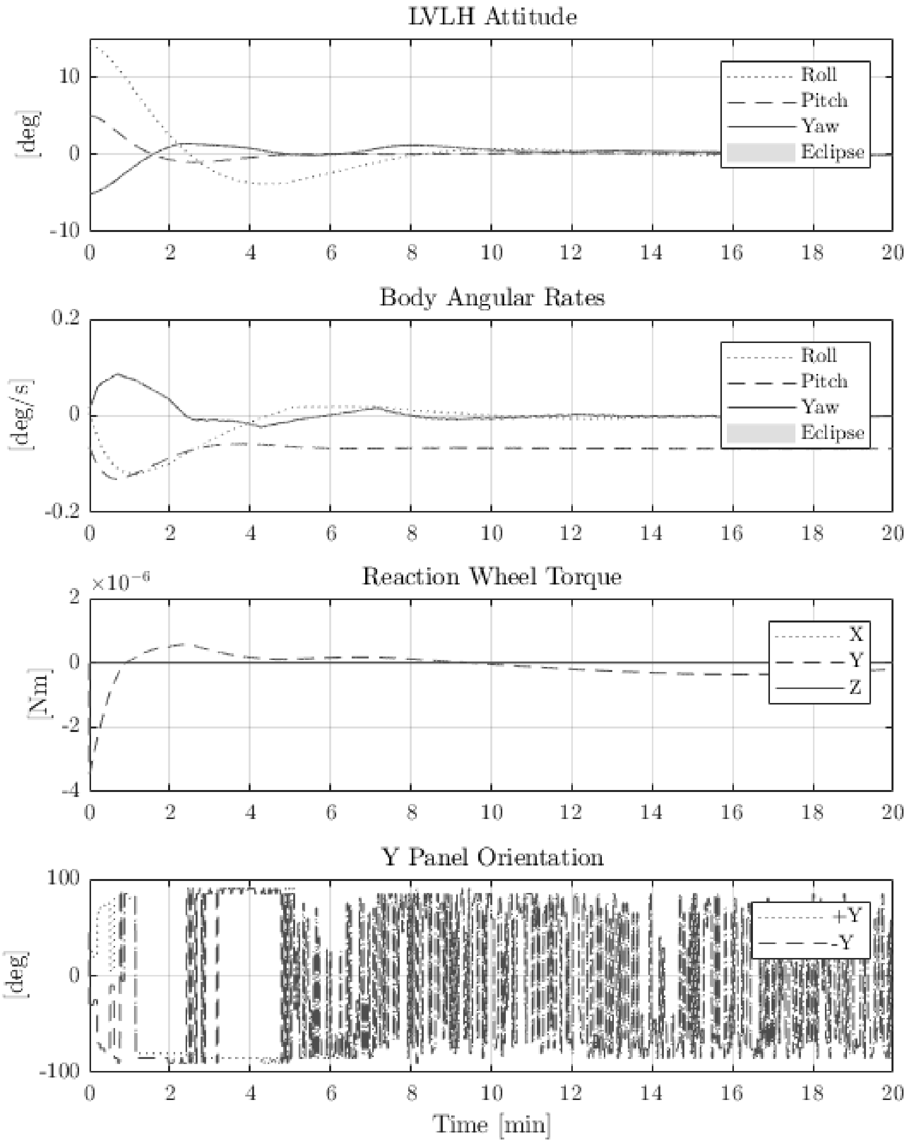

Figure 16: Aerodynamic roll & yaw control + reaction wheel pitch control for the disc satellite geometry: 1) Euler angles time history about the orbital LVLH reference frame; 2) Inertial angular body rates evolution with time; 3) Control torques provided by the reaction wheels in body axes; 4) Orientation of the panels extending along the Y_B body axis.

C Feathered Configuration (SOAR)

C1.1 Aerodynamic Roll Control + Reaction Wheel Pitch & Yaw Control

Similarly to the simulations performed for the shuttlecock and disc satellite design, feasibility of aerodynamic control manoeuvres was investigated for the feathered configuration in the form of SOAR. For the aerodynamic roll axis control task, the following initial conditions were selected:

Initial orbit parameters	$alt = 200\ km,\ i = 50°,\ e = 0,\ \Omega = 0°, \nu = 0°$
Initial attitude (RPY in LVLH)	$\varphi_0 = -15°,\ \vartheta_0 = 5°,\ \psi_0 = -5°$
Initial body rates (in LVLH) [°/s]	$\omega_{BO,i} = [0,0,0]$
Desired final attitude (RPY in LVLH)	$\varphi_f = 0°,\ \vartheta_f = 0°,\ \psi_f = 0°$
Desired final body rates (in LVLH) [°/s]	$\omega_{BO,f} = [0,0,0]$

Table 11: Initial and final parameters for aerodynamic roll control + reaction wheel pitch & yaw control for the SOAR feathered geometry.

The results shown in Figure 17 demonstrate that aerodynamic roll control is achievable for materials providing accommodation coefficients available at the current state of the art for low orbit altitudes in the VLEO range. The torques provided in 3-axis by the reaction wheels confirm that the traditional actuators do not interfere with the aerodynamic control task, which is entirely performed by the control panels. For this simulation, the control panel orientation is selected so that not only the desired roll control torque is produced, but such that pitch and yaw control are also supported. In this way, the production of torques which act contrary to the reaction wheels task are avoided. Looking at Figure 17, it is possible to notice that when the attitude departs from the desired target, the panels abandon the nominal configuration to correct the current offset. In this way, during the trim task the amount of drag induced by the interaction with the surfaces is minimised as much as possible.

With regards to the time history of the panel deflections (Figure 17, bottom), it is interesting to note that during the attitude control task, counter-rotation of the panels is preferentially selected. Once the attitude is stabilised, the panels do not return to their nominal position but exert aerodynamic trim in three axes to counteract the environmental disturbances perturbing the target attitude. In this time interval there are circumstances in which the controller selects co-rotated panel combinations. This is possibly due to the fact that the panels are trying to maintain the satellite attitude in the desired offset with regards to the flow reference frame. This implies that the panels constantly have to exert a control action in yaw to counteract the disturbance introduced in the system by the upper atmosphere co-rotation with the Earth and keep the satellite aligned with the LVLH reference frame.

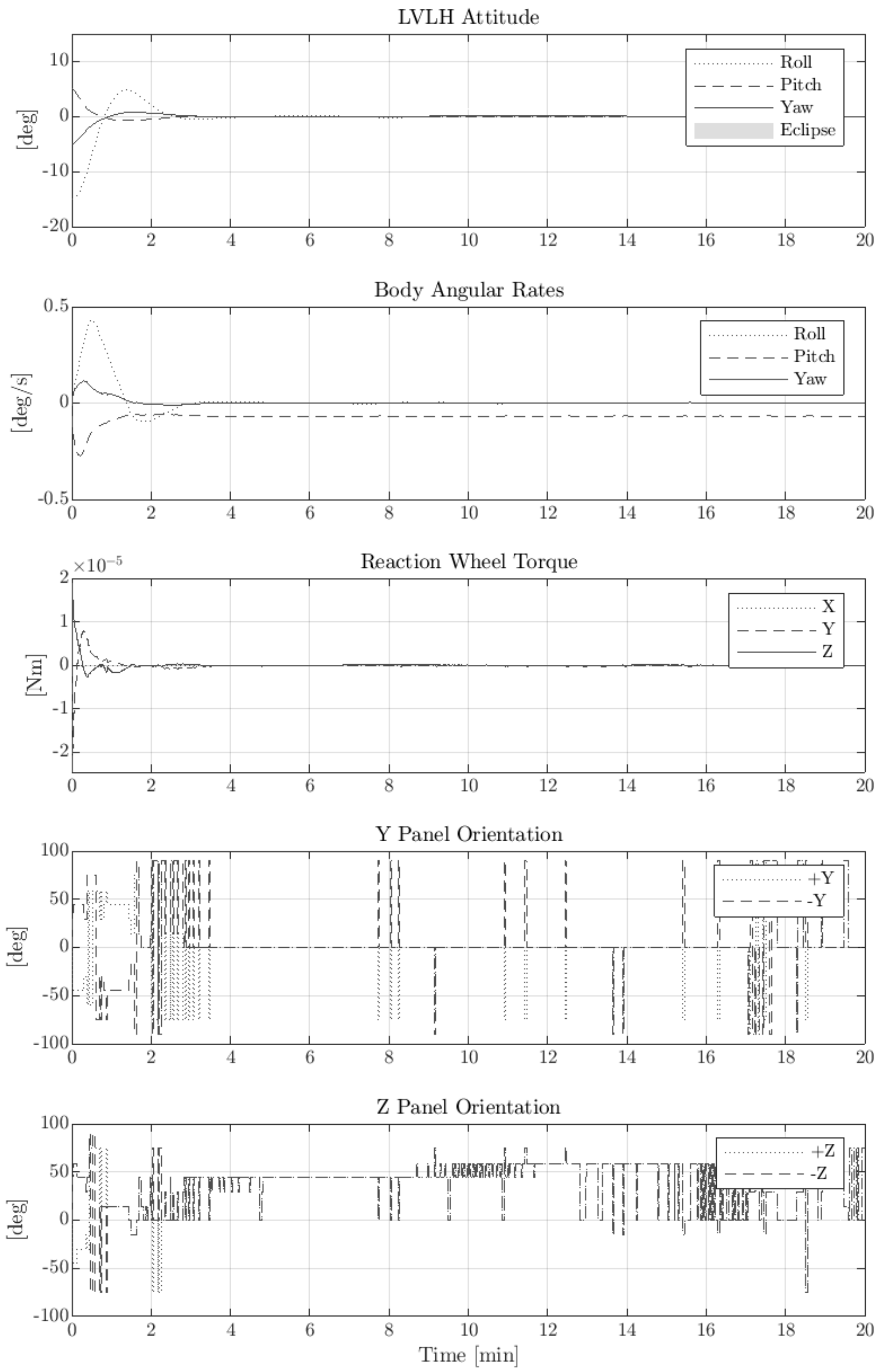

Figure 17: Aerodynamic roll + reaction wheel pitch & yaw control for SOAR feathered geometry: 1) Euler angles time history about the orbital LVLH reference frame; 2) Inertial angular body rates evolution with time; 3) Control torque provided by the reaction wheels in body axes; 4) Orientation of the panels extending along the Y_B body axis; 5) Orientation of the panels extending along the Z_B body axis.

For the aerodynamic attitude control task in roll, a second scenario was considered and the aerodynamic actuators feasibility to correct the satellite attitude and stabilise it with regards to a desired offset about the roll axis was investigated. Even in this case, the algorithm that controls the panel configuration was set so that the induced aerodynamic torques in pitch and yaw would support the reaction wheels control task, whenever possible.

Initial orbit parameters	$alt = 220\ km,\ i = 56°,\ e = 0,\ \Omega = 0°, \nu = 0°$
Initial attitude (RPY in LVLH)	$\varphi_0 = 5°, \vartheta_0 = -5°, \psi_0 = 5°$
Initial body rates (in LVLH) [°/s]	$\omega_{BO,i} = [0,0,0]$
Desired final attitude (RPY in LVLH)	$\varphi_f = -3°, \vartheta_f = 0°, \psi_f = 0°$
Desired final body rates (in LVLH) [°/s]	$\omega_{BO,f} = [0,0,0]$

Table 12: Initial and final parameters for aerodynamic roll control + reaction wheel pitch & yaw control for the SOAR feathered geometry. The control panels are actuated to maintain a desired offset in roll with regards to the LVLH reference frame.

Results obtained in Figure 18 show the feasibility of the aerodynamic control manoeuvre described above for very low altitude orbits in the VLEO range. Given an initial error in the attitude about the roll axis, the control panels are capable of providing sufficient control authority to achieve coarse pointing with regards to the desired offset in roll. The manoeuvre, for the case studied, also appears to be obtained with reasonable panel actuation (Figure 18, bottom). The performance are however likely to degrade with the selection of higher altitudes, for which the oscillatory behaviour about the roll axis observed at the top of Figure 18 is expected to increase and the time required to stabilise the satellite to an acceptable extent could be longer. Since the atmospheric density exponentially decrease with altitude, the same manoeuvre might be unfeasible for altitudes above 300 km during periods of minimum solar activity. More investigations are for this reason required to evaluate the aerodynamic performances obtained at higher VLEO altitudes: these could be useful not only to broadly define the range of feasibility of the attitude control manoeuvres selected but also to evaluate if any limitations are introduced by the controller structure in a more challenging environmental scenario.

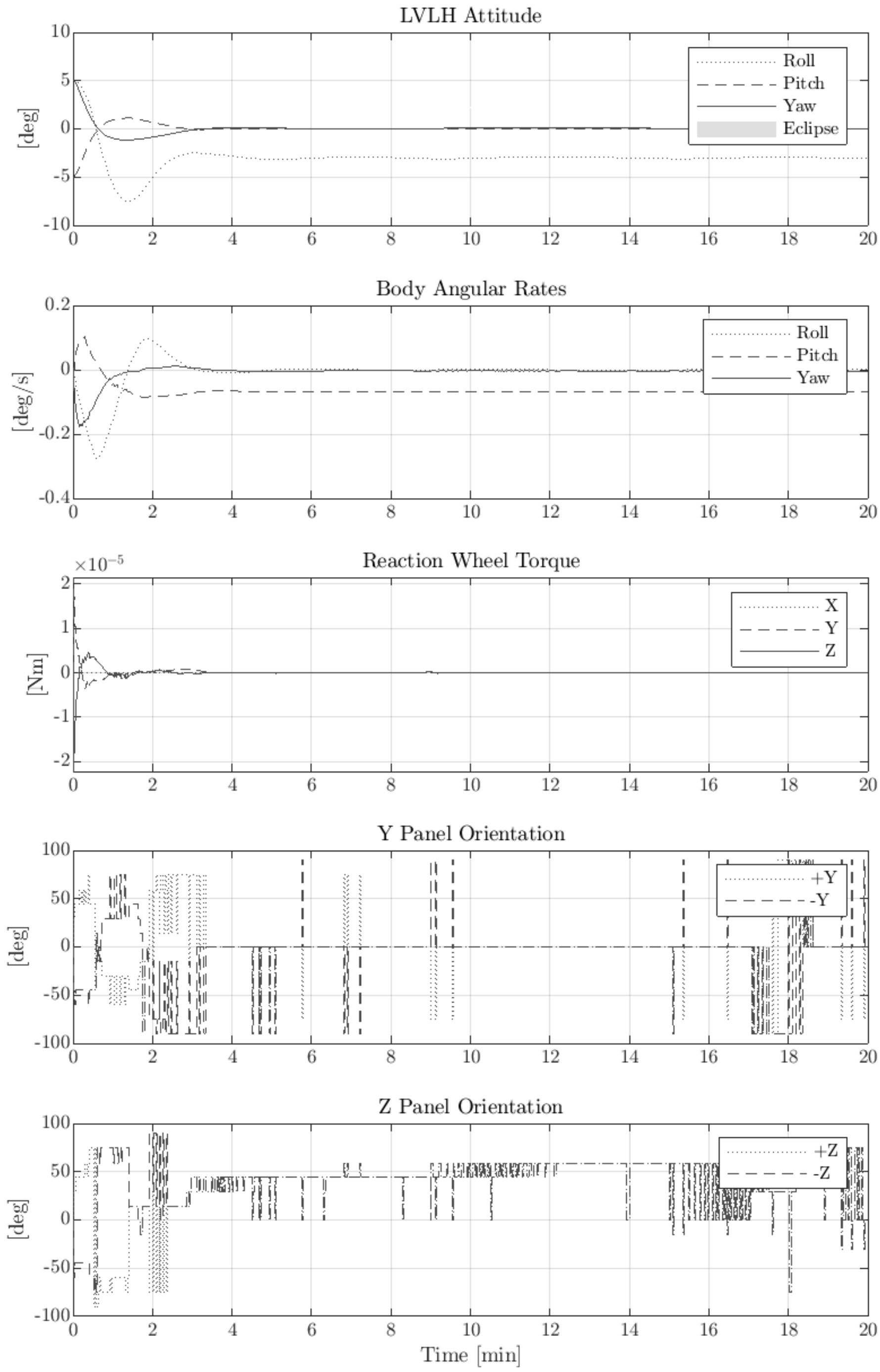

Figure 18: Aerodynamic roll + reaction wheel pitch & yaw control for the SOAR feathered geometry. In this case the aerodynamic paddles are actuated to provide and maintain a desired offset with regards to the LVLH reference frame: 1) Euler angles time history about the orbital LVLH reference frame; 2) Inertial angular body rates evolution with time; 3) Control torque provided by the reaction wheels in body axes; 4) Orientation of the panels extending along the Y_B body axis; 5) Orientation of the panels extending along the Z_B body axis.

C1.2 Aerodynamic Pitch & Yaw Control + Reaction Wheel Roll Control

Feasibility of aerodynamic control in pitch and yaw axes was evaluated for the following initial orbital conditions:

Initial orbit parameters	$alt = 250\ km,\ i = 56°,\ e = 0,\ \Omega = 0°, \nu = 0°$
Initial attitude (RPY in LVLH)	$\varphi_0 = 20°,\ \vartheta_0 = -10°,\ \psi_0 = 12°$
Initial body rates (in LVLH) [°/s]	$\omega_{BO,i} = [0,0,0]$
Desired final attitude (RPY in LVLH)	$\varphi_f = 0°,\ \vartheta_f = 0°,\ \psi_f = 0°$
Desired final body rates (in LVLH) [°/s]	$\omega_{BO,f} = [0,0,0]$

Table 13: Initial and final parameters for aerodynamic pitch & yaw control + reaction wheel roll control for the SOAR feathered geometry.

As the manoeuvre is performed in the lower VLEO range, the algorithm controlling the panel configuration was set so the desired control torques were provided (pitch and yaw axes) and the roll control task performed by the reaction wheels was supported whenever possible. In this way, any undesired disturbance torque in roll which may counteract the reaction wheel actuation and potentially lead to saturation is avoided. Results shown in Figure 19 show that the control task is achieved and that the final attitude in roll, pitch and yaw is kept very close to the target thanks to the panels counteracting external disturbances once the manoeuvre is accomplished (aerodynamic trim). The panels time history, however, suggest that the aerodynamic trim is performed in a way that would probably be mechanically unfeasible and that because of this, needs to be revisited and improved. These improvements are discussed later in Section 2.6.

Figure 19 shows the control torques produced in output by the reaction wheels and the satellite in its entirety. Since the reaction wheels do not interfere with the aerodynamic control task (Figure 19, third from the top), the short time required to perform the manoeuvre can be explained considering the dimensions of the four control panels and the very low altitudes selected to perform the task (increased density). The logic used to select the satellite geometric configuration that provides the desired control torques is also a contributing factor. Improvement in the performance may derive from the fact that the algorithm providing the panel deflections accounts for the contribution coming from the main body for the current angle of attack/angle of sideslip. In this way, the main body torques are not treated as disturbances but are usefully used to optimise the aerodynamic control task even if no control action can be exerted on them. Moreover, Figure 19 shows that the control supports the actuation of the reaction wheels, providing a roll torque in the direction prescribed by the control law.

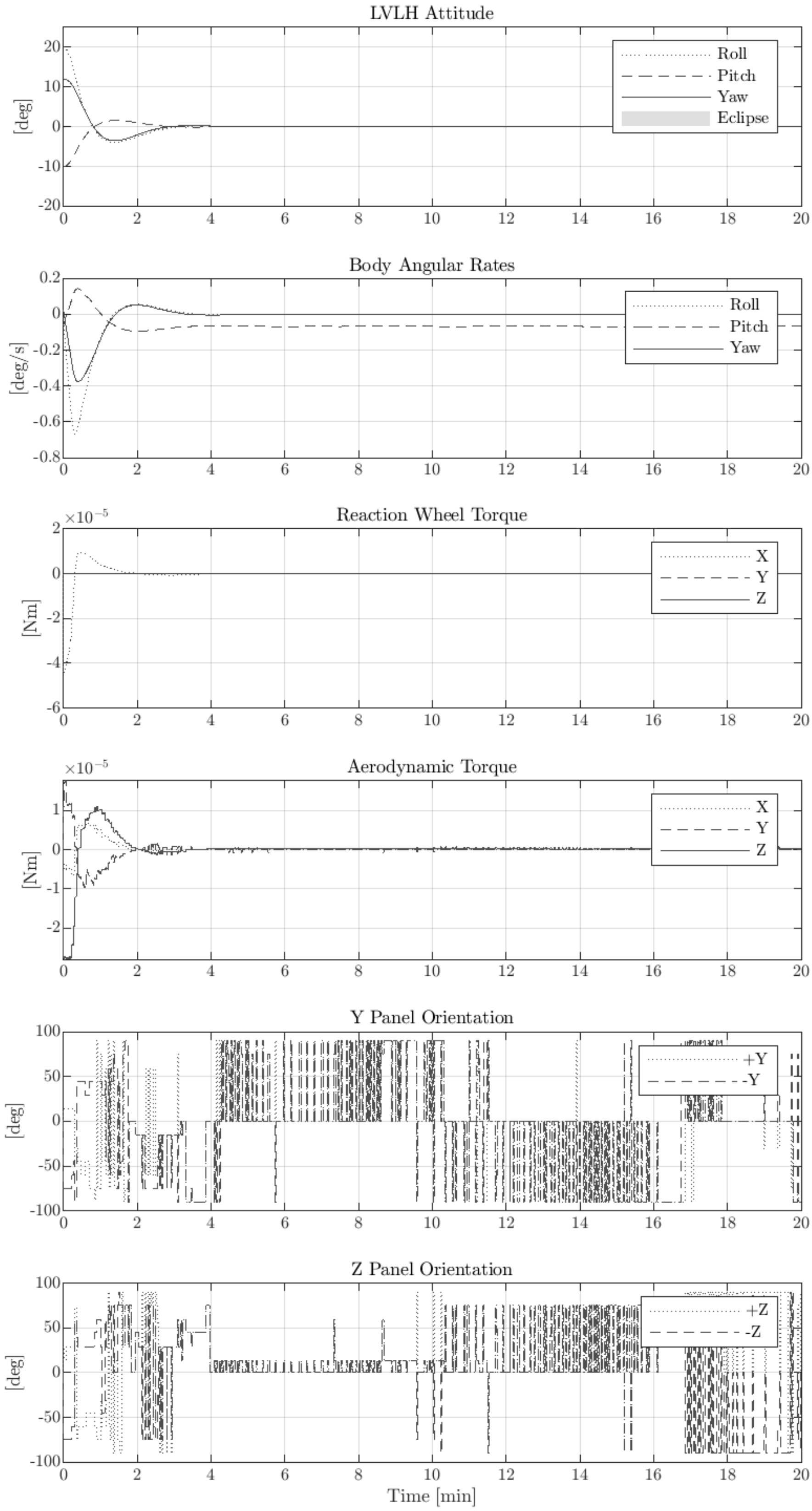

Figure 19: Aerodynamic pitch & yaw control + reaction wheel roll control for the SOAR feathered geometry: 1) Euler angles time history about the orbital LVLH reference frame; 2) Inertial angular body rates evolution with time; 3) Control torques provided by the reaction wheels in body axes; 4) Aerodynamic control torques provided in body axes; 5) Orientation of the panels extending along the Y_B body axis; 6) Orientation of the panels extending along the Z_B body axis.

For the pitch and yaw aerodynamic control manoeuvre a second slightly more challenging scenario was selected. An initial small tumble was added in roll, pitch and yaw, so that the conditions set for the simulation comprise:

Initial orbit parameters	$alt = 280\ km,\ i = 56°,\ e = 0,\ \Omega = 0°, \nu = 0°$
Initial attitude (RPY in LVLH)	$\varphi_0 = 5°,\ \vartheta_0 = -8°,\ \psi_0 = 8°$
Initial body rates (in LVLH) [°/s]	$\omega_{BO,i} = [0.1,0.1,0.1]$
Desired final attitude (RPY in LVLH)	$\varphi_f = 0°,\ \vartheta_f = 0°,\ \psi_f = 0°$
Desired final body rates (in LVLH) [°/s]	$\omega_{BO,f} = [0,0,0]$

Table 14: Initial and final parameters for aerodynamic pitch & yaw control + reaction wheel roll control for the SOAR feathered geometry. An initial tumble is assumed in the satellite initial inertial body rates.

In this case the control panels are not only required to compensate for the attitude error in pitch and yaw, but also to correct the initial offset in the satellite body rates velocities with regards to the orbital LVLH reference frame. Similarly to the case previously discussed, the reaction wheels are employed to control solely the motion about the roll axis. The time evolution of the system is shown in Figure 20. The initial tumble in the pitch and yaw angular velocity is successfully corrected by the panels and the desired final attitude is simultaneously successfully achieved. When it comes to panel actuation, considerations similar to those already made for the previous less demanding scenario are unfortunately still valid. The panel actuation required to achieve the control performance shown is particularly intense and likely to be achieved only in a very ideal scenario. Moreover, the preferential selection of high drag configurations during the trim task is likely to be unsuitable at the altitudes selected (increased orbital rate of decay). The performance of the panel configuration algorithm can however be improved keeping into account the considerations made in Section 2.6.

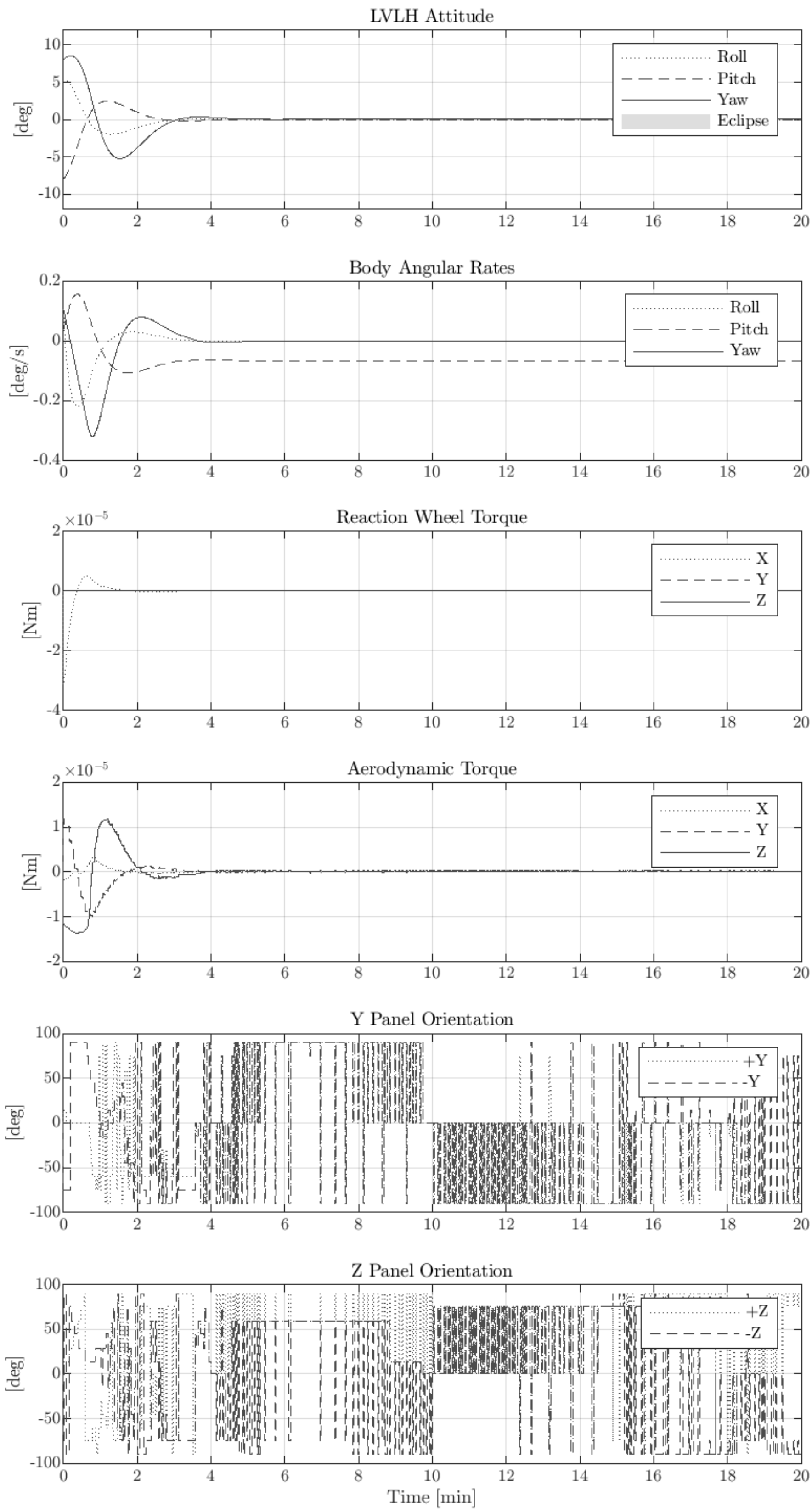

Figure 20: Aerodynamic pitch & yaw control + reaction wheel roll control for the SOAR feathered geometry, given an initial tumble in roll, pitch and yaw: 1) Euler angles time history about the orbital LVLH reference frame; 2) Inertial angular body rates evolution with time; 3) Control torques provided by the reaction wheels in body axes; 4) Aerodynamic control torques provided in body axes; 5) Orientation of the panels extending along the Y_B body axis; 6) Orientation of the panels extending along the Z_B body axis.

C2.1 Aerodynamic Momentum Management

A possible employment of the aerodynamic torques as a means to maintain the total momentum stored in the wheels within the saturation limits was investigated for the feathered geometry. An initial offset in roll, pitch and yaw was also assumed. In this way, it was be possible to address any major perturbation provided by the aerodynamic panels to the attitude control task performed by the reaction wheels. The overall simulation was run for 140 minutes, to evaluate any possible saturation occurrence over a larger timescale. The time interval chosen for the simulation is characterised by the alternation of eclipse and non-eclipse periods. In this way, the robustness of the controller and the feasibility of the manoeuvre with the achievable aerodynamic control authority were tested. It is to be kept in mind that the results shown in this section may possibly change with altitude, environmental conditions, initial orbit inclination since the aerodynamic torques provided by the panels change with any variation in each of this factor. Because of this, altitudes in the very low VLEO range and high orbit inclinations were selected as a representative and demanding case study. The initial orbital conditions consist in:

Initial orbit parameters	$alt = 200\ km,\ i = 70°,\ e = 0,\ \Omega = 0°, \nu = 0°$
Initial attitude (RPY in Flow)	$\varphi_0 = 5°,\ \vartheta_0 = 10°,\ \psi_0 = 8°$
Initial body rates (in LVLH) [°/s]	$\omega_{BO,i} = [0,0,0]$
Desired final attitude (RPY in LVLH)	$\varphi_f = 0°,\ \vartheta_f = 0°,\ \psi_f = 0°$
Desired final body rates (in LVLH) [°/s]	$\omega_{BO,f} = [0,0,0]$

Table 15: Initial and final parameters for the reaction wheel momentum management task for the SOAR feathered geometry.

As can be seen in Figure 21, very low altitudes and high orbit inclinations lead to fast saturation of the reaction wheels. Figure 22 on the other hand shows that when aerodynamic torques are employed, reaction wheels saturation is avoided and the angular momentum stored in each reaction wheel is kept in very close proximity to the null value after the attitude control manoeuvre is accomplished. The management task seems also to be achieved with a reasonable panel activity. The number of switches between the minimum and maximum drag configurations appears to be contained and limited to short periods of time. More intense panels activity, as expected is observed while the attitude control task is performed.

Figure 21 and Figure 22 compare the performance of the reaction wheels when the aerodynamic momentum management loop is not operating (Figure 21, top) and when it is operating in parallel to the attitude control loop (Figure 22, top). No substantial difference can be observed in the time history of the Euler angles about the LVLH orbit reference frame, thus suggesting in first analysis that the gains of the LQR were appropriately selected to grant wide time separation between the two closed loops. This results, however, needs to be confirmed by frequency response analysis.

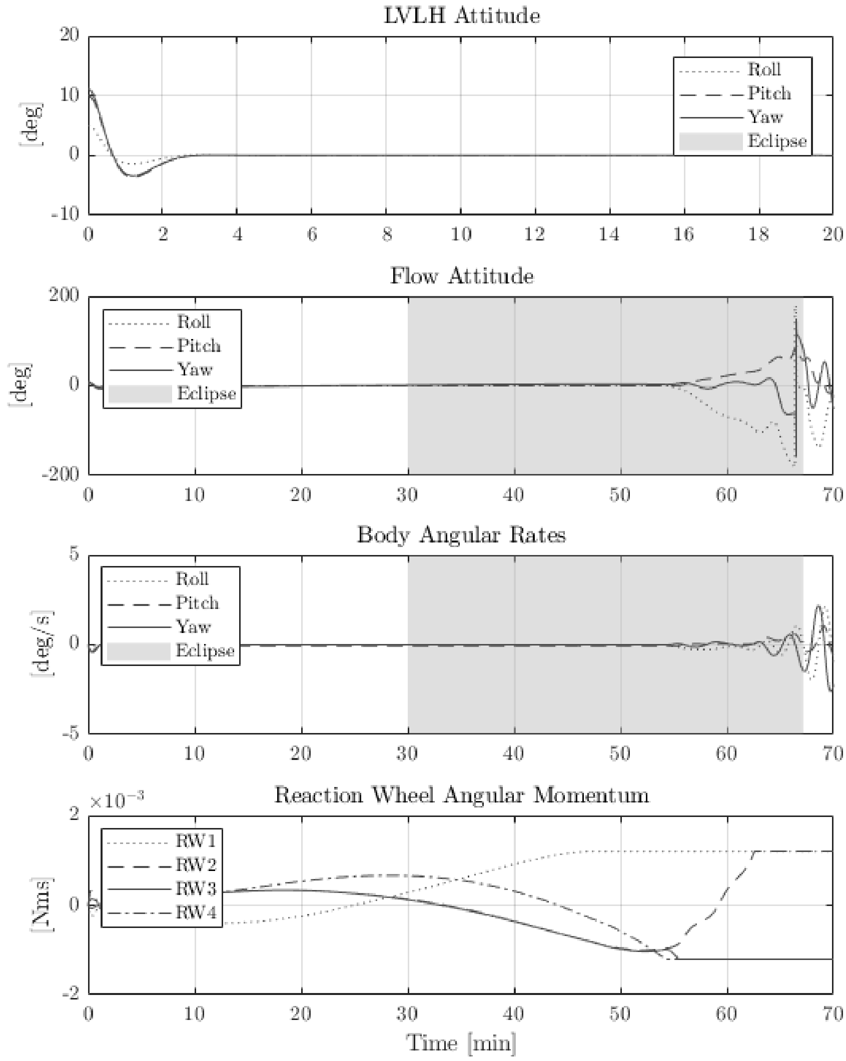

Figure 21: Time histories of the Euler angles and the satellite body rates for the SOAR feathered geometry under reaction wheel saturation. After the reaction wheels achieve the saturation condition (bottom), the satellite experiences an uncontrolled motion. Due to its aerostable configuration it starts oscillating about the flow direction with increasing angular body rates (middle). The required attitude control task is however achieved before the occurrence of the actuators saturation.

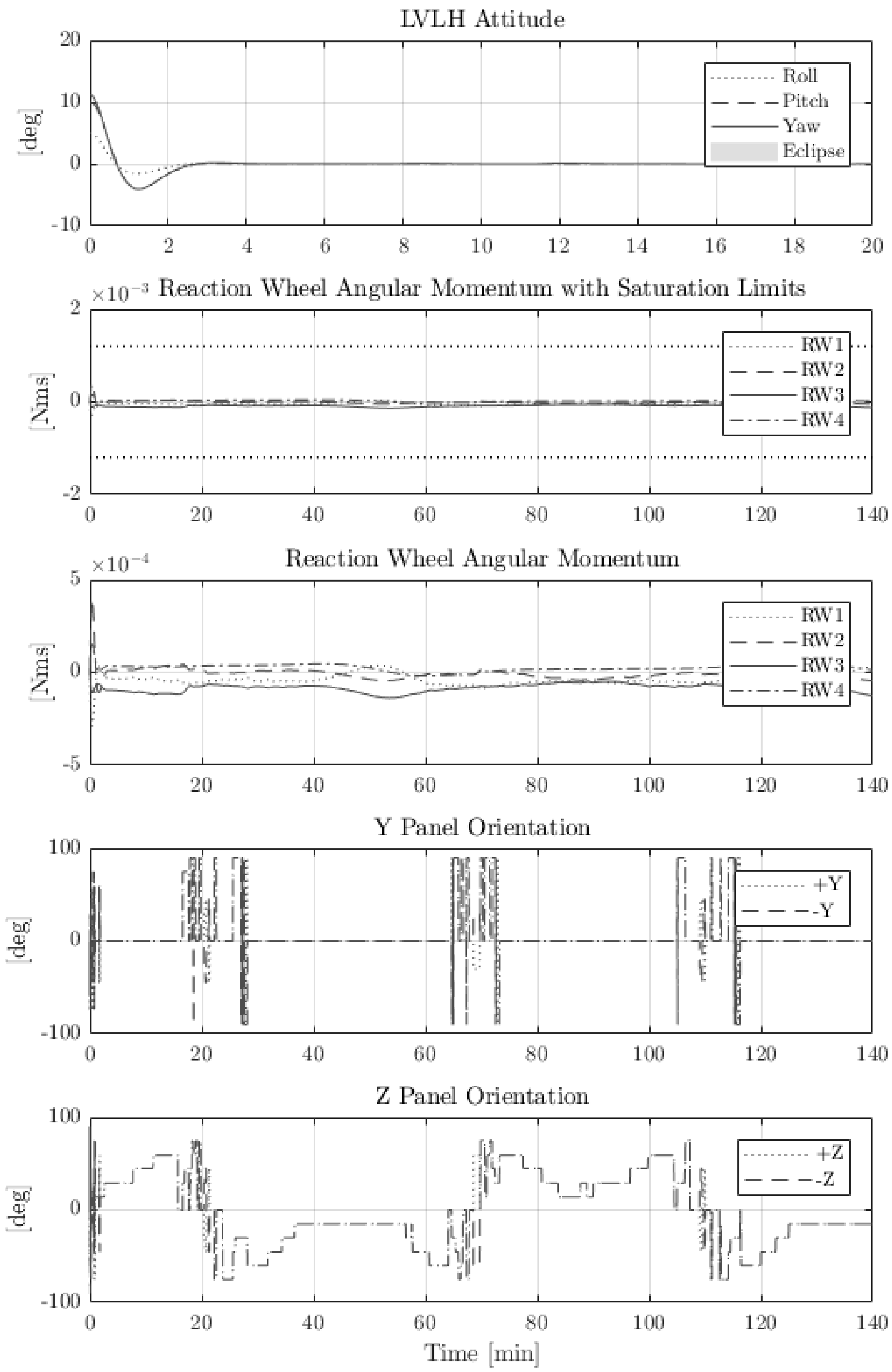

Figure 22: Aerodynamic management of the angular momentum stored in the reaction wheels: 1) Time history of Euler angles about the LVLH reference frame. The reaction wheels are commanded to perform an attitude control manoeuvre about the LVLH reference frame; 2) Evolution with time of the angular momentum stored in each reaction wheel. The dotted lines identify the upper and lower saturation limits; 3) Close-up view to the momentum stored in each reaction wheel. The results are the same of the plot in 2) but shown with a different scale; 4) Orientation of the panels extending along the Y_B body axis; 5) Orientation of the panels extending along the Z_B body axis

2.6. Proposed Controller Improvements

At present the algorithm implementation capably demonstrates the feasibility of aerodynamic control manoeuvres and that they can be *mathematically* achieved, even with currently characterised materials with accommodation coefficients close to 1. However, some further consideration needs to be given to the physical and practical implemented on spacecraft platforms, for example SOAR.

The variation of aerodynamic torques is susceptible to a high number of parameters and thus presents additional challenges to the implementation of the aerodynamic control algorithms. If only the dependency on the orientation of the aerodynamic control panels is considered, an efficient model capable of describing an aerodynamic geometry varying with four independent variables in a non-linear regime needs to be found. This model also has to respect some requirements in terms of speed to grant the overall stability of the control loop.

Further developments are needed and some possible strategies to achieve the desired result have already been identified for implementation:

- Translate the panel configuration algorithm into a Jacobian based approach. This mainly consists in translating the algorithm into a symbolic form, so that the variation of the aerodynamic coefficients in roll, pitch and yaw with the four panel deflections can be determined. The panels configuration providing the desired aerodynamic profile can subsequently be selected. The translation of the algorithm from a numerical to a symbolic form is sought for improved computational efficiency in selecting the panel configuration to provide the desired control torque. Alternatively, the angular range of each panel can be reduced so that a linear approximation of the aerodynamic torque with panel angle can be applied. This approach may however have an impact on the feasibility and performance of the control manoeuvres described above;
- Modify the PID gains in aerodynamic control axes to penalise panel actuation. In the pointing and trim simulations presented previously, it was observed that the selection of the control panel deflection was very sensitive to small changes in the desired output torque, resulting in frequent and large changes in the output panel deflection. In comparison, for the momentum management tasks, particularly for the shuttlecock and feathered configurations, it was noted that this behaviour was less prevalent. This improved performance is attributed to the gains for the aerodynamic panels which are selected to guarantee a wide separation between the time responses of the attitude and momentum management control loops. They are selected so that the aerodynamic momentum management task has a considerably slower time response compared to the reaction wheel attitude control task. This suggests that, for the attitude control task, a panel behaviour similar to that observed for the momentum management task can be achieved by penalising movement of the aerodynamic actuators. Practically, this means that substantial improvements in the aerodynamic pitch and yaw panels history are expected to be obtained if the PID gains corresponding to the aerodynamically control axes are reduced. Since a LQR approach is used to tune the modified PID algorithm, this objective can be achieved by increasing the weights of the Q matrix;
- Introduce saturation avoidance logic to avoid the selection of maximum aerodynamic drag configurations and preserve mission lifetime.

2.7. Demonstration of Aerodynamic Control Manoeuvres on SOAR

SOAR (Satellite for Orbital Aerodynamics Research) is a 3U CubeSat which is due to be launched from the ISS in 2020. The spacecraft features a set of four steerable panels (fins) which have been designed primarily to investigate the interaction between different materials and the residual gas flow in VLEO. These steerable fins can also be used as aerodynamic control actuators and therefore used to demonstrate some of the aerodynamic control manoeuvres described and implemented previously.

2.7.1. SOAR Hardware

The platform size, design, and specification of SOAR introduces a number of constraints to the aerodynamic control manoeuvres which can be implemented and the expected performance which can be achieved in orbit.

i) ADCS Subsystem

The attitude determination sensor-suite for SOAR is comprised of a set of fine sun sensors, a magnetometer and a 3-axis gyroscope. When combined using an unscented Kalman filter (UKF), these components provide an estimated attitude knowledge with a 3-sigma error in the range of 0.6-0.82° depending on the altitude, current attitude, and solar vector. The source of this error is principally due to the absolute accuracy of the different sensors and their associated noise.

As a result of this uncertainty, the ADCS is not able to reliably measure small attitude or rate errors (with respect to a reference set-point) and a process variable filter, hysteresis zone, or deadband should be implemented in the controller to avoid chattering or over-actuation in the output.

ii) System Sampling and Bus Rate

Whilst the previous simulations of control manoeuvres have been performed in continuous-time, implementation of the control methods on SOAR requires a discrete-time treatment. The spacecraft has a platform frequency of 1 Hz, resulting from the update rate of the ADCS system.

The implementation of discrete-time control requires some modification of the controller definition to account for the discretised signal input. For example, in PID controllers, alternative definitions of the derivative (approximation via backwards differencing) and integral terms (approximation by a finite sum) are required.

For discrete PID, an alternative, velocity form of the PID control algorithm can be implemented which can be more effective than the positional form for the hardware involved. For example, in reaction wheel control, the use of angular velocity as the control variable allows a simpler transformation to the incremental motor input needed to provide the demanded control torque.

$$\begin{aligned}\Delta u(k) &= u(k) - u(k-1)\\ &= K_p\left[e(k) - e(k-1) + \frac{T_0}{\tau_i}e(k-1) + \frac{\tau_d}{T_0}\left(e(k) - 2e(k-1) + e(k-2)\right)\right]\end{aligned}$$

In this form, summation in the integral term of the controller is no longer necessary, integral windup is avoided, and the controller can be resilient against system failure as only knowledge of the error in the previous two time steps (sample points) is necessary. However, this form can also be susceptible to noise and sampling of the control signal, resulting in possible overreaction of the controller. Implementation of control signal filters may therefore be required.

iii) Panel Deflection Rate

Hardware limitations will impose some constraint on the rate at which the aerodynamic control panels can be actuated or rotated. Including this in the controller implementation is important as it may impact the output aerodynamic control performance. It may be particularly important if there is high variability in the relative flow direction or magnitude (or alternatively fast body rates) that the aerodynamic control surfaces are expected to respond to. This effect will also become more pronounced as the altitude is reduced.

The variation in total angular momentum of the spacecraft with actuation of the external control surfaces should also be considered. Fast rates of actuation or rotation could result in significant contributions to the body rates, disturbing the satellite attitude and deteriorating the control performance.

iv) Aerodynamic Test Surfaces

The primary objective of SOAR is to investigate the GSI characteristics and associated lift and drag coefficients of reference and novel materials in the VLEO environment. As the requirement is to test multiple materials, the surfaces of the four steerable fins will not all be the same. The fins will therefore have different aerodynamic profiles that must be considered by any implemented control and panel selection algorithm.

Knowledge of the GSI properties of the novel materials is currently only theoretically based. Whilst it is hopeful that the materials will promote more specular reflection properties, ground-based experiments are required to provide more information on the true character and performance of the GSI. These ground-based experiments are due to be performed in The University of Manchester ROAR (Rarefied Orbital Aerodynamics Research) Facility, which is currently being assembled and commissioned within the scope of WP3. The first experiments are due to be started in late 2019. Further information from the initial in-orbit testing and material investigation of SOAR may also be able to improve the knowledge of the performance of these materials in the true environment and can subsequently be integrated into the aerodynamic control logic if it is possible to update these parameters during the flight campaign.

v) On-board Computer Capability and Performance

Implementation of the control algorithms on-board the spacecraft must also be compatible with the available computational resources. The on-board computer for SOAR is based on an Atmel AVR32 microcontroller architecture which is also responsible for performing other on-board tasks. The complexity of control algorithm which can be implemented must be able to operate at a maximum of 50% time on the 64 MHz processor. Memory and data storage are also limited to approximately 8MB SDRAM and 32MB NOR FLASH respectively, and must carefully managed.

For example, extensive databases of aerodynamic coefficients which are dependent on multiple variables (eg. angle of attack/sideslip, control surface deflections, altitude) can require storage on the order of hundreds of megabytes to gigabytes. This capacity is not available on board, and linearised expressions which estimate these databases must be implemented. Furthermore, querying these large databases can require significant memory and processing power and may not be feasible on the given hardware (in the required time) even if sufficient storage is available.

2.7.2. Aerostability

SOAR is characterised by an aerostable design capable of providing static stability in pitch and yaw with regards to the flow direction. For orbits lower than 600 km, this feature represents a considerable advantage especially if the mission requirements demands for the satellite to be aligned with the flow to achieve the mission objectives. Coarse aerodynamic pointing can be easily obtained with reduced control effort from the actuators. This condition is particularly advantageous in the lower VLEO altitudes range, where passive aerodynamic stabilisation can effectively postpone reaction wheel saturation, thus relaxing the frequency with which the desaturation task needs to be performed. The results shown in Figure 23 were obtained using the control adaption of ADBSat for control purposes. They show how satellite dimensional aerodynamic coefficients (mainly about the yaw and pitch axes) vary with the angle of attack and the angle of sideslip. Even though these graphs do not provide any detailed information about the real non-linear satellite behaviour, they represent a very simple and straightforward tool which design engineers can use to validate an aerostable design before actually starting performing simulations or to compare the results of this last with the expected theoretical behaviour.

Figure 23 shows that the simplified conditions for passive aerodynamic stabilisation [20] are met. Because of the number of assumptions on which these conditions rely on, simulations of the real non-linear satellite dynamics need to be performed to asses in a realistic scenario, the expected SOAR aerostability characteristic against the purely theoretical results. An initial simulation (Figure 24) was run for a simple case scenario, an equatorial ($i = 0°$) orbit at 200 km altitude. Whilst all the modelled perturbations were included in this analysis, the equatorial inclination chosen minimises perturbations in yaw that arise from atmospheric co-rotation. An initial offset with regard to the flow reference frame of $\varphi_0 = 10°$, $\vartheta_0 = -10°$ and $\psi_0 = 10°$ is provided about the roll, pitch and yaw axes. To study the evolution of the uncontrolled motion of the satellite, the gains of the controller described in the previous sections were all set a null value and SOAR was assumed in its nominal minimum drag configuration.

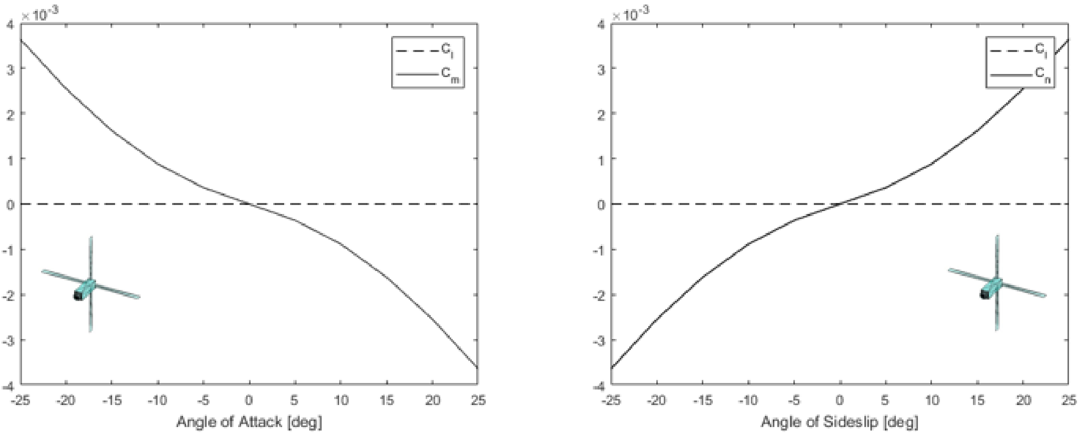

Figure 23: SOAR aerostability characteristics for the nominal configuration. A proper selection of the relative distance between the centre of mass and the centre of pressure provide aerodynamic passive stabilisation. Stability is granted in pitch when the derivative of the pitch momentum coefficient with regards to the angle of attack is negative. Passive stability in yaw is given by the yaw momentum coefficient having a positive derivative with regards to the angle of sideslip.

Figure 24 demonstrates aerodynamic stability of SOAR about the roll, pitch and yaw axes with regards to the flow reference frame. The results appear to be in reasonable agreement with what was expected for the selected orbit. The amplitude of oscillations is dependent on the initial value of the offset with regards to flow and it is expected to be even smaller if a flow pointing condition is assumed as initial condition. Despite this, both the amplitude and the frequency of oscillation appear to be reasonably constrained: these two properties are indeed dependent on the magnitude of the induced aerodynamic torques. Smaller amplitudes and increased frequency are expected at lower altitudes where the aerodynamic stiffness is increased and therefore restoring torques are greater in magnitude.

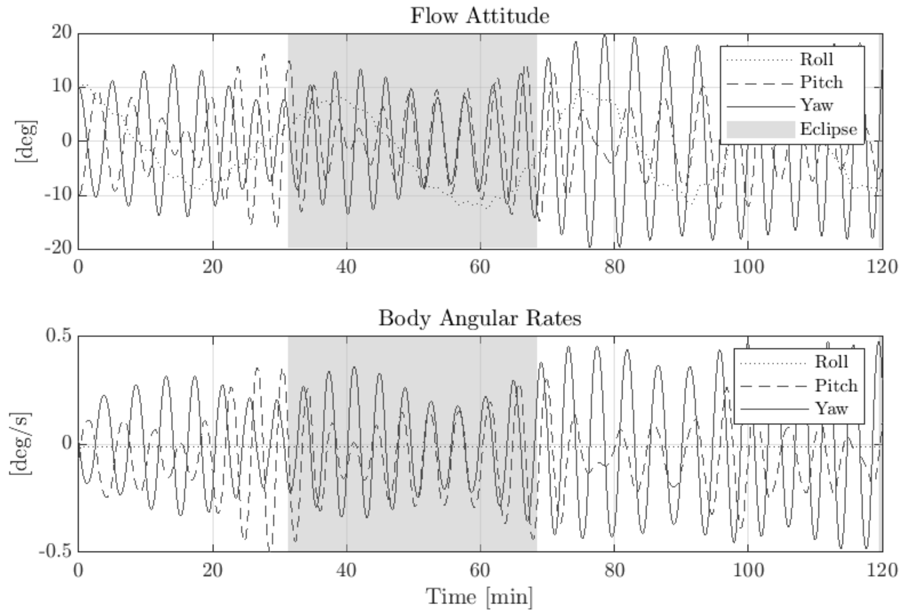

Figure 24: Uncontrolled motion of SOAR in its nominal configuration about the flow reference frame, given an initial offset of 10° in roll, -10° in pitch and 10° in yaw (top) in an equatorial orbit at 200 km of altitude. The corresponding evolution with time of the inertially referenced angular body rates is shown at the bottom.

The aerostability characteristic of SOAR was evaluated for a second simplified but more relevant scenario. For this second test, the satellite was initially assumed to be pointing in the flow reference frame and to be characterised by a small tumble in pitch and yaw of - 0.05 deg/s and 0.05 deg/s, respectively. Even for this scenario, the evolution of the satellite uncontrolled motion about the flow reference frame was investigated for a circular equatorial orbit at 200 km altitude. No initial tumble was given about the roll axis to simplify the discussion of the results. As Figure 23 shows, SOAR design does not provide any aerodynamic stabilisation in roll and because of this any initial perturbation is expected to be amplified unless other stabilisation devices are assumed to be installed. To assess the truthfulness of the theoretical results (Figure 23), we are particularly interested in the uncontrolled pitch and yaw motion in a realistic simulation environment. Results obtained for this scenario are displayed in Figure 25, where the inertial referenced body rate component in pitch (Figure 25, bottom) not only keeps into account the initial tumble in the satellite body reference frame but also the orbit angular rate component. The aerostability behaviour predicted by the theoretical results of Figure 23 is even in this case confirmed. Similarly to the previous case discussed, the high frequencies observed in the pitch and yaw oscillations about the flow reference frame depend on the increased aerodynamic torques experienced by the satellite at the selected orbital altitudes.

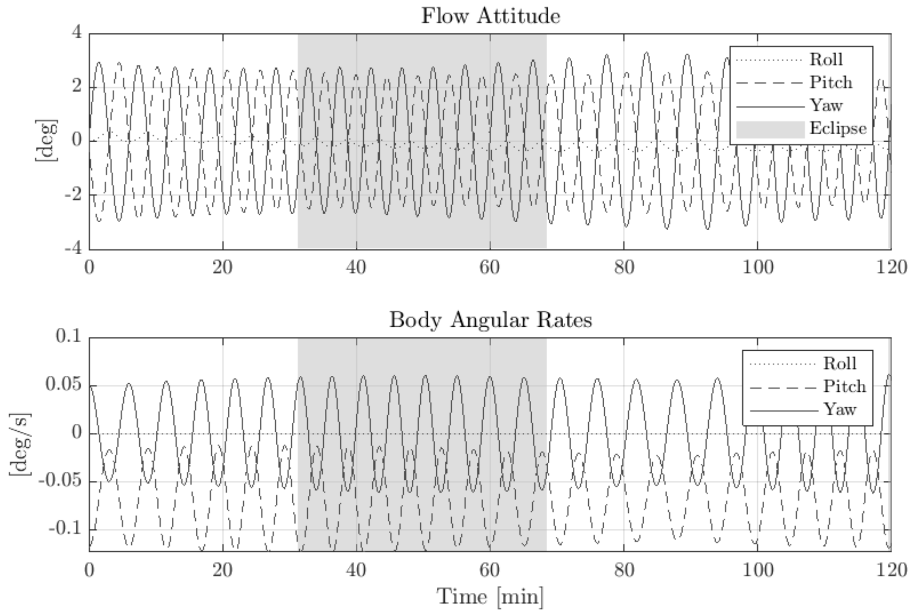

Figure 25: Uncontrolled motion of SOAR in its nominal configuration about the flow reference frame, given an initial tumble of -0.05°/s in pitch and 0.05°/s in yaw (top) in an equatorial orbit at 200 km of altitude. The corresponding evolution with time of the inertially referenced angular body rates is shown at the bottom.

The capability of the induced aerodynamic torques to grant passive static stabilisation about the desired flow direction is however expected to be affected by increasing orbital altitudes and inclinations. The thermospheric density decreases exponentially with altitude with more significant variations to be expected during period of low solar activity [2]. According to this, even the magnitude of the restoring aerodynamic torques is expected to decrease, with possibly a little effect on the stabilisation of the satellite dynamics. On the other hand, satellite in non-null inclination orbits are affected by perturbations in the yaw motion that changes sign each half orbital period and which are due to the atmosphere co-rotation with the Earth. Some disturbances are thus expected to be observed especially in the yaw motion when non-equatorial orbit are considered.

According to this the same simulation described before was repeated considering an initial tumble in pitch and yaw of - 0.05 °/s and 0.05 °/s, but modifying the initial orbital conditions according to more realistic and challenging scenarios. Figure 26 shows SOAR aerostable behaviour in a 300 km orbit inclined at 51.6°. Both the uncontrolled pitch and yaw motion appears to be affected by the increase in orbital altitude and inclination, with more considerable effects noticeable on the yaw motion. The variation of the amplitude of the oscillation in pitch might find explanation both in the coupling with external disturbances and in the reduced aerodynamic restoring torques achievable at this altitude. The satellite, however, seems to preserve overall a good aerostable characteristic about this axis.

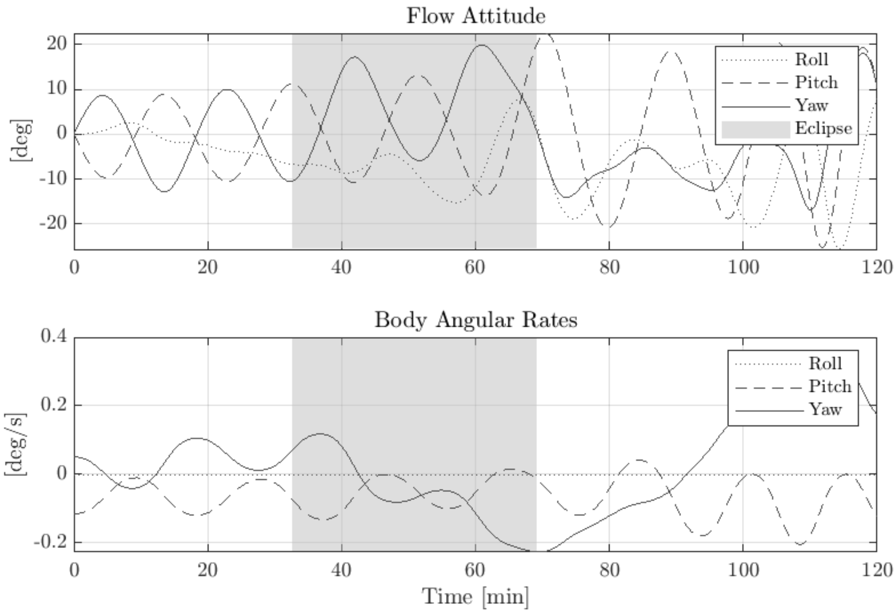

Figure 26: Uncontrolled motion of SOAR in its nominal configuration about the flow reference frame, given an initial tumble of -0.05°/s in pitch and 0.05°/s in yaw (top) in a 51.6° inclined orbit at 300 km of altitude. The corresponding evolution with time of the inertially referenced angular body rates is shown at the bottom.

As expected, the yaw motion is non-negligibly affected by the selection of inclined orbits in the middle altitudes VLEO range, with the aerostable characteristic effectively being lost. It is also interesting to notice that, given the same initial condition, the evolution about the roll axis is noticeably worsened with regards to the more ideal equatorial orbit scenario. Moreover, the reduced aerodynamic experienced at these altitudes translates in the reduced frequencies of oscillation about the pitch and yaw axes. The attitude error with regards to the flow pointing direction increases as well, if compared to the 200 km scenario.

Figure 27 similarly shows the aerostable performance of SOAR for a 400 km orbit inclined at 51.6°, given an initial tumble in pitch and yaw of - 0.05°/s and 0.05°/s as in the cases discussed above. It is possible to notice how at this altitude, the order of magnitude of the induced aerodynamic torques is not sufficient to provide an adequate restoring torque to passively stabilise the satellite about the desired flow direction. Deteriorated performance are observed not only for the yaw motion, but also for the pitch motion that hardly meets the aerostability characteristics observed in Figure 24, Figure 25 and Figure 26. These results thus seem to suggest that the aerostable design of the satellite in its nominal configuration loses its effectiveness in the higher VLEO altitude ranges and that it can only be successfully employed at lower altitudes. According to this the satellite is not able to produce the restoring torques required to re-align the velocity vector when the system is subjected to perturbations. If increments in aerodynamic drag associated with non-minimum drag configurations are not acceptable, more traditional solutions need to be employed to achieve the desired velocity vector orientation.

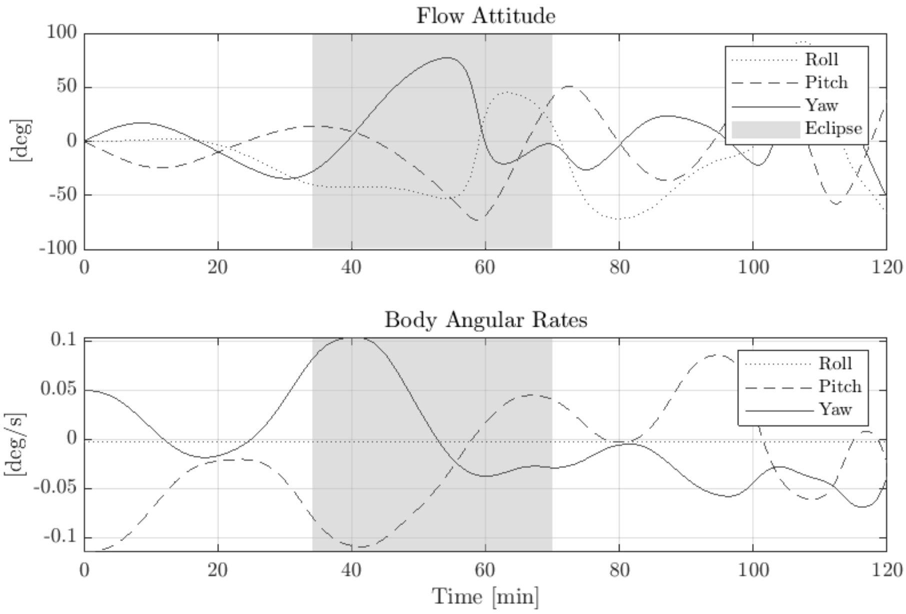

Figure 27: Uncontrolled motion of SOAR in its nominal configuration about the flow reference frame, given an initial tumble of -0.05°/s in pitch and 0.05°/s in yaw (top) in a 51.6° inclined orbit at 400 km of altitude. The corresponding evolution with time of the inertially referenced angular body rates is shown at the bottom.

2.7.3. Proposed In-Orbit Demonstration Manoeuvres

Accounting for the previously presented simulations and results a set of manoeuvres for in-orbit demonstration using the SOAR spacecraft can be proposed.

The previously developed control methods and associated algorithms are proposed to implement these demonstration manoeuvres but require the previously noted modifications and improvements in order to provide improved performance and compatibility with the spacecraft on-board systems. Considerations also need to be made for the specific design of SOAR, the aerodynamic surfaces/materials, and the associated hardware limitations of the platform.

The proposed demonstration manoeuvres encompassing pointing, trim, and momentum management tasks are as follows:

- Aerodynamic roll control with reaction wheel pitch and yaw control
- Aerodynamic pitch control combined with reaction wheel yaw and roll control
- Aerodynamic yaw control combined with reaction wheel pitch and roll control
- Three axis aerodynamic-assisted pointing with reaction wheel inputs

- Aerodynamic momentum management of reaction wheels in the presence of disturbing environmental torques (in a nominally aerostable attitude)
- Reaction wheel control in pitch/yaw with aerodynamic trim for momentum management
- Reaction wheel desaturation using 1-3 axis aerodynamic control

2.8. Conclusions

The feasibility of a range of aerodynamic attitude control manoeuvres was investigated and proved for varying initial orbital conditions and aerodynamic geometries. The investigation mainly concerned a range of combined aerodynamic and reaction wheel attitude control manoeuvres, disturbance rejection through aerodynamic trim, and aerodynamic management of the momentum stored in the reaction wheels.

Despite adaptive techniques are more suitable to cope with uncertain environments, variations in the aerodynamic control authority due to altitudes and hardware performances deterioration, initial attempts to implement a self-tuning adaptive PID based on the principles of adaptive interaction proved to be unsuccessful. This result is probably depending on the increased level complexity of this controller and the consequent increase in expertise required in order to achieve successful implementation. According to this, a simple robust modified PID and a LQR controller was selected. LQRs are well known for their intrinsic stability and robust characteristics in presence of uncertainties. The low sensitivity of the robust modified PID was tested with good results against uncertainties in the satellite inertia matrix and in the environmental disturbance torques, with special attention to transitions between eclipse periods.

The applicability of the above mentioned attitude manoeuvres was discussed for two aerostable configurations and one nominally neutrally stable geometry. The purpose of this operation was to demonstrate the feasibility of aerodynamic control for three independent designs with variations in performances mainly subjected to the aerodynamic effectiveness of the geometry selected. The performances achieved through the implementation of the control strategy on the three geometries selected were discussed. The shuttlecock configuration was expected to have limited aerodynamic roll control capability, but aerodynamic pitch and yaw control and momentum management appeared to be feasible. Similarly, the disc satellite configuration was proved to have no aerodynamic control authority in pitch due to the relative location of the centre of mass with regards to the aerodynamic centre of pressure. This control pitch can be however easily achieved for this geometry if the neutrally-stable characteristic of the geometry is removed, ie. moving the centre of mass or the control panels. Good performances were however achieved for the implementation of an aerodynamic roll control manoeuvre.

Higher aerodynamic performances are achievable with feathered configurations (SOAR) due to the increased control authority obtainable with the panel actuation. Feasibility of aerodynamic pointing was demonstrated in roll and combined pitch and yaw. For the attitude task two more challenging scenarios characterised by a final offset in roll and initial tumble in 3-axes were also discussed. Similarly to the shuttlecock configuration, good performances were obtained for the momentum management task. For SOAR, an aerostability analysis was also performed to test the expected aerostable behaviour against the results predicted by theory.

Aerodynamic trim was shown to be feasible for all the three geometries. However, the analysis of the results obtained especially for this task highlighted the need for some improvements. In particular, it is thought that more optimal selection of the panel deflections can be achieved by further penalising the actuation level in the aerodynamic controlled axes (ie. lower gains). Higher efficiency of the panel selection algorithm can may also be able to be achieved by translating the logic currently implemented into a Jacobian formulation. A saturation avoidance logic can also be added to prevent the undesired selection of high drag configurations.

Whilst the presented results demonstrate feasibility and appear promising for operational implementation, further development and analysis is required to enable implementation with hardware limitations. These aspects were neglected in this study to preserve the generality of the discussions and specific requirements and limitations will vary with the mission and platform design. Forthcoming developments will specifically address the specifications of SOAR within the controller logic and the performance achievable on this in-orbit test platform will be explored in more detail.

3. References

[1] P.C.E. Roberts, N.H. Crisp, S. Edmondson, S.J. Haigh, R.E. Lyons, V.T.A. Oiko, A. Macario-Rojas, K.L. Smith, J. Becedas, G. González, I. Vázquez, Á. Braña, K. Antonini, K. Bay, L. Ghizoni, V. Jungnell, J. Morsbøl, T. Binder, A. Boxberger, G. Herdrich, F. Romano, S. Fasoulas, D. Garcia-Almiñana, S. Rodriguez-Donaire, D. Kataria, M. Davidson, R. Outlaw, B. Belkouchi, A. Conte, J.S. Perez, R. Villain, B. Heißerer, A. Schwalber, DISCOVERER – Radical Redesign of Earth Observation Satellites for Sustained Operation at Significantly Lower Altitudes, in: 68th Int. Astronaut. Congr., International Astronautical Federation (IAF), Adelaide, Australia, 2017.

[2] D. Mostaza-Prieto, B.P. Graziano, P.C.E. Roberts, Spacecraft drag modelling, Prog. Aerosp. Sci. 64 (2014) 56–65. doi:10.1016/j.paerosci.2013.09.001.

[3] D. Mostaza-Prieto, Characterisation and Applications of Aerodynamic Torques on Satellites, The University of Manchester, 2017.

[4] P.M. Mehta, A. Walker, C.A. McLaughlin, J. Koller, Comparing Physical Drag Coefficients Computed Using Different Gas–Surface Interaction Models, J. Spacecr. Rockets. 51 (2014) 873–883. doi:10.2514/1.A32566.

[5] J.R. Wertz, ed., Spacecraft Attitude Determination and Control, Springer Netherlands, Dordrecht, 1978. doi:10.1007/978-94-009-9907-7.

[6] F.. Lemoine, S.C. Kenyon, J.K. Factor, R.G. Trimmer, N.K. Pavlis, D.S. Chinn, C.M. Cox, S.M. Klosko, S.B. Luthcke, M.H. Torrence, Y.M. Wang, R.G. Williamson, E.C. Pavlis, R.H. Rapp, T.R. Olson, The Development of the Joint NASA GSFC and the National Imagery and Mapping Agency (NIMA) Geopotential Model EGM96, Greenbelt, MD, 1998. doi:10.1007/978-3-662-03482-8_62.

[7] N.K. Pavlis, S.A. Holmes, S.C. Kenyon, J.K. Factor, The development and evaluation of the Earth Gravitational Model 2008 (EGM2008), J. Geophys. Res. Solid Earth. 117 (2012). doi:10.1029/2011JB008916.

[8] AIAA Atmospheric and Space Environments Comimittee on Standards, Guide to Reference and Standard Atmosphere Models, Reston, VA, 2010.

[9] S. Bruinsma, The DTM-2013 thermosphere model, J. Sp. Weather Sp. Clim. 5 (2015). doi:10.1051/swsc/2015001.

[10] J.M. Picone, A.E. Hedin, D.P. Drob, A.C. Aikin, NRLMSISE-00 Empirical Model of the Atmosphere: Statistical Comparisons and Scientific Issues, J. Geophys. Res. 107 (2002). doi:10.1029/2002JA009430.

[11] D.P. Drob, J.T. Emmert, G. Crowley, J.M. Picone, G.G. Shepherd, W. Skinner, P. Hays, R.J. Niciejewski, M. Larsen, C.Y. She, J.W. Meriwether, G. Hernandez, M.J. Jarvis, D.P. Sipler, C.A. Tepley, M.S. O'Brien, J.R. Bowman, Q. Wu, Y. Murayama, S. Kawamura, I.M. Reid, R.A. Vincent, An empirical model of the Earth's horizontal wind fields: HWM07, J. Geophys. Res. Sp. Phys. 113 (2008) 1–18. doi:10.1029/2008JA013668.

[12] D.P. Drob, J.T. Emmert, J.W. Meriwether, J.J. Makela, E. Doornbos, M. Conde, G. Hernandez, J. Noto, K.A. Zawdie, S.E. McDonald, J.D. Huba, J.H. Klenzing, An Update to the Horizontal Wind Model (HWM): The Quiet Time Thermosphere, Earth Sp. Sci. (2015) n/a-n/a. doi:10.1002/2014EA000089.

[13] M.F. Larsen, J.W. Meriwether, Vertical winds in the thermosphere, J. Geophys. Res. Sp. Phys. 117 (2012) n/a-n/a. doi:10.1029/2012JA017843.

[14] A.J. Ridley, Y. Deng, G. Tóth, The global ionosphere–thermosphere model, J. Atmos. Solar-Terrestrial Phys. 68 (2006) 839–864. doi:10.1016/j.jastp.2006.01.008.

[15] P.B. Dandenault, MENTAT: A New Wind Model for Earth's Thermosphere, J. Geophys. Res. Sp. Phys. 123 (2018) 7124–7147. doi:10.1029/2018JA025551.

[16] D.A. Vallado, Fundamentals of Astrodynamics and Applications, 4th ed., Microcosm Press/Springer, Hawthorne, CA, 2013.

[17] J.-F. Oehler, D. Rouxel, M.-F. Lequentrec-Lalancette, Comparison of global geomagnetic field models and evaluation using marine datasets in the north-eastern Atlantic Ocean and western Mediterranean Sea, Earth, Planets Sp. 70 (2018) 99. doi:10.1186/s40623-018-0872-y.

[18] E. Thébault, C.C. Finlay, C.D. Beggan, P. Alken, J. Aubert, O. Barrois, F. Bertrand, T. Bondar, A. Boness, L. Brocco, E. Canet, A. Chambodut, A. Chulliat, P. Coïsson, F. Civet, A. Du, A. Fournier, I. Fratter, N. Gillet, B. Hamilton, M. Hamoudi, G. Hulot, T. Jager, M. Korte, W. Kuang, X. Lalanne, B. Langlais, J.-M. Léger, V. Lesur, F.J. Lowes, S. Macmillan, M. Mandea, C. Manoj, S. Maus, N. Olsen, V. Petrov, V. Ridley, M. Rother, T.J. Sabaka, D. Saturnino, R. Schachtschneider, O. Sirol, A. Tangborn, A. Thomson, L. Tøffner-Clausen, P. Vigneron, I. Wardinski, T. Zvereva, International Geomagnetic Reference Field: the 12th generation, Earth, Planets Sp. 67 (2015) 79. doi:10.1186/s40623-015-0228-9.

[19] C.C. Finlay, S. Maus, C.D. Beggan, T.N. Bondar, A. Chambodut, T.A. Chernova, A. Chulliat, V.P. Golovkov, B. Hamilton, M. Hamoudi, R. Holme, G. Hulot, W. Kuang, B. Langlais, V. Lesur, F.J. Lowes, H. Lühr, S. Macmillan, M. Mandea, S. McLean, C. Manoj, M. Menvielle, I. Michaelis, N. Olsen, J. Rauberg, M. Rother, T.J. Sabaka, A. Tangborn, L. Tøffner-Clausen, E. Thébault, A.W.P. Thomson, I. Wardinski, Z. Wei, T.I. Zvereva, International Geomagnetic Reference Field: The eleventh generation, Geophys. J. Int. 183 (2010) 1216–1230. doi:10.1111/j.1365-246X.2010.04804.x.

[20] D. Mostaza-Prieto, P.C.E. Roberts, Methodology to Analyze Attitude Stability of Satellites Subjected to Aerodynamic Torques, J. Guid. Control. Dyn. 39 (2016) 437–449. doi:10.2514/1.G001481.

[21] T. Bak, R. Wisniewski, Passive Aerodynamic Stabilization of a Low Earth Orbit Satellite, in: Third Int. Conf. Spacecr. Guid. Navig. Control Syst., European Space Agency (ESA), Noordwijk, the Netherlands, 1997: pp. 469–474.

[22] Y.H. Chen, Z.C. Hong, C.H. Lin, J.S. Chern, Aerodynamic and gravity gradient stabilization for microsatellites, Acta Astronaut. 46 (2000) 491–499. doi:10.1016/S0094-5765(99)00191-5.

[23] M.L. Psiaki, Nanosatellite Attitude Stabilization Using Passive Aerodynamics and Active Magnetic Torquing, J. Guid. Control. Dyn. 27 (2004) 347–355. doi:10.2514/1.1993.

[24] J. Armstrong, C. Casey, G. Creamer, G. Dutchover, Pointing Control for Low Altitude Triple Cubesat Space Darts, in: 23rd Annu. AIAA/USU Conf. Small Satell., American Institute of Aeronautics and Astronautics (AIAA), Logan, UT, 2009.

[25] J. Auret, W.H. Steyn, Design of an Aerodynamic Attitude Control System for a Cubesat, 62nd Int. Astronaut. Congr. (2011).

[26] S.A. Rawashdeh, J.E. Lumpp, Aerodynamic Stability for CubeSats at ISS Orbit, J. Small Satell. 2 (2013) 85–104.

[27] J. Virgili Llop, P.C.E. Roberts, S.E. Hobbs, J. Kingston, Aerostability for Low Altitude Flying CubeSats, in: 2nd IAA Conf. Univ. Satell. Mission. Cubesat Work., International Academy of Astronautics (IAA), Rome, Italy, 2013.

[28] V.A. Sarychev, S.A. Mirer, A.A. Degtyarev, E.K. Duarte, Investigation of equilibria of a satellite subjected to gravitational and aerodynamic torques, Celest. Mech. Dyn. Astron. 97 (2007) 267–287. doi:10.1007/s10569-006-9064-3.

[29] R.R. Kumar, D.D. Mazanek, M.L. Heck, Simulation and Shuttle Hitchhiker validation of passive

satellite aerostabilization, J. Spacecr. Rockets. 32 (1995) 806–811. doi:10.2514/3.26688.

[30] M.R. Drinkwater, R. Haagmans, D. Muzi, A. Popescu, R. Floberghagen, M. Kern, M. Fehringer, The GOCE Gravity Mission: ESA'S First Core Earth Explorer, in: 3rd Int. GOCE User Work., European Space Agency (ESA), Frascati, Italy, 2007: pp. 1–7. doi:ISBN 92-9092-938-3.

[31] M.L. Gargasz, Optimal Spacecraft Attitude Control Using Aerodynamic Torques, Air Force Institute of Technology, 2007.

[32] J. Virgili Llop, P.C.E. Roberts, Z. Hao, Aerodynamic Attitude and Orbit Control Capabilities of The ΔDsat CubeSat, in: 37th Annu. AAS Guid. Control Conf., American Astronautical Society (AAS), Breckenridge, CO, 2014.

[33] B. Tossman, F. Mobley, G. Fountain, K. Heffernan, J. Ray, C. Williams, MAGSAT attitude control system design and performance, in: Guid. Control Conf., American Institute of Aeronautics and Astronautics (AIAA), Danvers, MA, 1980. doi:10.2514/6.1980-1730.

[34] T.H. Stengle, MagSat Attitude Dynamics and Control: Some Observations and Explanations, in: J. Teles (Ed.), Fiifth Annu. Flight Mech. Theory Symp., Greenbelt, MD, 1980.

[35] C.L. Leonard, W.M. Hollister, E.V. Bergmann, Orbital Formationkeeping with Differential Drag, J. Guid. Control. Dyn. 12 (1989) 108–113. doi:10.2514/3.20374.

[36] D.N.J. du Toit, J.J. du Plessis, W.H. Steyn, Using Atmospheric Drag for Constellation Control of Low Earth Orbit Micro-satellites, in: 10th Annu. AIAA/USU Conf. Small Satell., American Institute of Aeronautics and Astronautics (AIAA), Logan, UT, 1996.

[37] G.B. Palmerini, S. Sgubini, G. Taini, Spacecraft Orbit Control using Air Drag, in: 56th Int. Astronaut. Congr., American Institute of Aeronautics and Astronautics (AIAA), Fukuoka, Japan, 2005. doi:10.2514/6.IAC-05-C1.6.10.

[38] R. Bevilacqua, M. Romano, Rendezvous Maneuvers of Multiple Spacecraft Using Differential Drag Under J2 Perturbation, J. Guid. Control. Dyn. 31 (2008) 1595–1607. doi:10.2514/1.36362.

[39] C. Lambert, B.S. Kumar, J.F. Hamel, A. Ng, Implementation and performance of formation flying using differential drag, Acta Astronaut. 71 (2012) 68–82. doi:10.1016/j.actaastro.2011.08.013.

[40] O. Ben-Yaacov, P. Gurfil, Long-Term Cluster Flight of Multiple Satellites Using Differential Drag, J. Guid. Control. Dyn. 36 (2013) 1731–1740. doi:10.2514/1.61496.

[41] A.S. Li, J. Mason, Optimal Utility of Satellite Constellation Separation with Differential Drag, in: AIAA/AAS Astrodyn. Spec. Conf., American Institute of Aeronautics and Astronautics (AIAA), San Diego, CA, 2014. doi:10.2514/6.2014-4112.

[42] M. Horsley, S. Nikolaev, A. Pertica, Small Satellite Rendezvous Using Differential Lift and Drag, J. Guid. Control. Dyn. 36 (2013) 445–453. doi:10.2514/1.57327.

[43] C. Traub, G.H. Herdrich, S. Fasoulas, Influence of energy accommodation on a robust spacecraft rendezvous maneuver using differential aerodynamic forces, CEAS Sp. J. (2019). doi:10.1007/s12567-019-00258-8.

[44] D. Mishne, E. Edlerman, Collision-Avoidance Maneuver of Satellites Using Drag and Solar Radiation Pressure, J. Guid. Control. Dyn. 40 (2017) 1191–1205. doi:10.2514/1.G002376.

[45] A.W. Lewin, Low-Cost Operation of the ORBCOMM Satelliet Constellation, in: 11th Annu. AIAA/USU Conf. Small Satell., American Institute of Aeronautics and Astronautics (AIAA), Logan, UT, 1997.

[46] J.W. Gangestad, B.S. Hardy, D.A. Hinkley, Operations, Orbit Determination, and Formation Control of the AeroCube-4 CubeSats, in: 27th Annu. AIAA/USU Conf. Small Satell., American Institute of Aeronautics and Astronautics (AIAA), Logan, UT, 2013.

[47] C. Foster, J. Mason, V. Vittaldev, L. Leung, V. Beukelaers, L. Stepan, R. Zimmerman, Differential Drag Control Scheme for Large Constellation of Planet Satellites and on-Orbit Results, in: 9th Int. Work. Satell. Constellations Form. Fly., Boulder, CO, 2017: pp. 1–18.

[48] H. Leppinen, Deploying a single-launch nanosatellite constellation to several orbital planes using drag maneuvers, Acta Astronaut. 121 (2016) 23–28. doi:10.1016/j.actaastro.2015.12.036.

[49] J. Virgili Llop, P.C.E. Roberts, N.C. Hara, Atmospheric Interface Reentry Point Targeting Using Aerodynamic Drag Control, J. Guid. Control. Dyn. 38 (2015) 403–413. doi:10.2514/1.G000884.

[50] J. Virgili Llop, P.C.E. Roberts, K. Palmer, S.E. Hobbs, J. Kingston, Descending Sun-Synchronous Orbits with Aerodynamic Inclination Correction, J. Guid. Control. Dyn. 38 (2015) 831–842. doi:10.2514/1.G000183.

[51] D. González, V. Cañas, J. Becedas, R.M. Domínguez, P.C.E. Roberts, N.H. Crisp, V.T.A. Oiko, S. Edmondson, S.D. Worrall, S.J. Haigh, K.L. Smith, R.E. Lyons, S. Livadiotti, C. Huyton, L.A. Sinpetru, S. Rodriguez-Donaire, D. Garcia-Almiñana, M. Nieto, C. Muñoz, M. Sureda, D. Kataria, G.H. Herdrich, F. Romano, T. Binder, A. Boxberger, S. Fasoulas, C. Traub, R. Outlaw, L. Ghizoni, V. Jungnell, K. Bay, J. Morsbøl, R. Villain, J.S. Perez, A. Conte, B. Belkouchi, A. Schwalber, B. Heißerer, Modelling and Simulation of Very Low Earth Orbits, in: 8th Eur. Conf. Aeronaut. Sp. Sci., Madrid, Spain, 2019.

[52] D. González, V. Cañas, J. Becedas, R.M. Domínguez, P.C.E. Roberts, N.H. Crisp, V.T.A. Oiko, S. Edmondson, S.D. Worrall, S. Haigh, K. Smith, R.E. Lyons, S. Livadiotti, C. Huyton, L.A. Sinpetru, S. Rodriguez-Donaire, D. Garcia-Almiñana, M. Nieto, C. Muñoz, M. Sureda, D. Kataria, G.H. Herdrich, F. Romano, T. Binder, A. Boxberger, S. Fasoulas, C. Traub, R. Outlaw, L. Ghizoni, V. Jungnell, K. Bay, J. Morsbøl, R. Villain, J.S. Perez, A. Conte, B. Belkouchi, A. Schwalber, B. Heißerer, Scilab and Xcos for VLEO satellites modelling, in: Scilab Conf., Berlin, Germany, 2019: p. 14.

[53] C. Traub, F. Romano, T. Binder, A. Boxberger, G. Herdrich, S. Fasoulas, P.C.E. Roberts, K.L. Smith, S. Edmondson, S.J. Haigh, N.H. Crisp, V.T.A. Oiko, R.E. Lyons, S.D. Worrall, S. Livadiotti, J. Becedas, R.M. Dominguez, L. Ghizoni, V. Jungnell, K. Bay, J. Morsbøl, D. Garcia-Almiñana, S. Rodriguez-Donaire, M. Sureda, D. Kataria, R. Outlaw, R. Villain, J.S. Perez, A. Conte, B. Belkouchi, A. Schwalber, B. Heißerer, A Review and Gap Analysis of Exploiting Aerodynamic Forces as a Means to Control Satellite Formation Flight, in: 67th Dtsch. Luft- Und Raumfahrtkongress, German Aerospace Society, Friedrichshafen, German, 2018.

[54] C. Traub, F. Romano, T. Binder, A. Boxberger, G. Herdrich, S. Fasoulas, P.C.E. Roberts, K.L. Smith, S. Edmondson, S.J. Haigh, N.H. Crisp, V.T.A. Oiko, R.E. Lyons, S.D. Worrall, S. Livadiotti, J. Becedas, G. González, R.M. Dominguez, D. González, L. Ghizoni, V. Jungnell, K. Bay, J. Morsbøl, D. Garcia-Almiñana, S. Rodriguez-Donaire, M. Sureda, D. Kataria, R. Outlaw, R. Villain, J.S. Perez, A. Conte, B. Belkouchi, A. Schwalber, B. Heißerer, On the exploitation of differential aerodynamic lift and drag as a means to control satellite formation flight, CEAS Sp. J. (2019). doi:10.1007/s12567-019-00254-y.

[55] M. Walther, C. Traub, G.H. Herdrich, S. Fasoulas, Improvements to the Feasibility Range of Rendezvous Maneuvers using Aerodynamic Forces, in: 68th Dtsch. Luft-Und Raumfahrtkongress, Darmstadt, Germany, 2019.

[56] Y. Yang, Spacecraft attitude determination and control: Quaternion based method, Annu. Rev. Control. 36 (2012) 198–219. doi:10.1016/j.arcontrol.2012.09.003.

[57] S. De Florio, S. D'Amico, Optimal autonomous orbit control of remote sensing spacecraft, Adv. Astronaut. Sci. 134 (2009) 949–967.

[58] N.H. Crisp, P.C.E. Roberts, S. Edmondson, S.J. Haigh, C. Huyton, S. Livadiotti, V.T.A. Oiko, K.L.

Smith, S.D. Worrall, J. Becedas, D. González, G. González, R.M. Dominguez, K. Bay, L. Ghizoni, V. Jungnell, J. Morsbøl, T. Binder, A. Boxberger, S. Fasoulas, G. Herdrich, F. Romano, C. Traub, D. Garcia-Almiñana, S. Rodriguez-Donaire, M. Sureda, D. Kataria, R. Outlaw, B. Belkouchi, A. Conte, J.S. Perez, R. Villain, B. Heißerer, A. Schwalber, SOAR – Satellite for Orbital Aerodynamics Research, in: 69th Int. Astronaut. Congr., International Astronautical Federation (IAF), Bremen, Germany, 2018.

[59] J. Virgili Llop, P.C.E. Roberts, ΔDsat, a QB50 CubeSat mission to study rarefied-gas drag modelling, Acta Astronaut. 89 (2013) 130–138. doi:10.1016/j.actaastro.2013.04.006.

[60] H. Bang, M.-J. Tahk, H.-D. Choi, Large angle attitude control of spacecraft with actuator saturation, Control Eng. Pract. 11 (2003) 989–997. doi:10.1016/S0967-0661(02)00216-2.

[61] B. Wie, H. Weiss, A. Arapostathis, Quarternion feedback regulator for spacecraft eigenaxis rotations, J. Guid. Control. Dyn. 12 (1989) 375–380. doi:10.2514/3.20418.

[62] E. Doornbos, H. Klinkrad, Modelling of space weather effects on satellite drag, Adv. Sp. Res. 37 (2006) 1229–1239. doi:10.1016/j.asr.2005.04.097.

[63] L.H. Sentman, Free molecule flow theory and its application to the determination of aerodynamic forces, Sunnyvale, CA, 1961.

[64] K. Moe, M.M. Moe, Gas–Surface Interactions and Satellite Drag Coefficients, Planet. Space Sci. 53 (2005) 793–801. doi:10.1016/j.pss.2005.03.005.

RD-1 DISCOVERER Deliverable 2.1 VLEO Aerodynamics Requirements Document

4. Acknowledgement and Disclaimer

This project has received funding from the European Union’s Horizon 2020 research and innovation programme under grant agreement No 737183. This publication reflects only the author's view and the Agency is not responsible for any use that may be made of the information it contains.